UNIVERSITY OF CALIFORNIA
Santa Barbara

STRATIFICATION AMD MIXING IN HYPERSALINE MONO LAKE (CALIFORNIA)

A Dissertation submitted in partial satisfaction
of the requirements for the degree of

Doctor of Philosophy

in

Biology

by

José R. Romero

Committee in charge:

Professor John M. Melack, Chairman

Professor Alice A. Alldredge

Professor Roger M. Nisbet

Doctor Sally MacIntyre

December 1996

UMI Number: 9724592

The dissertation of José R. Romero is approved

Alvin Alderson

Ross W. Nesbit

Sally MacIntyre

Jack Wallace

Committee Chairperson

December 1996

ACKNOWLEDGEMENTS

Financial support was provided by grants from the Los Angeles Department of Water and Power. The first three years of graduate study was supported by the Patricia Roberts Harris Fellowship from the University of California. The FORTRAN compiler used in the dissertation analyses was provided at reduced cost by Lahey Computer Systems, Inc.

Dr. John Patterson, formerly of the Centre for Water Research, Perth, Australia, provided the vertical mixing model, DYRESM, and was helpful in my familiarization of the model during two extended stays at UC Santa Barbara. Dr. Patterson also provided contributions to Chapter 1. Dr. Sally MacIntyre provided invaluable input into the organization and presentation of Chapter 2 which I gratefully acknowledge. Dr. Robert Jellison was responsible for most of the field research presented in this dissertation and provided support and perspective throughout my graduate career. I thank Dr. John Melack for providing guidance, financial support, flexibility, and patience as an advisor. In addition, I wish to thank the other members of my committee, Dr. Roger Nisbet and Dr. Alice Alldredge.

Most of the data presented in this dissertation was collected by Gayle Dana and Darla Heil as part of the monitoring program at Mono Lake. Present and former graduate student colleagues Steve Hamilton, Suzanne Sippel, Solange Filoso, Mike Williams, Al Lydecker, Veronique LaCapra, and Diana Engle made graduate study pleasurable. I thank friends Natalie Rimmele, Chris Day, Ray Miller, Vance Vredenberg, Ari Martinez, Peter Lee, Mark Britton, and Tyler Trull for wonderful and needed diversions from study. Finally, and most importantly, a special thanks to my family (José Sr., Anita, Nick, Hugo, and Soraya) for support and perspective during my 12 years of higher education.

VITA

José R. Romero

Born: September 10, 1966, Eureka, California.

EDUCATION

1989 M.S. in Environmental Engineering, Stanford University, Stanford.

1989 B.S. in Civil Engineering, Stanford University, Stanford.

PROFESSIONAL EXPERIENCE

1992-1996 Teaching Assistant, University of California, Santa Barbara, California.

1991-1996 Research Assistant, Dr. J.M. Melack, University of California, Santa Barbara, California. Physical limnological investigations of Mono Lake, California.

1994, 1996 Research assistant, Dr. S. MacIntyre, University of California, Santa Barbara, California. Physical limnological investigations of Lake Victoria, Uganda.

PUBLICATIONS

Romero, J.R., J.C. Patterson, and J.M. Melack. 1996. Simulation of the effect of methane bubble plumes on vertical mixing in Mono Lake. Aquatic Sciences 55: *In Press*.

Romero, J.R. and J.M. Melack. 1996. Sensitivity of vertical mixing in a large saline lake to variations in runoff. Limnol. Oceanogr. 41:955-965.

ABSTRACT

Stratification and Mixing in Hypersaline Mono Lake (California)

by

José R. Romero

Application of a one-dimensional (1D) vertical mixing model to hypersaline (*ca.* 94 g l^{-1}) Mono Lake during 1-yr reproduced mixed-layer dynamics well, but hypolimnetic heating was underestimated. One possible source of hypolimnetic heating is vertical mixing by methane bubble plumes rising from the sediments. Simulations with the inclusion of a bubble plume algorithm required an ebullition rate 300x greater than the maximum estimate to simulate observed hypolimnetic heating.

The influence of lake level and salinity changes on seasonal mixing was modeled with the 1D model where the diffusivity was based on the Lake Number (L_N). The simulation reproduced salinity dynamics for 2-yr of monomixis and 6-yr of meromixis. Assuming climate change causes less precipitation, the frequency and duration of meromixis for 100, 87.5, and 75% of the freshwater inputs over a 50-yr period (1940-1990) was simulated with the assumption of no streamflow diversion. Simulations indicate the lake is susceptible to meromixis over a large lake level range for all scenarios during large runoff years.

The effect of freshwater inputs on stratification, vertical mixing, and upward ammonia flux was evaluated during a 6-yr (1989-1994) monomicitic period. Five years had falling lake level and periods of inverse salinity stratification with double diffusive salt fingering conditions during the last several months of thermal stratification. Bi-weekly to monthly summer (June-September) diffusivities estimates in the thermocline from the heat-flux

gradient method ranged from 9.5×10^{-7} m^2 s^{-1} during wet 1993 to 4.2×10^{6} m^2 s^{-1} during a drought in 1989. Estimated seasonal and interannual differences in the upward ammonia flux can be partly explained by variations in freshwater inputs and wind forcing.

The 1D model simulated mixed-layer dynamics adequately for 5-yr from 1989-1994. The destabilizing influence of inverse salinity stratification resulted in the inapplicability of the 1D assumption during 1989. During the other 5-yr modeled diffusivities within the pycnocline were underestimated by 10-20x. Three approaches were tested to increase mixing: 1) sub-daily wind speed input, 2) benthic boundary layer turbulence, and 3) the L_N as an index of mixing. The L_N parameterization yielded the best results and suggests boundary mixing along the margins and perhaps shear mixing in the interior during high wind forcing predominate as the major vertical transport mechanisms.

TABLE OF CONTENTS

INTRODUCTION

Saline lakes occur on every continent and have a total volume almost as large as that of the world's freshwater lakes and rivers. Saline lakes are usually the only natural lakes in closed-basins and are particularly responsive to climatic variations as lake level and salinity are closely coupled with the water balance in these systems (Hammer 1986). Further, diversion of freshwater inputs for anthropogenic uses have resulted in diminished size and increased salinity in many saline lakes throughout the world (Micklin 1988, Cooper and Koch 1990, Galat 1990, Anati and Stiller 1991).

Variations in the size and salinity of saline lakes, whether anthropogenically or climatically induced, can cause changes in stratification. The stratification regime of temperate endoheric saline lakes is commonly monomictic (one period of complete mixing per year), but can be meromictic (incomplete mixing over the course of a year). Some lakes such as Mono (Jellison and Melack 1993) or Pyramid (Galat 1990) have undergone periods of temporary meromixis with persistent chemical stratification over a multi-year duration. Other lakes have undergone long-term meromixis such as the Dead Sea (Steinhorn 1985), which was meromictic for more than 100 years, or Big Soda (Hutchinson 1957, Kimmel *et al.* 1978), which has been meromictic since 1910-1920. Meromictic periods are characterized by decreased vertical transport rates (Jellison and Melack 1993) and the accumulation of nutrients below the persistent chemocline (Jellison *et al.* 1993, Cloern *et al.* 1985).

Saline lakes are also characterized by low algal and zooplankton species diversity relative to freshwater lakes, and often do not have fish. Relative to freshwater lakes, saline lakes have simple trophic complexity which makes ecological modeling of these lacustrine systems attractive. Climatic or anthropogenic perturbations can cause interannual variations in seasonal salinity stratification which may lead to direct physical effects on ecosystem dynamics. In N-limited Pyramid Lake, a large influx of riverine freshwater associated with the 1982-1983 El Niño shifted the dominant algae to N-fixing cyanobacteria presumably as a consequence of a lower vertical N-flux because of salinity stratification (Galat *et al.* 1990). One approach to assess the effect of variations in freshwater inputs on saline lacustrine ecosystem response is to couple a model of vertical mixing with an ecological model.

Two classes of vertical mixing models have been developed over the past 30 years, diffusion models and mixed-layer models (Harleman 1982). Diffusion models are based upon the one-dimensional (1D), non-linear heat transfer equation,

$$\frac{\partial T}{\partial t} = \frac{1}{\partial A(z)} \frac{\partial}{\partial z}\left[A(z)(\mu + K)\frac{\partial T}{\partial z} \right] + \frac{1}{\rho c}\frac{\partial N}{\partial z}$$

where T is temperature (°C), t is time (s), z is the depth below the water surface (m), $A(z)$ is the cross-sectional area of the lake at depth z (m^2), K is the eddy diffusivity ($m^2\ s^{-1}$), μ is the molecular diffusivity ($m^2\ s^{-1}$), N is the heat input from absorption of solar radiation ($W\ m^{-2}$), ρ is the density of the water ($kg\ m^{-3}$), and c is the specific heat of water ($J\ kg^{-1}\ °C^{-1}$). The eddy diffusivity, K, is usually expressed under stratified conditions as a neutral eddy diffusivity, K_N, multiplied by a function of the gradient Richardson Number, R_i, as:

$$K = K_N f(R_i)$$

and

$$R_i = \frac{N^2}{(\partial u/\partial z)^2}.$$

Difficulties have arisen in the analytical specification of both K_N and $f(R_i)$ (*see* Henderson-Sellers 1985).

The surface dynamics of mixed-layer models are based on the integral turbulent kinetic energy (TKE) model (Sherman *et al.* 1978). In the mixed-layer model, DYRESM (Imberger and Patterson 1981, 1990), TKE is partitioned into four discrete processes: wind stirring at the surface, convective overturn from density instabilities, interfacial shear production at the base of the mixed-layer, and Kelvin-Helmoltz billowing at the base of the mixed-layer. The available TKE is compared to the potential energy required to combine the mixed layer with layer immediately below it. Parameterization of the available TKE is:

$$KE = \frac{C_K}{2}(w_*^{\,2} + n^3 u_*^{\,3})\Delta t + \frac{C_S}{2}\left(u^2 + \frac{u^2}{6}\frac{d\delta}{dh} + \frac{u\delta}{3}\frac{du}{dh}\right)\delta h$$

and for the required potential energy is:

$$PE = \frac{C_T}{2}\left[(w_*^{\,3} + \eta^3 u_*^{\,3}) + \frac{\Delta\rho g h}{\rho_0} + \frac{g\delta^2}{24\rho_0}\frac{d(\Delta\rho)}{dh} + \frac{g\Delta\rho\delta}{12\rho_0}\frac{d\delta}{dh}\right]\delta h$$

where u_* and w_* are the velocity scales for wind shear and penetrative convection (m s^{-1}), u is the shear velocity of the mixed-layer (m s^{-1}), $\Delta\rho$ is the density jump between the mixed-layer with depth h and the layer below it with depth dh, ρ_0 is the reference density (kg m^{-3}), δ is the Kelvin-Hemoltz billow thickness scale (m), Δt is the time step (s), and g is the acceleration due to gravity (m s^{-2}) (Imberger and Patterson 1990). The efficiency of the individual mixing mechanisms (η, C_K, C_T, *and* C_S) are fixed constants derived from laboratory and field studies. Mixing below the mixed-layer is described in the dissertation chapters.

DYRESM has been applied to small reservoirs such as Wellington Reservoir (area = 16 km^2, z_{max}=30 m) in southern Australia (Imberger and Patterson 1981), moderate-sized (area = 360 km^2, z_{avg}=100 m) Kootenay Lake in British Columbia (Patterson *et al.* 1984), and large-sized (width = 70 km, length=190 km, z_{avg}=22 m) Lake Erie (Ivey and Patterson 1984). The model has also been applied to lakes with seasonal ice cover (Patterson and Hamblin 1988). The model's validation over a wide range of lake sizes and latitudinal locations without calibration were important considerations in the decision to apply the model to Mono Lake.

This dissertation examines the vertical mixing dynamics of moderately-sized (*ca.* 150 km^2), hypersaline Mono Lake. Chapters 1, 2, and 4 present DYRESM simulations of Mono Lake. Chapter 3 describes the physical limnology of the lake from 1989-1994, a period of monomixis.

In some lakes, after the onset of thermal stratification, anoxic conditions develop in the hypolimnion and reduced solutes accumulate. Several techniques have been developed to ameliorate poor water quality in the hypolimnion of reservoirs and lakes including direct infusion of oxygen into the hypolimnion (Wüest *et al.* 1992), bubble plume destratification (Schladow 1992, 1993), and a number of mechanical mixing devices. Bubble plume algorithms in a stratified fluid (McDougall 1978) were incorporated into DYRESM (Asaeda and Imberger 1989) to develop a management tool which has been successfully used to increase the efficiency of bubble plume destratification systems in water storage reservoirs (Schladow 1992, 1993).

A DYRESM simulation of the 1992 Mono Lake stratification dynamics adequately simulated mixed-layer deepening, but underestimated hypolimnetic heating. Both biogenic and thermogenic methane bubble sources have been identified in Mono Lake (Oremland *et al.* 1987). Chapter 1 evaluates whether methane bubble plumes are a significant hypolimnetic heating mechanism in Mono Lake. Chapter 1, 'Simulation of the effect of methane bubble plumes on vertical mixing in hypersaline Mono Lake", is *In Press* in *Aquatic Sciences.*

With the extension of the Los Angeles Aqueduct into the Mono Basin in 1941, stream diversions resulted in falling lake level (14 m from 1947 to 1982), decreased volume (5.4×10^9 m^3 to 2.6×10^6 m^3), and increased salinity (45 to 94 g l^{-1}). The high salinity and decreased surface area made the lake susceptible to ectogenic meromixis during exceptionally large discharge years such as the 1982-83 El Niño (Jellison and Melack 1993). In Chapter 2, "Sensitivity of a large saline lake to variations in runoff", long-term simulations were used to evaluate the likely stratification dynamics (i.e. meromictic or monomictic) from the past 50 years (1941-1990) of freshwater inputs, assuming no stream diversions and the 1992 lake level (1943 m above sea level) as an initial condition. Paleoclimatic reconstructions (Graumlich 1993, Stine 1994) indicate the past 50 years were an exceptionally wet period, so additional scenarios with reductions in precipitation and stream discharge were evaluated. The incorporation of the Lake Number (Imberger and Patterson 1990) into the vertical diffusivity parameterization was necessary to model the observed deep mixing in the lake. Chapter 2 has been published in *Limnology and Oceanography*, volume 41 in a special climate change issue.

Chapter 3, "Effect of hydrologic variations on stratification and upward ammonia flux in hypersaline Mono Lake", evaluates a 6 year (1989-1994) period of monomixis which complements earlier research on the 1983-1988 meromictic period (Jellison and Melack 1993, Jellison *et al.* 1993). Temperature and conductivity profiles were measured with a conductivity-temperature-depth (CTD) profiler from 1991 to 1994 and had greater accuracy and resolution than methods employed from 1982 to 1990. Though the lake level fluctuated within a small range over the period (*ca.* 1.25 m), variations in stratification dynamics were substantial. Conditions for double diffusive salt fingering (Turner 1985) across the pycnocline are likely during years with falling lake level from August to November. Comparisons of vertical eddy diffusivities and upward ammonia fluxes between meromixis and monomixis are presented. Further, the Lake Number is shown to be an indicator of deep mixing.

Chapter 4, "Simulations of vertical mixing in a hypersaline lake", presents a critical comparison between field and model estimates of mixed-layer and hypolimnetic properties, pycnocline indices, and eddy diffusivities within the pycnocline. Many vertical models have been developed to evaluate water quality management alternatives or serve as the physical basis of ecological models. However, verification of modeled vertical transport rates have not been presented in previous publications. Simulations with the Lake Number as an index of deep mixing yielded vertical diffusivities within the pycnocline similar to estimates from the heat flux gradient method (Jassby and Powell 1974).

Further improvements to the mixing model are expected. On-going research is identifying deep mixing mechanisms which may result in the development of improved vertical mixing parameterizations below the base of the mixed-layer. Climatic effects on the ecology of saline lakes, water resource strategies to manage salinity stratification, and investigations of the significance of physical mixing mechanisms are questions in which a vertical mixing model can provide insight.

References

Anati, D.A. and M. Stiller. 1991. The post-1979 thermohaline structure of the Dead Sea and the role of double-diffusive mixing. Limnol. Oceanogr. 36:342-354.

Asaeda, T. and J. Imberger. 1989. Behavior of bubble plumes in a linear stratification. J. Jpn. Soc. Civ. Eng. 411:55-62.

Cloern, J.E., B.J. Cole, and R.S. Oremland. 1983. Seasonal changes in chemistry and biology of a meromictic lake (Big Soda Lake, Nevada, U.S.A.). Hydrobiologia 105:195-206.

Cooper, J.J. and D.L. Koch. 1984. Limnology of a desertic terminal lake, Walker Lake, Nevada, U.S.A. Hydrobiologia 118:275-292.

Galat, D.L., J.P. Verdin, and L.L. Simis. 1990. Large-scale patterns of *Nodularia spumigena* blooms in Pyramid lake, Nevada, determined from Landsat imagery: 1972-1986. Hydrobiologia 197:147-164.

Graumlich, L.J. 1993. A 1000-year record of temperature and precipitation in the Sierra Nevada. Quat. Res. 39:249-255.

Hammer, U.T. 1986. Saline lake ecosystems of the world. Junk.

Harleman, D.R.F. 1982. Hydrothermal analysis of lakes and reservoirs. J. Hydr. Div. ASCE 108:302-325.

Henderson-Sellers, B. 1985. New formulation of eddy diffusion thermocline models. Appl. Math. Modelling 9:441-446.

Hutchinson, G.E. 1957. A treatise on limnology, v. 1. Wiley.

Imberger, J. and J.C. Patterson. 1981. A dynamic reservoir simulation model, DYRESM: 5. In: Transport Models for Inland and Coastal Waters. Ed. H. B. Fischer, pp. 310-361, Academic Press, New York.

Imberger, J. and J.C. Patterson. 1990. Physical Limnology. In: Advances in applied mechanics. Ed. T. Wu, 27:303-475, Academic Press, Boston.

Ivey, G.N. and J.C. Patterson. 1984. A model of the vertical mixing in Lake Erie in summer. Limnol. Oceanogr. 29:553-563.

Jassby, A. and T. Powell. 1975. Vertical patterns of eddy diffusion during stratification in Castle Lake, California. Limnol. Oceanogr. 20:530-543.

Jellison, R. and J.M. Melack. 1993*a*. Meromixis in hypersaline Mono Lake, California. 1. Stratification and vertical mixing during the onset, persistence, and breakdown of meromixis. Limnol. Oceanogr. 38:1008-1019.

Jellison, R., L.G. Miller, J.M. Melack, and G.L. Dana. 1993. Meromixis in hypersaline Mono Lake, California. 2: Nitrogen fluxes. Limnol. Oceanogr. 38:1020-1039.

Kimmel, B.L., R.M. Gersberg, L.J. Paulson, R.P. Axler, and C.R. Goldman. 1978. Recent changes in the meromictic status of Big Soda Lake, Nevada. Limnol. Oceanogr. 23:1021-1025.

McDougall, T.J. 1978. Bubble plumes in stratified environments. J. Fluid Mech. 85:655-672.

Micklin, P.P. 1988. Desiccation of the Aral Sea: a water management disaster in the Soviet Union. Science 241:1170-1176.

Oremland, R.S., L.G. Miller, and M.J. Whiticar. 1987. Sources and flux of natural gases from Mono Lake, California. Geochim. Cosmochim. Acta 51:2915-2929.

Patterson, J.C. and P.F. Hamblin. 1988. Thermal simulation of a lake with winter ice cover. Limnol. Oceanogr. 33:323-338.

Patterson, J.C., P.F. Hamblin, and J. Imberger. 1984. Classification and dynamic simulation of the vertical density structure of lakes. Limnol. Oceanogr. 29:845-861.

Schladow, S.G. 1992. Bubble plume dynamics in a stratified medium and the implications for lake water quality amelioration in lakes. Wat. Resour. Res. 28:313-321.

Schladow, S.G. 1993. Lake destratification by bubble-plume systems: design methodology. J. Hydr. Engr. 119:350-368.

Sherman, F., J. Imberger, and G.M. Corcos. 1978. Turbulence and mixing in stable stratified waters. Ann. Rev. Fluid Mech. 10:267-288.

Steinhorn, I. 1985. The disappearance of the long term meromictic stratification of the Dead Sea. Limnol. Oceanogr. 30:451-472.

Stine, S. 1994. Extreme and persistent drought in California and Patagonia during medieval time. Nature 369:546-549.

Turner, J.S. 1985. Multicomponent convection. Ann. Rev. Fluid Mech. 17:11-44.

Wüest, A., N.H. Brooks, and D.M. Imboden. 1992. Bubble plume modeling for lake restoration. Wat. Resour. Res. 28:3235-3250.

CHAPTER 1

Simulation of the Effect of Methane Bubble Plumes on Vertical Mixing in Mono Lake

Introduction

Recent research on bubble plumes has emphasized the potential of destratification systems (Patterson and Imberger 1989, Schladow 1993) and artificial oxygenation of the hypolimnion (Wüest *et al.* 1992) to improve the quality of inland waters. In destratification systems a continuous release of bubbles results in the entrainment of ambient water to form a combined bubble and water plume; this combined plume is called a bubble plume. The bubble plume rises through the water column entraining ambient water until a level is reached at which the air-water mixture is neutrally buoyant. The water then detrains from the bubble plume, falls to a level of neutral buoyancy and horizontally intrudes. The mechanism transports denser fluid up the water column and, in reservoir destratification systems, is used to increase the potential energy of the reservoir so that the entire water column mixes periodically.

Natural bubble seeps occur in lakes with much lower gas flow rates than destratification systems. However, the contribution of natural bubble plumes to mixing dynamics in lakes has not been evaluated and there is some potential for these natural seeps to provide significant vertical transport in the hypolimnion. In this paper we evaluate the vertical mixing induced by methane bubble plumes in Mono Lake with a one-dimensional lake stratification model which includes an algorithm simulating the effect of bubble plumes.

Study Site

During 1992 Mono Lake (38°N, 119°W) covered 160 km^2 with a mean depth of 17 m and surface elevation of 1943 m (Fig. 1). The lake is hypersaline with a salinity of *ca.* 91 g L^{-1} with a chemical composition as reported in Jellison and Melack (1993). Mono Lake lies in a closed hydrologic basin where streamflow is primarily from the accumulation of snowpack along the eastern escarpment of the Sierra Nevada during the winter and subsequent melt in the spring and early summer. The lake is usually monomictic (Mason 1967, Melack 1983), but a 6 year meromictic episode occurred from 1983 to 1988 as a result of a large influx of freshwater accompanying an El Niño-Southern Oscillation (Jellison and Melack 1993).

During 1986 Oremland *et al.* (1987) estimated the methane bubble ebullition rates at Mono Lake. Twelve thermogenic seeps were found with methane flow rates greater than 0.033 L s^{-1}. Oremland *et al.* (1987) estimated a maximum of 20 seeps with flow-rates of 0.067 L s^{-1} resulting in an ebullition of 1.3 L s^{-1}. Oremland *et al.* (1987) also estimated 600 to 1000 low flow seeps (8.3×10^{-4} to 1.7×10^{-3} L s^{-1}) which result in a total low flow ebullition of 0.6 to 1.7 L s^{-1}.

Lake and Bubble Plume Models

DYRESM (Imberger and Patterson 1981), a one-dimensional vertical mixing model, was used to simulate the mixing dynamics of Mono Lake. The model is based on a Lagrangian structure which models the lake as horizontal layers of uniform properties (i.e. temperature and salinity). The layers move vertically, expanding and contracting in response to surface mass fluxes and mixing processes.

The model explicitly simulates fundamental mixing mechanisms in stratified lakes and reservoirs. Mixed-layer deepening is modeled as penetrative convection from surface cooling and evaporative concentration of salt at the surface, stirring by the wind, seiche induced shear at the pycnocline, and billowing at the pycnocline resulting from shear. DYRESM calculates the eddy diffusivity using Weinstock's (1981) formulation given by:

$$K_z = \alpha \frac{\varepsilon}{N^2 + 0.6k_0{}^2u^2}$$

where ε is the dissipation of turbulent kinetic energy, k_0 is the wave number of the energy bearing eddies, u is the root mean square velocity of the motion in the turbulent patch, N is the buoyancy frequency, and α is a constant whose value lies between 0.2 and 0.8. We used a value of 0.5. The model has been successfully applied to reservoirs (Imberger and Patterson 1981) and freshwater lakes (Patterson *et al.* 1984). Some modifications were required for its application to hypersaline Mono Lake (see below).

The algorithm describing the behavior of bubble plume aerators in the model is described by Schladow (1992), following an earlier version by Patterson and Imberger (1989). The algorithm is based on the assumption that the rising bubbles constitute a simple buoyant plume with a density equal to the air-water mixture (McDougall 1978). As the plume rises through the decreasing density of the ambient stratification, it entrains water, increasing the density of the air-water mixture, and causing the plume to slow until it reaches a height at which the mixture is neutrally buoyant, as observed in laboratory experiments, and detrainment occurs (McDougall 1978, Asaeda and Imberger 1989). The detrained water no longer contains bubbles and is therefore locally heavy; it falls back through the water column until it reaches a level of equal density and is inserted horizontally. The level of the intrusion will be above that of the seep as the plume has entrained lighter water from above the seep. The bubble component of the plume continues to rise, and a new buoyant plume begins. The whole process of rise and ejection may be repeated several times, depending on the water depth, airflow rate, and density stratification.

The process may be modeled as a buoyant plume with the effects of the bubbles included. A bubble plume differs from usual sources of buoyancy in two ways. First, a continuous increase in buoyancy results from expansion of the bubbles as they rise through the water column. Secondly, the bubbles ascend faster than the surrounding water so that there is a slip at the bubble-water interface. The equations solved are the standard integral plume equations for conservation of mass, momentum, and buoyancy (List 1982), with the latter equation including the provision for bubble expansion, bubble slip, and a variable ambient density stratification (McDougall 1978). A 4th-order Runge-Kutta scheme is used to solve the equations (Schladow 1992), with the initial conditions coming from the assumption that near the source stratification may be neglected (McDougall 1978).

As with all integral models, this model simplifies the true complexity of a bubble plume rising in a density stratified fluid. However, from the perspective of predicting the changes in density that result, the key is the prediction of the total entrainment flux, and the model has been shown to perform well in that regard when compared with experimental data (Schladow

1992). The algorithm requires specification of the airflow rate, the number of seeps, and the depth of the seeps.

The model simulates a continuous column of bubbles. The dynamics and entrainment efficiencies of discontinuous bubble seeps are unknown. Here it is assumed that all seeps emit continuous bubble plumes.

Simulation Inputs

Temperature and conductivity profiles were obtained bi-weekly at three sampling locations (Fig. 1) from March through October 1992 and monthly during the remainder of the year with a Sea-Bird Seacat SBE-19. Temperature measurements had a vertical resolution of 0.125 m and accuracy of 0.005°C, and conductivity measurements had a vertical resolution of 1 m and accuracy of 0.1 mS cm^{-1} after data processing. Raw conductivity measurements were standardized to 25 °C. Conductivity at 25°C was assumed to act conservatively and was used as a measure of salinity. Measured temperature and conductivity profiles from the three stations were laterally averaged and used to initialize and verify the simulations.

The model requires a formulation of the density as a function of temperature and conductivity. For Mono Lake, the density equation is $\rho=1204.41-0.2164T-0.00326T^2-4.265C_{25}+0.03166C_{25}^2$ where ρ is the density of Mono Lake water (kg m^{-3}), T is the water temperature (°C), and C_{25} is the conductivity at 25 °C (mS cm^{-1}) (Jellison and Melack 1993). The density equation is valid within the conductivity range of 77 to 92 mS cm^{-1} and temperature range of 0 to 25 °C.

Other parameters describing the properties of Mono Lake water are required by the model. A latent heat of evaporation of 2.477×10^6 J kg^{-1} for

Mono Lake water was estimated from linear interpolation between the values of seawater (Gill 1982) and the Dead Sea (Steinhorn 1991). A kinematic viscosity of 1.27×10^{-6} m^2 s^{-1} and specific heat of 3865 J kg^{-1} $°C^{-1}$ were obtained from Mason (1967).

Hourly averaged measurements of shortwave and longwave radiation were recorded at a meteorological station located 7 km southwest of the lake. Ten minute averages of wind speed, relative humidity, and air temperature and total hourly rainfall (not shown) were measured at a meteorological station on the southern tip of Paoha Island in the center of the lake. Relevant meteorological measurements were standardized to 10 m and computed as daily averages with the exception of average shortwave radiation data which was computed with a constant day length of 12 hours. These data are shown in figures 2A-C.

Photosynthetically available radiation (PAR) through the water column was measured with a submersible Li-Cor quantum sensor. Attenuation coefficients ranged from 0.35 to 1.1 m^{-1} in 1992. Daily values were estimated by interpolating between dates of field surveys (Fig. 2A). Attenuations at other wavelengths are reported in Jellison and Melack (1993). The surface reflectivity of incoming shortwave radiation is a function of sun angle and surface roughness, but is usually taken as a constant for averaged data (Imberger and Patterson 1990). A constant surface reflectivity of 5% was used here. PAR was computed as 45% of the incoming shortwave radiation and is very close to the findings of Jellison and Melack (1993).

Lake surface elevations were recorded weekly to monthly from staff gauges by the Los Angeles Department of Water and Power. Daily lake elevations were computed by linear interpolation between dates of measured lake surface elevations. A thirteen point moving average was applied to smooth the interpolated daily elevations (Fig. 2D). Total daily stream discharges into the lake from the five major creeks were provided by the Los Angeles Department of Water and Power and Southern California Edison (Fig. 2D). Stream gauges are approximately 5 km upstream from the lake and there is considerable uncertainty in the water loss estimates below the weirs to groundwater and evapotranspiration (Vorster 1985). Rather than estimating the groundwater and evaporation, the lake elevation was used as the major hydrological input. The amount of water required to raise the simulated lake level to the daily input elevation was added to the surface layer on a sub-daily time step. The 1992 Convict Creek temperatures (not shown) at the Sierra Nevada Aquatic Research Laboratory located 45 km from Mono Lake at an elevation of 2160 m served as stream temperature inputs. Simulations with ±3 °C variations in stream temperature inputs indicated that stream temperature was not a sensitive input parameter during 1992.

For all simulations reported here the model is initialized with the 18 January 1992 profile, and run for a period of 330 days until 12 December 1992, the final field survey of 1992. The model requires the daily data described above and runs independently of the subsequent profiles which are used only for validation.

1992 Mono Lake Seasonal Stratification

During 1992 Mono Lake was monomictic (Fig. 3). The onset of thermal stratification during late February and early March coincided with increased solar irradiance and high underwater attenuation (Fig. 2A). By the end of May the structure and gradient of the seasonal thermocline had setup and persisted through September (Fig. 3A). The midpoint of the thermocline deepened from approximately 10 m at the end of May to 16 m by October. The average hypolimnetic temperature increased from 2.5 (March) to 4.2 °C (September) (Fig. 3B).

During February and March low evaporation rates led to a steady lake level increase which resulted in the dilution of the mixed-layer as evident from the 90.0 mS cm^{-1} isopleth of conductivity (Fig. 3C). From April to December the lake level decreased as evaporation from the lake surface exceeded hydrologic inputs. From April to July, a period of increasing evaporation rates, the lake level decreased slowly as high stream discharges (Fig. 2D) nearly balanced evaporation. By late April falling lake levels and increasing evaporation resulted in inverse chemical stratification where the average mixed-layer conductivity was greater than the average hypolimnetic conductivity. Peak stream discharges in May and June (Fig. 2D) resulted in the dilution of the upper 2 to 5 m (90.5 and 90.75 mS cm^{-1} isopleths of conductivity, Fig. 3C) with inverse chemical stratification below 5 m. During August through October high evaporation rates and low stream inputs resulted in a relatively rapid lake level decrease. By October 5, about a month prior to turnover, the mixed-layer conductivity was 1.5 mS cm^{-1} greater than the hypolimnion.

A 2 to 3 kg m^{-3} density difference between the mixed-layer and the hypolimnion persisted throughout much of the stratified period (Fig. 3D). During July temperature contributed 2.3 kg m^{-3} to the density difference across the pycnocline (15 to 7 °C) whereas inverse conductivity stratification reduced the density difference by 0.7 kg m^{-3}. Autumn turnover occurred in mid-November from a combination of cooling and unstable chemical stratification.

Simulation without Bubble Plumes

Initially DYRESM was run with no methane gas release and simulated the seasonal mixed-layer thermal dynamics well (Fig. 4A). The onset of thermal stratification during early to mid-March, mixed-layer deepening, and the timing of autumn turnover matched well with the field data. The lower boundary of the simulated thermocline deepened too slowly whereas field profiles indicate that the thermocline deepened at approximately the same rate as the mixed-layer. A small increase in the simulated hypolimnetic heat content was mainly from thermal diffusion of the warmer overlying metalimnion (Fig. 4B).

The seasonal mixed-layer conductance dynamics were not predicted adequately during the onset of stratification (Fig. 4C). The simulated dilution of the upper 10 m from February to April (89.75 and 90.0 mS cm^{-1} isopleths of conductivity) was caused by rising lake level (Fig. 2D). The 90.25 mS cm^{-1} isopleth of conductance mixed to 22 m during the first 20 days of the simulation and remained at 22 m until just prior to autumn turnover. Mixed-layer conductivity increased from mid-April to autumn turnover which coincided with falling lake level. By May the conductivity of the mixed-layer was greater than the remainder of the water column which resulted in inverse chemical stratification. Sharpening of the pycnocline in April and May resulted from mixed-layer deepening without concurrent deepening of the thermocline (Fig. 4D).

Potential Hypolimnetic Heat Sources

Estimates of the sediment and geothermal heat fluxes into the hypolimnion were made to assess the relative importance of these heat sources.

In 1992 the heat content of the lower 25 m increased from 6.1×10^9 MJ to 9.6×10^9 MJ from late March to late August. During this 146 day period the measured heat content of the bottom 25 m increased linearly ($r^2 = 0.98$) at a rate of 2.5×10^7 MJ day^{-1} (0.34 MJ m^{-2} day^{-1}) (Fig. 5).

Mono Lake is located in an active geothermal region. The possibility of geothermal hot springs at depth in the lake contributing to hypolimnetic heating is plausible. The heat content gain from deep geothermal springs was calculated as, $H_{Spr}=Q\rho_{Spr}C_P\Delta T$, where H_{Spr} is the heat input from the springs (J day^{-1}), Q is the total spring discharge rate (m^3 day^{-1}), ρ_{Spr} is the spring water density($\approx$1000 kg m^{-3}), C_p is the specific heat of the spring water ($\approx$4000 J kg^{-1} °C^{-1}), and ΔT is the temperature difference between the spring water temperature and the hypolimnion temperature (°C). For 50 °C and 100 °C geothermal spring temperatures, flow rates of $\approx 1\times10^5$ and $\approx 5\times10^4$ m^3 d^{-1} would account for the measured heat increase. For the 100 °C temperature difference the amount of water required per day is impossibly high (¼ of the base stream flow rate). However, it is plausible that perhaps 1% of the heating may occur with this mechanism (i.e. $\approx$1000 m^3 day^{-1} at 50 °C). Jellison and Melack (1993) estimated from 1985 to 1987 during meromixis that the geothermal heat contributed a maximum of 2-8% of the measured heat flux across the thermocline which corroborates the 1992 estimate here.

Heat transfer from the sediments is another potential mechanism of hypolimnetic heating. An upper estimate of the sediment heat flux can be made by assuming a constant input of heat from the sediments into the hypolimnion during stratification. Calculations of sediment heat transfer with the equation, $J_{Sed}=H_{Sed}/A_{Sed}$, where J_{Sed} is the heat flux from the sediments

(J m^{-2} day^{-1}), H_{Sed} is daily heat requirement (J day^{-1}), and A_{Sed} ($7.5x10^7$ m^2) is the lake area below 25 m yields a J_{Sed} of $3.3x10^5$ J m^{-2} day^{-1}. Likens and Johnson (1969) determined a sediment heat transfer rate of $7.3x10^3$ J m^{-2} day^{-1} for two small Wisconsin Lakes. Assuming similar sediment heat transfer rates, this mechanism could provide a maximum of 2% of the heat flux into the hypolimnion. Jellison and Melack (1993) estimated the sediment heat flux to always be <5% of the observed heat flux below the thermocline. These estimates indicate the sediment and geothermal heat fluxes are minor sources of hypolimnetic heating in Mono Lake.

Simulations with Methane Bubble Plumes

The potential contribution of methane ebullition to the mixing dynamics of Mono Lake was modeled analogously to a bubble destratification system with all methane originating at one depth. Simulations of 20 and 1000 seeps released at a depth of 5 m relative to the maximum depth were done. Total methane ebullition rates of 1 (Mono Lake ebullition estimate), 3, 10, 33, 100, 330, and 1000 L s^{-1} served as inputs to the model.

Figure 5 summarizes the heat content of the bottom 25 m of the lake throughout the simulated period for the field profiles, the simulation with no bubble plumes, and the simulations of 330 and 1000 L s^{-1} methane ebullition rates with 20 bubble plumes. The rapid heat increase from October to November occurred at autumn turnover. The simulation with a methane ebullition rate of 330 L s^{-1} gave a result close to the observed rate of hypolimnetic heating (Fig.s 5 and 6B) but simulated autumn turnover a month to early (Fig. 6). The mixed-layer depth was several meters lower than the simulation with no bubbles.

A methane ebullition rate approximately 300x greater than the Mono Lake methane estimate was required to simulate the observed 1992 seasonal hypolimnetic heating. Simulations with rates closer to the estimated rates (1 L s^{-1} and 3 L s^{-1}) gave hypolimnetic heating rates almost indistinguishable from the case with no methane bubbles. This result confirms that methane bubbles do not contribute to hypolimnetic heating in Mono Lake.

The 330 day simulations often resulted in a sharp metalimnion-hypolimnion boundary that may have affected the simulated heat transfer of the bubble plume. Fourteen to thirty day simulations with initial field profiles throughout the stratified period which retained the more diffuse metalimnion-hypolimnion interface were also performed. The short term simulations agreed well with the results of the 330 day simulation and suggest that the structure at the interface does not significantly influence the results.

Discussion

In previous DYRESM applications the vertical density structure of Wellington Reservoir (Imberger and Patterson 1981) and Kootenay Lake (Patterson *et al.* 1984) were dominated by temperature and the hypolimnetic heat dynamics were dominated by inflow or outflow processes or a combination of both. In Mono Lake both temperature and salinity strongly influence the vertical density structure. Furthermore, the stream inputs overflow on the surface of the lake and do not influence hypolimnetic mixing directly by plunging below the pycnocline. While DYRESM simulated the Mono Lake mixed-layer dynamics adequately, deficiencies of the model included prediction of a sharp thermocline and a lack of hypolimnetic mixing relative to field profiles. A rate of methane ebullition 100x greater than the rates measured in Mono Lake (1-3 L s^{-1}) are required to simulate the observed hypolimnetic heating with a bubble plume algorithm (Fig. 5) and strongly supports that heat transfer from methane ebullition is insignificant.

Patterson *et al.* (1984) speculated for Kootenay Lake where a sharp pycnocline was also simulated that boundary mixing may broaden the pycnocline. The Weinstock (1981) vertical eddy diffusivity parameterization models turbulent patches within and below the pycnocline induced by wind-driven turbulent kinetic energy. Other processes may significantly increase diffusivities below the mixed-layer in Mono Lake. High wind speeds may cause upwelling and do generate large amplitude internal waves in Mono Lake (*ca.* > 4 m in the hypolimnion, *ca.* > 2 m in the metalimnion) (Romero and MacIntyre, *unpub. data*). Internal waves in Lake Alpnach, Switzerland, were shown to produce significant bottom currents and the generation of a well mixed benthic boundary layer (BBL) (Gloor *et al.* 1994). Imberger and Ivey (1993) show that the turbulent mixing in a BBL along a sloping boundary leads to an exchange flow between the boundary layer and the interior. We predict the mechanism of exchange between the BBL and the interior of the hypolimnion will be important in Mono Lake with its gently sloping sides and larger sediment area to volume ratios relative to Lake Alpnach. Although Münnich *et al.* (1992) found negligible mixing in the interior of the hypolimnion due to horizontal velocity variations induced by internal wave displacements in Lake Alpnach, the mechanism may be important in Mono Lake where internal waves lead to larger hypolimnetic volume displacements on a percentage basis, resulting in higher velocities within the interior.

The Lake Number, L_N, has been shown by Imberger and Patterson (1990) to be an indicator of mixing below the base of the mixed-layer and is defined as:

$$L_N = \frac{gS_t(1 - z_t/H)}{\rho_0 u_*^2 A_0^{1.5}(1 - z_g/H)}$$

where g is the gravitational acceleration, S_t is the lake stability, z_t the height to the center of the metalimnion, z_g is height to the center of volume of the lake, u_* is the shear velocity, and A_0 is the lake surface area. For large L_N (>>1), the bottom of pycnocline remains horizontal. For small L_N (<1), the entire pycnocline tilts with the generation of currents below the pycnocline which results in active hypolimnetic mixing. Figure 7 shows the calculated L_N for the field profiles and the simulation with no methane bubbles. There are occasions throughout the simulated stratified period where the L_N approaches 1 which suggests pycnocline tilting, the setup of internal waves, and the generation of hypolimnetic currents.

References

Asaeda, T. and J. Imberger. 1989. Behavior of bubble plumes in a linear stratification. J. Jpn. Soc. Civ. Eng. 411:55-62.

Gill, A.E.. 1982. Atmosphere-Ocean Dynamics. International Geophysics Series. Vol. 30. Academic Press, New York.

Gloor, M., A. Wüest, and M. Münnich. 1994. Benthic boundary mixing and resuspension induced by internal seiches. Hydrobiologia 284:59-68.

Imberger, J. and G.N. Ivey. 1993. Boundary mixing in stratified reservoirs. J. Fluid Mech. 248:477-491.

Imberger, J. and J.C. Patterson. 1981. A dynamic reservoir simulation model, DYRESM: 5. In: Transport Models for Inland and Coastal Waters. Ed. H. B. Fischer, pp. 310-361, Academic Press, New York.

Imberger, J. and J.C. Patterson. 1990. Physical Limnology. In: Advances in applied mechanics. Ed. T. Wu, 27:303-475, Academic Press, Boston.

Jellison, R. and J.M. Melack. 1993. Meromixis and vertical diffusivities in hypersaline Mono Lake, California. Limnol. Oceanogr. 38:1008-1019.

Likens, G.E. and N.M. Johnson. 1969. Measurement and analysis of the annual heat budget for the sediments in two Wisconsin Lakes. Limnol. Oceanogr. 14:115-135.

List, J. 1982. Turbulent jets and plumes. Annu. Rev. Fluid Mech. 14:189-212.

Mason, D.T. 1967. Limnology of Mono Lake, California. Univ. Calif. Publ. Zool. 83:1-110.

McDougall, T.J. 1978. Bubble plumes in stratified environments. J. Fluid Mech. 85:655-672.

Melack, J.M. 1983. Large, deep salt lakes: a comparative limnological analysis. Hydrobiologia 158:1-14.

Münnich, M., A. Wüest, and D.M. Imboden, 1992. Observations of the second vertical mode of the internal seiche in an alpine lake. Limnol. Oceanogr. 37:1705-1719.

Oremland, R.S., L.G. Miller, and M.J. Whiticar. 1987. Sources and flux of natural gases from Mono Lake, California. Geochim. Cosmochim. Acta 51:2915-2929.

Patterson, J.C. and J. Imberger. 1989. Simulation of bubble plume destratification systems in reservoirs. Aquatic Sciences 51:3-18.

Patterson, J.C., P.F. Hamblin, and J. Imberger. 1984. Classification and dynamic simulation of the vertical density structure of lakes. Limnol. Oceanogr. 29:845-861.

Schladow, S.G. 1992. Bubble plume dynamics in a stratified medium and the implications for lake water quality amelioration in lakes. Wat. Resour. Res. 28:313-321.

Schladow, S.G. 1993. Lake destratification by bubble-plume systems: design methodology. J. Hydr. Engr. 119:350-368.

Steinhorn, I. 1991. On the concept of evaporation from fresh and saline water bodies. Wat. Resour. Res. 27:645-648.

Vorster, P. 1985. A water balance forecast model for Mono Lake. Calif. Water Resour. Monogr. 10. U.S. Dep. Agric. Forest Serv. Region 5.

Weinstock, J. 1981. Vertical turbulence diffusivity for weak or strong stable stratification. J. Geophys. Res. 86:9925-9928.

Wüest, A., N.H. Brooks, and D.M. Imboden. 1992. Bubble plume modeling for lake restoration. Wat. Resour. Res. 28:3235-3250.

Figure 1. Bathymetry of Mono Lake with sampling stations (•) and the Paoha Island meteorological station (◆). Dashed contour is 20 m depth.

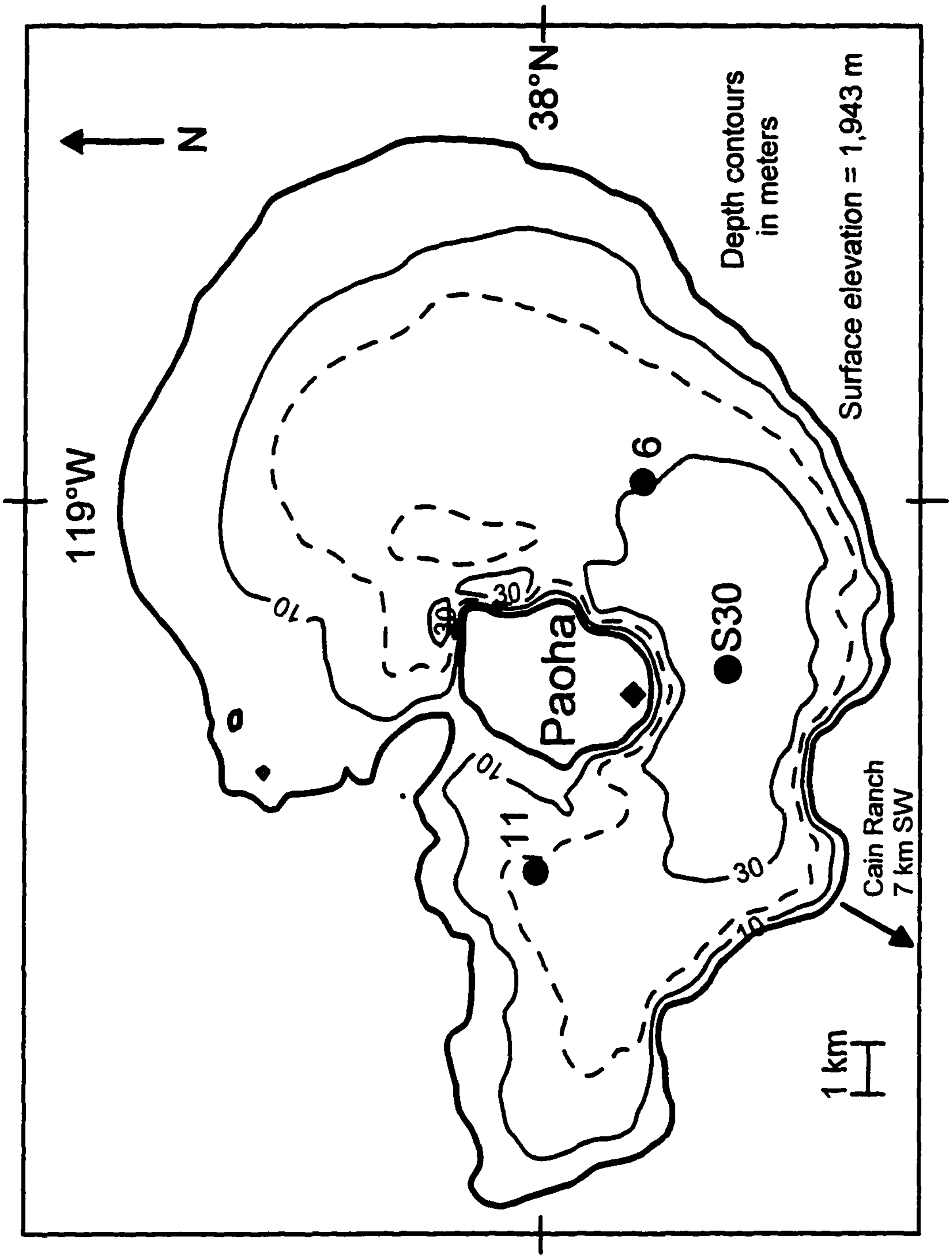
N
38°N
119°W
Depth contours
in meters
Surface elevation = 1,943 m
6
S30
Paoha
11
10
30
Cain Ranch
7 km SW
1 km

Figure 2. Simulation inputs - (A) incoming shortwave radiation (SW) and attenuation (Atten) (B) air temperature (Air T) and long wave radiation (LW) (C) wind speed (Wind) and vapor pressure (VP) (D) discharge (Dis) and lake surface elevation (Elev).

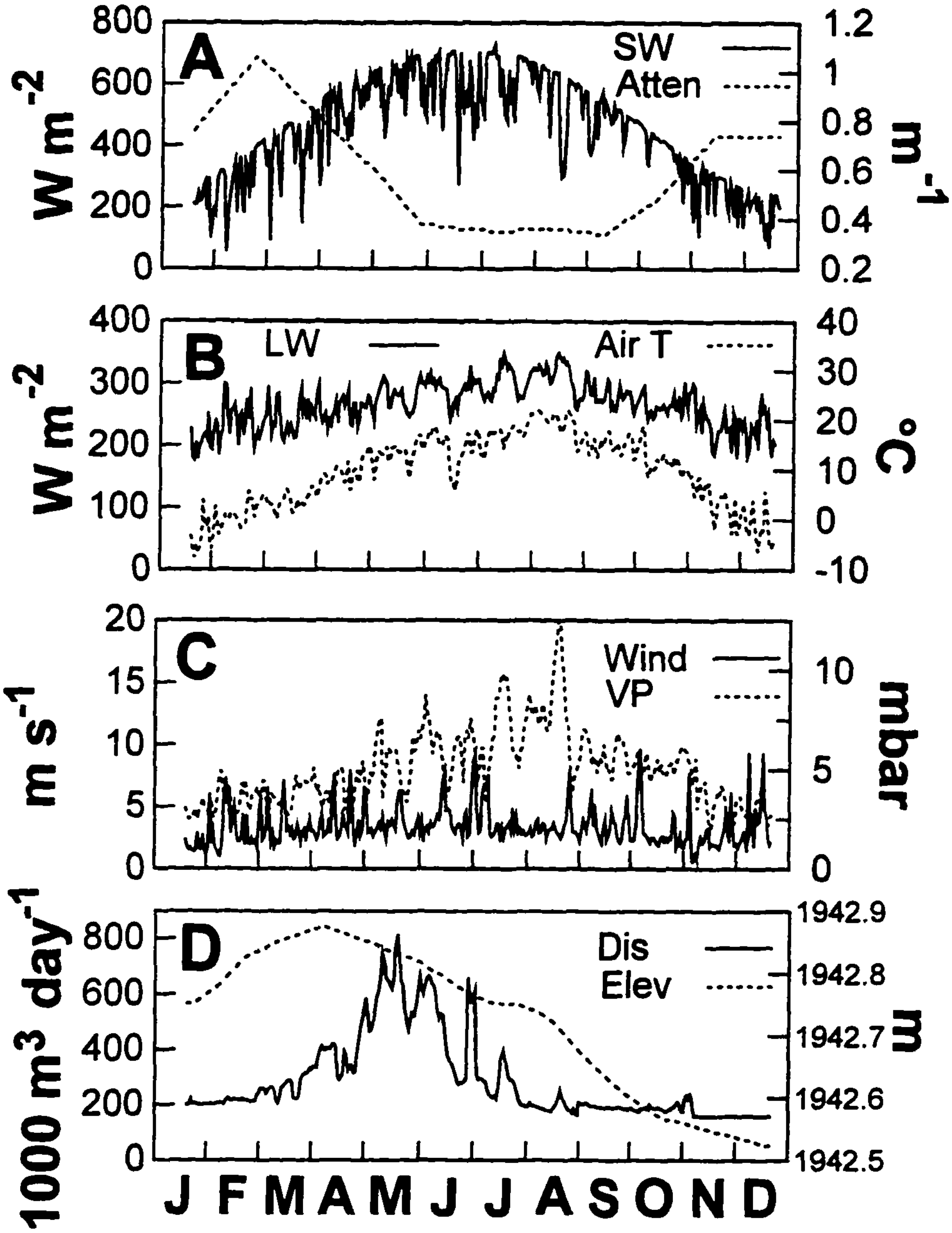
A
SW
Atten
W m-2
m-1
B
LW
Air T
°C
C
Wind
VP
m s-1
mbar
D
Dis
Elev
1000 m3 day-1
m
J F M A M J J A S O N D

Figure 3. (A) Temperature (°C) (B) temperature from 15 to 30 m and 2 to 5 °C (C) conductivity at 25 °C (mS cm^{-1}) (D) excess density [(ρ-1000) kg m^{-3}] profiles.

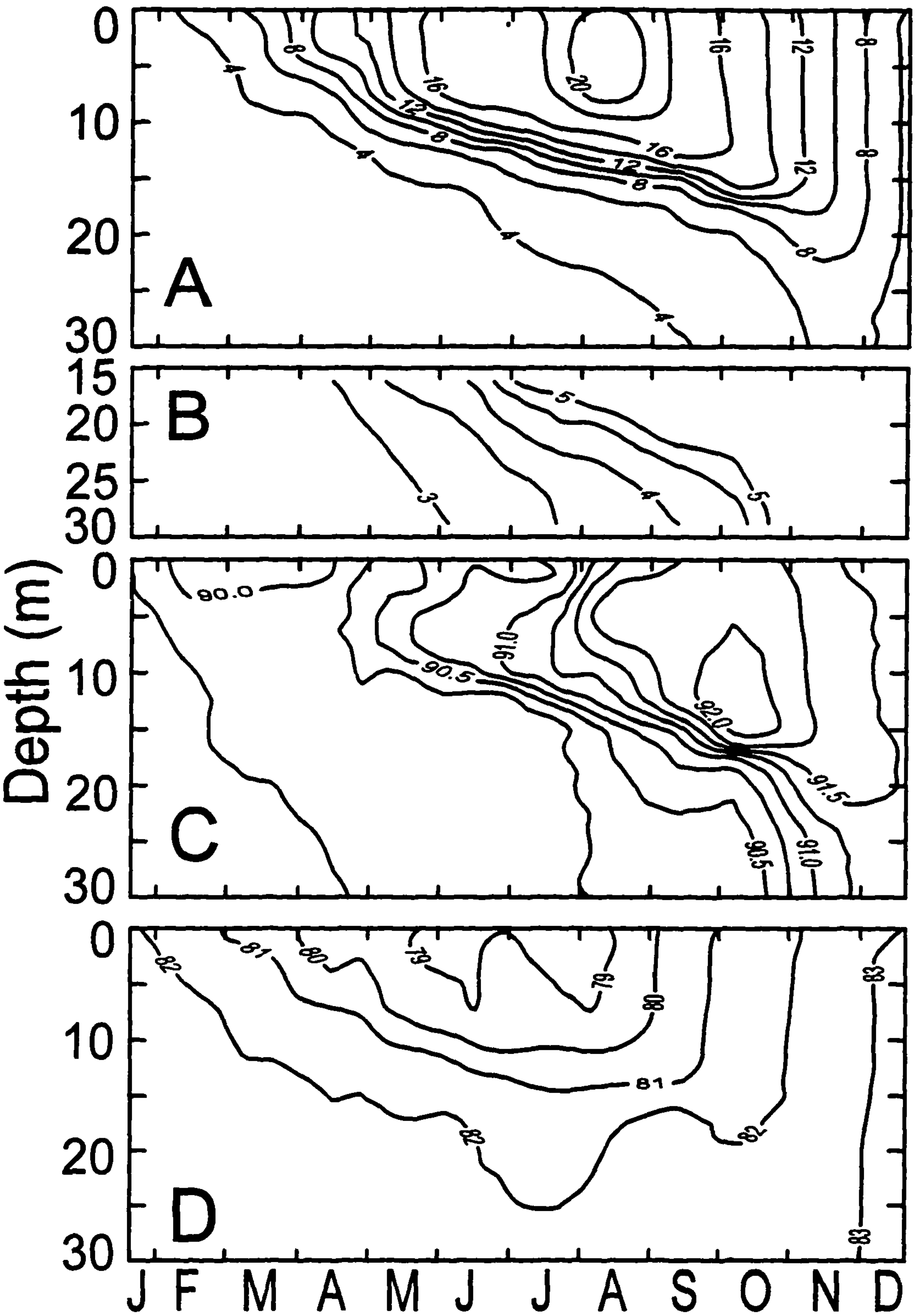

Depth (m)
A
B
C
D
0
10
20
30
15
20
25
30
4
8
12
16
20
3
5
90.0
90.5
91.0
91.5
92.0
79
80
81
82
83
J F M A M J J A S O N D

Figure 4. As fig. 3 for a DYRESM simulation without methane bubble plumes.

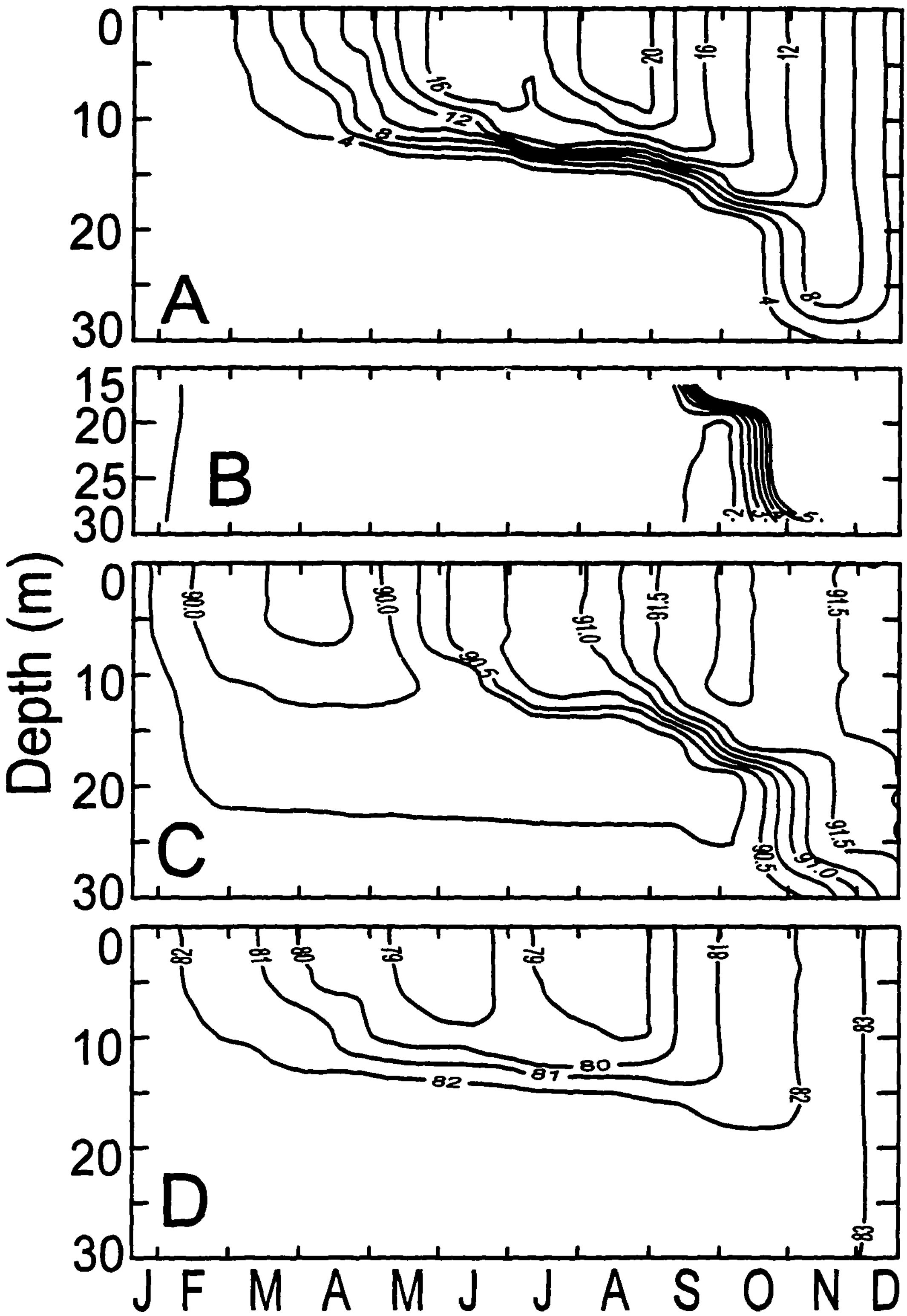
Depth (m)
A
B
C
D
J F M A M J J A S O N D

Figure 5. Heat content of the bottom 25 m for field profiles (◆), simulation with no methane bubbles (solid line), simulation with 20 seeps at 330 L s^{-1} (dashed line), and simulation with 20 seeps at 1000 L s^{-1} (dashed-dotted line).

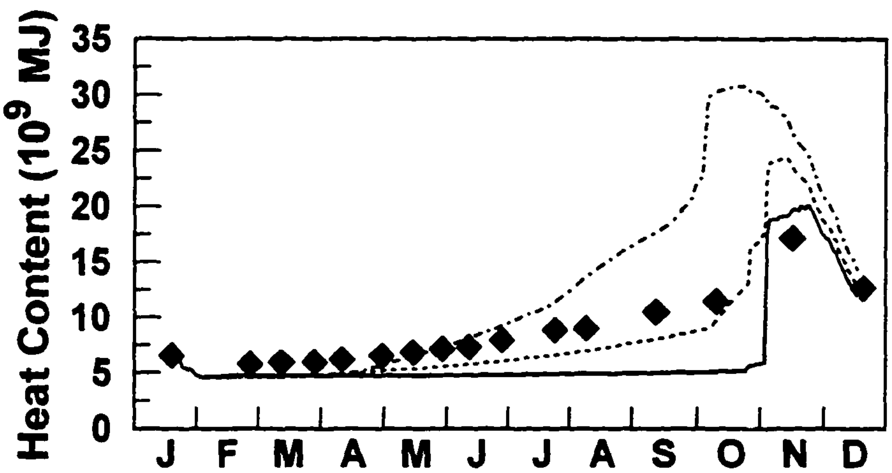
Heat Content (10^9 MJ)
35
30
25
20
15
10
5
0
J F M A M J J A S O N D

Figure 6. As fig. 3 for a DYRESM simulation of 20 plumes with a total ebullition of 330 L s^{-1}.

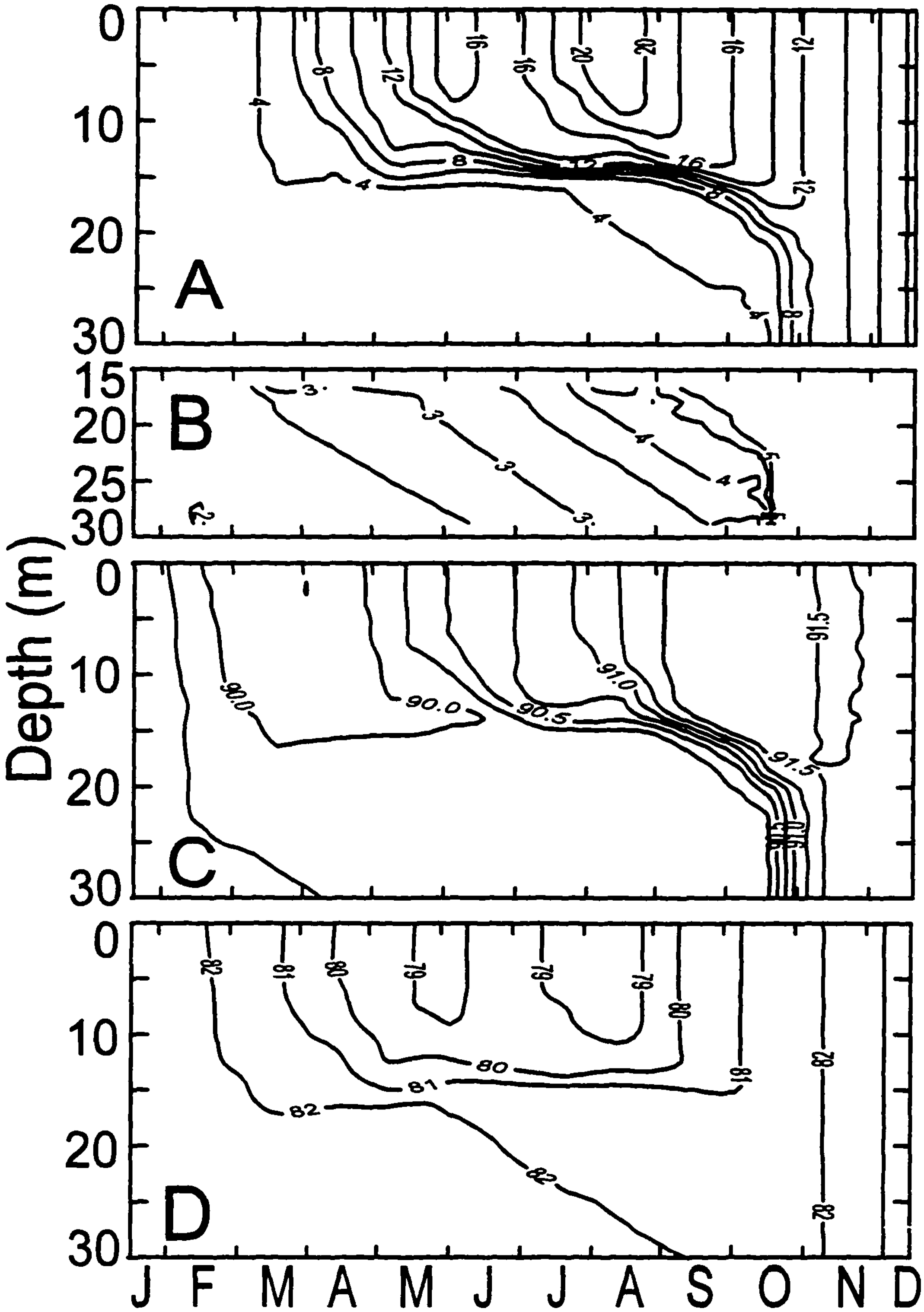
Depth (m)
A
B
C
D
J F M A M J J A S O N D

Figure 7. Daily Lake Number, L_N, for field profiles (◆) and simulation with no methane bubbles (solid line).

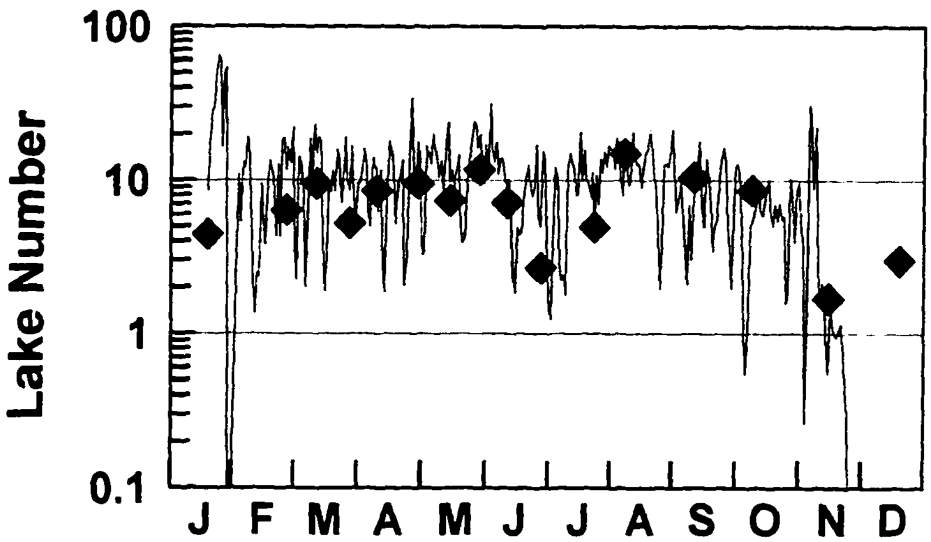

Lake Number
100
10
1
0.1
J F M A M J J A S O N D

CHAPTER 2

Sensitivity of Vertical Mixing in a Large Saline Lake to Variations in Runoff

Introduction

Meromixis is a condition of persistent chemical stratification with incomplete mixing over the course of a year, and usually results in anoxia and the accumulation of nutrients in the monimolimnion (MacIntyre and Melack 1982) and reduced vertical mixing (Jellison and Melack 1993*a*). Numerous saline lakes, worldwide, are known to be meromictic (Hammer 1986), and in the western United States there are several large (>100 km^2), saline lakes including Mono, Pyramid, Abert, Salton, Walker, and Great Salt lakes, with Mono Lake (Jellison and Melack 1993*a*) and Great Salt Lake (Lin 1976) at least known to undergo a period of meromixis. Moreover, most saline lakes lie in hydrologically closed basins where the balance between inputs of freshwater and evaporation from the lake surface determines changes in size, salinity, and ultimately the stability of the water column. Consequently, mixing in saline lakes is likely to be responsive to climatic variations.

Clusters of extreme wet and dry years have been evident in recent years for streams of the eastern slope of the Sierra Nevada (Kattelmann 1992). Five of the largest snowmelt floods (in terms of volume) since the 1920s occurred from 1978 to 1986; five of the smallest floods occurred from 1987 to 1991. These events support theories of some climatologists that extreme events are becoming more common in the western United States (Granger 1977, Michaelson *et al.* 1987).

Climatic variability along the Pacific coast of North America on an interannual scale often is associated with mid- and high-latitude variations in the polar jetstream (Roden 1989). One to three times a decade, low-latitude disturbances, i.e. El Niño-Southern Oscillation (ENSO), link to mid-latitude circulation and cause climatic anomalies such as warm and rainy periods. These periods have caused changes in the mixing regime of Mono Lake (Jellison and Melack 1993*a*), as well as in subalpine Castle Lake of the Sierra Nevada (Jassby *et al.* 1990).

Evidence for climatic variability in the Sierra and western Great Basin also indicate century to decadal drought periods in the past. Stine (1994), studying relict tree stumps in or near Mono Lake, concluded that a severe drought of 200 years duration occurred prior to AD 1112 and another of 140 years duration occurred before AD 1350, and suggested that the severe droughts were caused by a reorientation of the mid-latitude storm tracks. Temperature and precipitation in the southern Sierra based on tree-ring reconstruction (Graumlich 1993) corroborates Stine's 140-year drought prior to AD 1350, but not the 200-year drought prior to AD 1112.

The primary emphasis of this study is to determine the sensitivity of the interannual vertical mixing dynamics of Mono Lake to variations in runoff for several climate change scenarios. The past 50 years of stream discharge and precipitation for the period 1940 to 1990 served as the hydrological inputs to a model of vertical mixing. We assumed no diversion of incoming streams. The period 1940 to 1990 encompasses an anomalously wet period during the past 1000 years (Graumlich 1993), so simulations with 12.5% and 25% reductions in runoff and precipitation were run to assess a drier climate. To assess the recent trend of higher interannual variability of streamflow (Kattelmann 1992) and precipitation (Michaelson *et al.* 1987, Granger 1977) on the frequency of meromixis, simulations were performed with 12.5% and 25% reductions in freshwater inputs in the moderately wet to dry years and with no reductions in eight of the largest runoff years. The same meteorological year was used for each year of the simulation so that interannual differences in the extent of vertical mixing resulted from variations in lake level, salinity, and freshwater inputs.

Simulations with the one-dimensional vertical mixing model, DYRESM (Imberger and Patterson 1981), were used to assess the incidence of meromixis. During model verification, DYRESM did not predict the timing of turnover for one of two monomictic years. The Lake Number (Imberger and Patterson 1990), an index of mixing below the mixed-layer, was incorporated into the parameterization of the vertical diffusivity to increase the vertical transport in the thermocline and hypolimnion. The modified diffusivity parameterization modeled the timing of turnover for the two year monomictic verification period and a nine year period which included a six year meromictic period from 1983 to 1988. The model was then run with the fifty year hydrological inputs to assess the interannual vertical mixing dynamics.

Study Site

Mono Lake lies in a hydrologically closed basin with an area of 1800 km^2 located on the western edge of the North American Great Basin just east of the Sierra Nevada, California (38°N, 119°W) (Fig. 1). At an elevation of 1943 m above sea level Mono Lake has a 160 km^2 surface area, a 17 m mean depth, a 45 m maximum depth, and salinity of *ca.* 94 g L^{-1}. The lake was monomictic when it was studied in the early 1960s (Mason 1967) and late 1970s through early 1980s (Melack 1983). Diversion of freshwater inflow from Mono Lake began in 1941 with the extension of the Los Angeles Aqueduct into the Mono Basin. By 1982 the lake's surface elevation had dropped 14 m and the salinity had doubled. During 1982 and 1983, the lake's surface rose 2.6 m accompanying an ENSO event which resulted in the initiation of meromixis. Meromixis persisted until 1988 and was characterized by a marked decrease in vertical mixing (Jellison and Melack 1993*a*) and nutrient transport across the pycnocline (Jellison *et al.* 1993) which resulted in diminished algal productivity (Jellison and Melack 1993*b*).

Most of the precipitation in the Mono Basin is derived from Pacific storms and orographic lifting over the Sierra Nevada (Houghton 1969). Approximately 75% of the annual precipitation onto the lake surface occurs between October and March (Vorster 1985). Most of the precipitation in the Mono Basin falls in the high elevations of the Sierra Nevada as snow (Patten *et al.* 1987). Stream discharge is the major hydrologic input into Mono Lake and is derived largely from snowmelt in the spring and summer (Patten *et al.* 1987).

Model Application

Vertical Mixing Model

DYRESM (Imberger and Patterson 1981), a one-dimensional vertical mixing model, was used to simulate the vertical mixing dynamics of Mono Lake. DYRESM is based on a Lagrangian structure which models the lake as horizontal layers of uniform properties (i.e. temperature and salinity). The layers move vertically, expanding and contracting in response to surface mass fluxes and mixing processes. The model explicitly simulates mixing mechanisms in stratified lakes and reservoirs. Processes causing deepening of the mixed-layer include penetrative convection from surface cooling and evaporative concentration of salt at the surface, stirring by the wind, seiche induced shear at the pycnocline, and billowing at the pycnocline resulting from shear. Hypolimnetic transport is modeled as a diffusive process whose magnitude depends on the local density gradient and rate of energy dissipation (Weinstock 1981). The model has been successfully applied to reservoirs (Imberger and Patterson 1981) and freshwater lakes (Patterson *et al.* 1984).

Physical Properties of Mono Lake Water

The equation for density of Mono Lake water, based on temperature and conductivity corrected to 25°C (Jellison and Melack 1993*a*), is valid for the range 74 (69.5 g kg^{-1}) to 92 mS cm^{-1} (95 g kg^{-1}). As the salinity range of the simulations reported here range from 40 to 95 g kg^{-1}, we modified the density equation to be a linear function of salinity (g kg^{-1}). Salinity, as total dissolved solids (*TDS*), over the range of conductivities from 74 to 92 mS cm^{-1} at 25°C is given by,

$$TDS\ (\mathrm{g\ L^{-1}}) = (1.421 \times C_{25}) - 35.64 \qquad n=22,\ r^2=0.978,\ SE=1.23\ \mathrm{g\ L^{-1}}$$

(Jellison and Melack 1993*a*). A linear regression between specific gravity and salinity measurements from 55 to 270 g kg^{-1} (r^2=0.99, n=11 Los Angeles Department of Water and Power, LADWP, *unpub. data*) when combined with the temperature-density equation (Jellison and Melack 1993*a*) resulted in the density equation:

$$\rho = 993.6 + 0.927\,S - 2.164 \times 10^{-1}\,T - 3.26 \times 10^{-3}\,T^2$$

where ρ is density (kg m^{-3}), T is temperature (°C), and S is salinity (g kg^{-1}).

A latent heat of evaporation of 2.477×10^6 J kg^{-1} for Mono Lake water was estimated from linear interpolation between the values of seawater (S=35 g kg^{-1}) (Gill 1982) and the Dead Sea (S=275 g kg^{-1}) (Steinhorn 1991). A kinematic viscosity of 1.27×10^{-6} m^2 s^{-1} and specific heat of 3.865 J kg^{-1} °C^{-1} were obtained from Mason (1967). Salinity-induced variations for these parameters are small (<10%) over the range considered here so that constant values were used in the simulations.

Verification Data and Simulation Inputs

Hourly averaged measurements of shortwave and longwave radiation were recorded at a meteorological station located 7 km southwest of the lake. Ten minute averages of readings made every second for wind speed, relative humidity, and air temperature were measured at a meteorological station on the southern tip of Paoha Island in the center of the lake (Fig. 1). Relevant meteorological measurements were standardized to 10 m and computed as daily averages with the exception of radiation data which are required as daily totals in DYRESM. Examples of these data are shown for January 1, 1992 through December 31, 1993 in Figures 2A-C. Downwelling photosynthetically available radiation (PAR) was measured with a submersible Li-Cor quantum sensor. Attenuation coefficients ranged from 0.35 to 1.1 m^{-1}. Daily values were estimated by interpolating between dates of field surveys (Fig. 2A). A surface reflectivity of 5% for incoming shortwave radiation was used in the simulations. PAR was computed as 45% of the incoming shortwave radiation. Attenuations at other wavelengths are reported in Jellison and Melack (1993*a*).

Lake surface elevations were recorded weekly to monthly from staff gauges by the LADWP (Fig. 2D and 3). Daily lake elevations were computed by interpolation between dates of measured surface elevations. Daily total discharge of four major streams was measured by the LADWP (Fig. 2D). Stream gauges are approximately 5 km upstream from the lake and there is uncertainty in the amount of water loss between the weirs and the lake (Vorster 1985). Rather than estimating these hydrologic terms, we used the volume of water derived from changes in lake level as the major hydrological input for the verification simulations. Temperatures of Convict Creek for 1992 (not shown), at the Sierra Nevada Aquatic Research Laboratory located 45 km from Mono Lake at an elevation of 2160 m, served as stream temperature inputs.

Water temperature and conductivity profiles were obtained bi-weekly in 1992 and 1993 from March to August at three sampling locations (Fig. 1) and monthly during the remainder of the year with a Sea-Bird Seacat SBE-19. Temperature measurements had a vertical resolution of 0.125 m and accuracy of 0.005°C, and conductivity measurements had a vertical resolution of 1 m and accuracy of 0.25 mS cm^{-1} after data processing.

With a few exceptions, temperature profiles were measured at three stations (Fig. 1) biweekly from March to August and monthly during the remainder of the year from 1982 to 1990. October through February were not sampled from 1982 to 1984 and station 30 was not sampled in 1982. Readings were taken every meter with a thermistor and Wheatstone bridge circuit readable to 0.01 °C. The conductivity of monthly samples at 5 depths (2, 8, 12, 20, and 28 m) from two stations (6 and 11) collected with a van Dorn sampler were measured in the laboratory with a conductivity meter (Yellow Springs, Model 30) between 24 and 26 °C and standardized to 25 °C. An additional 2 to 5 depths were sampled across major gradients dependent on the previous temperature and conductivity profiles. The accuracy of conductivity measurements was ± 1 mS cm^{-1}. Conductivity was not measured in 1982.

1940 to 1990 Simulation Inputs

Total annual precipitation (Fig. 4A) and basin runoff (Fig. 4B) based on the water year (October 1 to September 30) had substantial interannual variability from 1940 to 1990. The average precipitation over the fifty year period was 28.0 cm yr^{-1} (S.D.=10.4 cm yr^{-1}) and the average runoff 150 Mm^3 yr^{-1} (S.D.=49.2 Mm^3 yr^{-1}). Lake level fluctuations are predominately a function of runoff and evaporation, as the fifty year average of precipitation is approximately a fourth of the annual evaporation rate (*ca.* 1.0 m yr^{-1}). Eight of the years with highest runoff (from highest to lowest: 1983, 1969, 1982, 1967, 1986, 1952, 1941, 1984) all had total annual discharge greater than 206 Mm^3 yr^{-1} and accounted for approximately 25% of the total discharge over the fifty year period. Significant multiple year drought events with annual total discharge less than 120 Mm^3 yr^{-1} occurred from 1947 to 1950, 1953 to 1954, 1959 to 1961, 1976 to 1977, and 1987 to 1990. The variability in runoff and precipitation was much greater for the last fifteen years (1976 to 1990) and corroborates Kattelmann's (1992) finding of increased interannual runoff variability in the eastern Sierra for this period.

The Los Angeles Aqueduct Model (LAAMP) is a monthly water balance model of the Mono Lake basin. LAAMP utilizes the fifty year historical record of the monthly totals of precipitation from a site 7 km southwest of the lake and Mono basin runoff from April 1, 1940 to March 30, 1990. LAAMP generated a fifty year sequence of monthly elevations (Fig. 4C) assuming no diversion of Mono Basin water. The quantity of ungauged and groundwater inflow into the lake is dependent on the monthly evaporation rate specified in LAAMP. Monthly total evaporation rates from the 1992 DYRESM simulation were used in LAAMP to determine the ungauged streamflow and groundwater. The LAAMP stream discharge to the lake for the case with no diversions (Fig. 4D) and precipitation onto the lake surface were used as the hydrological inputs for the long-term simulations.

One hundred year simulations were run for five hydrological scenarios (Table 1). Precipitation and LAAMP runoff served as inputs for the first and second fifty years of the simulation. The second fifty years of the simulation were done to evaluate the incidence of meromixis for an additional range of elevations. Case 1 had no reductions in freshwater inputs. A linear regression between annual precipitation and runoff (based on the water year) explained 68% of the variance so we applied reductions to both precipitation and runoff in cases 2 to 5. Cases 2 and 3 had constant reductions in precipitation and runoff inputs of 12.5% and 25% for all years, and simulated drier climates than the past fifty years. Cases 4 and 5 were the same as cases 2 and 3, except the eight years with the largest runoff had no reductions in freshwater inputs. Cases 4 and 5 simulated a drier climate with higher interannual runoff variability than the period from 1940 to 1990.

We assume that freshwater inputs are the primary determinant of meromixis in Mono Lake so we used the 1992 daily meteorology and underwater extinction coefficients of PAR for every year of the one hundred year simulations. The 1982 to 1990 verification simulation which includes a six year meromictic event supports this assumption and is discussed below.

We compared equilibrium lake level predictions (z_{eq}, level at which inflow of water equals loss from evaporation) of cases 2 and 3 to z_{eq}

predictions of two other Mono Lake water balance models (Table 2) as a verification of lake level modeling. Direct comparisons between our z_{eq} predictions and those of the other two models cannot be made for several reasons. Our z_{eq} predictions were based on a reduction of precipitation onto the lake surface whereas the other models did not. Secondly, results from the other two water balance models utilized synthetic streamflow inputs generated from a forty year runoff and precipitation record, whereas our predictions were based on the recent fifty year historical precipitation and runoff record. However, even with the differences in lake level modeling inputs, our z_{eq} predictions as a function of runoff are bracketed by the Vorster (1985) model.

Model Verification

To test the applicability of using DYRESM in a lake with combined thermal and salinity stratification, model verification was done with data from 1992 and 1993, both monomictic years. These initial tests were done without modification of the mixing parameterizations in the published version of DYRESM (Imberger and Patterson 1990). As will be seen below, these parameterizations did not adequately predict the mixing dynamics of 1993. In consequence, we made a simple modification to the vertical diffusivity parameterization by incorporating the Lake Number (Imberger and Patterson 1990), a dimensionless index of mixing below the mixed-layer. Results from the two approaches follow.

1992 and 1993 Field Profiles and Simulations

Mono Lake was monomictic during 1992 and 1993 (Figs. 5A and 5B). The onset of thermal stratification during late February to early March coincided with increases in solar irradiance and high underwater attenuation for both years (Fig. 2A). By the end of May, 1992, and June, 1993, the structure and gradient of the seasonal thermocline was established (Fig. 5A). From May to October, the mixed-layer deepened two times more rapidly in 1992 than in 1993.

During February and March, 1992, a steady lake level increase (*ca.* 0.15 m) resulted in the dilution of the mixed-layer (92.5 g kg^{-1} isohaline, Fig. 5B). From April to December the lake level decreased as evaporation from the lake surface exceeded hydrologic inputs. By late April falling lake levels and increasing evaporation resulted in inverse chemical stratification; the average mixed-layer salinity was greater than the average hypolimnetic salinity. Autumn turnover in November, 1992, resulted from a combination of lake cooling and unstable chemical stratification.

From January to April, 1993 the lake level increased 0.4 m, the increases led to the establishment of a seasonal chemocline by March (Fig. 5B). The chemocline deepened to 15 m by May and persisted through the remainder of stratification. Two freshening periods above the seasonal chemocline were induced by high precipitation onto the lake surface and low evaporation rates (January to March) and high stream discharge (June to

August). Strong winds in November and December (Fig. 2C) caused autumn turnover by December 5.

A 2 to 3 kg m^{-3} density difference between the mixed-layer and the hypolimnion persisted throughout much of the stratified period during 1992. During July, temperature contributed 2.3 kg m^{-3} to the density difference across the pycnocline (15 to 7 °C) whereas inverse salinity stratification reduced the density difference 0.7 kg m^{-3}. During 1993, there was a 3 to 6 kg m^{-3} density difference between the mixed-layer and the hypolimnion through the stratified period. During July, temperature contributed 2.5 kg m^{-3} and stable salinity stratification contributed 2 kg m^{-3} to the density difference between the mixed-layer and hypolimnion.

DYRESM simulated the 1992 and 1993 seasonal mixed-layer thermal dynamics well in several respects (Fig. 5C). The onset of thermal stratification, mixed-layer deepening, and timing of autumn turnover matched the field data. However, the simulation of 1993 did not predict isothermal conditions by the end of the simulation and the thermocline was too sharp in both 1992 and 1993. Simulated diffusivities through the thermocline and hypolimnion were near the molecular diffusivities of heat and salt throughout the stratified period during both years.

Predictions of the seasonal dynamics of salinity within the mixed-layer were adequate in 1992 but not in 1993 (Fig. 5D). The simulated dilution of the upper 10 m from February to April, 1992 (93 g kg^{-1} isohaline) was caused by rising lake level (Fig. 2D). Mixed-layer salinity increased from mid-April to autumn. By May the salinity of the mixed-layer was greater than the remainder of the water column which resulted in inverse chemical stratification through turnover. The simulation of 1993 incorrectly predicted the development of a strong chemocline in spring which ultimately led to the prediction of meromixis. In consequence, the published version of the model could not be used to predict the onset and duration of meromixis, precisely the goal here.

Modifications to DYRESM to Improve Simulations of Hypolimnetic Mixing

Insufficient mixing below the mixed-layer was modeled during the setup of salinity stratification during February, 1993. We hypothesize that the eddy diffusivity parameterization underestimates mixing below the mixed-layer and advance a simple modification. DYRESM calculates the eddy diffusivity, K_Z, using Weinstock's (1981) formulation given by:

$$K_z = \alpha \frac{\varepsilon}{N^2 + 0.6 k_0^2 u^2}$$

where ε is the dissipation of turbulent kinetic energy, k_0 is the wave number of the energy bearing eddies, u is the root mean square velocity of the motion in the turbulent patch, N is the buoyancy frequency, and α is a constant whose value lies between 0.2 and 0.8. We used a value of 0.5. The Weinstock (1981) vertical eddy diffusivity parameterization models turbulent patches within and below the pycnocline induced by wind-driven turbulent kinetic energy.

Other processes may significantly increase diffusivities below the mixed-layer in Mono Lake. High wind speeds may cause upwelling and do generate large amplitude internal waves in Mono Lake (*ca.* > 5 m) (Romero and MacIntyre, *unpub. data*). Internal waves in Lake Alpanch, Switzerland, were shown to produce significant bottom currents and the generation of a well mixed benthic boundary layer (BBL) (Gloor *et al.* 1994). Imberger and Ivey (1993) show that the turbulent mixing in a BBL along a sloping boundary leads to an exchange flow between the boundary layer and the interior. We predict the mechanism of exchange between the BBL and the interior of the hypolimnion will be important in Mono Lake with its gently sloping sides and larger sediment area to volume ratios relative to Lake Alpanch. Although, Munnich *et al.* (1992) found negligible mixing in the interior of the hypolimnion due to horizontal velocity variations induced by internal wave displacements in Lake Alpanch, the mechanism may be important in Mono Lake where internal waves lead to larger hypolimnetic volume displacements on a percentage basis, resulting in higher velocities within the interior.

The Lake Number, L_N is an excellent indicator of mixing below the base of the mixed-layer and is defined as:

$$L_N = \frac{g S_t (1 - z_t/H)}{\rho_0 u_*^2 A_0^{1.5} (1 - z_g/H)}$$

where g is the gravitational acceleration, S_t is the lake stability, z_t the height to the center of the metalimnion, ρ_0 is the reference density, z_g is height to the center of volume of the lake, H is the lake depth, u_* is the shear velocity, and A_0 is the lake surface area (Imberger and Patterson 1990). L_N is a balance between the overturning moment which arises from wind acting over the lake's surface counterbalanced by the restoring moment of the density stratification. For large L_N (>>1), the bottom of the pycnocline remains horizontal. For small L_N (<1), the entire pycnocline tilts resulting in the generation of currents below the pycnocline and active hypolimnetic mixing.

We modeled the equation for K_z by making α a function of L_N: $\alpha = 0.5 a L_N^{-b}$ where a and b are constants. With a power functional dependence on L_N, we assume that as L_N approaches 1 the dissipation of turbulent kinetic energy increases more rapidly. We ran several simulations using these parameterization and varying values of a and b. The best results for the 1992 and 1993 simulation were obtained using a=10 and b=-0.8. During simulations a minimum α of 0.5 (L_N > 15) and maximum α of 5.0 (L_N < 1) were imposed.

The modified diffusivity parameterization resulted in an improved simulation of the structure of both the thermocline and chemocline, hypolimnetic heat dynamics and timing of turnover for 1993 (Fig. 6). Although there were some problems with the new simulations, such as a deeper mixed-layer and premature turnover in 1992, the revised model gave much better predictions of water column structure and turnover in 1993. We next tested its ability to predict meromixis.

Further Model Validation: 1982 to 1990 Field Profiles and Simulations

Further model verification for an additional nine year period, 1982 to 1990, which includes a six year period of meromixis was performed with the modified diffusivity parameterization. Prior to 1983, Mono Lake had declining lake levels, increasing salinity, and a monomictic thermal regime. From the autumn of 1982 to the summer of 1983, a large influx of freshwater from an abnormally high Sierran snowpack resulted in a 2.6 m lake elevation increase (Fig. 3). Freshwater dilution of the mixed-layer salinity during winter and spring of 1983 led to the onset of meromixis (Fig. 7A). A salinity difference of approximately 10 g kg^{-1} between the mixolimnion and the monimolimnion was measured in the spring and summer of 1983. Evaporative concentration of the mixed-layer, reduced inflows, and mixed-layer entrainment reduced the salinity difference to about 4 g kg^{-1} by the 1985-6 winter. In 1986, another large influx of freshwater caused a lake level rise of 0.7 m (Fig. 3) and the establishment of a secondary chemocline above the original one. Chemical stratification weakened from 1986 to 1988 with the complete breakdown of meromixis occurring in November 1988 (Jellison and Melack 1993*a*).

The meromictic event of the 1980s was simulated to determine if DYRESM predicted the vertical mixing dynamics adequately with the modified diffusivity formulation determined from the 1992 to 1993 simulation. Meteorological data and PAR extinction coefficients from 1992 were used for each year of the simulation. The salinity dynamics, downward migration of the chemocline and termination of meromixis were predicted accurately (Fig. 7B). The simulation shows that multi-year meromictic events in Mono Lake are predominately a function of the freshwater inputs.

Results

Lake levels, as will be seen below, strongly influence whether Mono Lake will become meromictic. Modeled lake level fluctuations (Fig. 8) were significantly different for each case. Case 1 inputs resulted in rapid long-term lake level increases of 10 m during the first fifty years, 5 m during the second fifty years and high lake levels by the end of the simulation. Cases 2 and 4 had long-term lake level increases of 5 and 6 m during the first fifty years and 2 and 2.5 m during the second fifty years. Case 3 was at a z_{eq} of approximately 46 m throughout the simulation. Case 5 had lake level rises of 3 and 0.5 m for the two fifty year periods. Except for case 3, all cases had smaller annual lake level increases during the second fifty years due to higher lake levels and larger surface areas. Cases 4 and 5 had significantly greater annual lake level increases for each of the eight years with no reductions in freshwater inputs than did cases 2 and 3, respectively.

An example of output from a simulation is given for case 1 in figure 9, which is a plot of two week averages of the mixed-layer salinity and salinity at 15 m relative to the maximum depth. The mixed-layer salinity was defined as the depth from the surface to a density gradient of 0.25 kg m^{-3} m^{-1}. Because the volume of water in the bottom 15 m is only 2.9% of the total volume when z_{max}=45 m and only 1.3% of the total volume when z_{max}=60 m, we assumed meromixis was terminated once the mixed-layer was within 15 m of the maximum depth. Two meromictic periods of approximately twenty years were predicted. Meromixis during simulation years 1 to 21 resulted from a large average lake level rise of 0.25 m yr^{-1} over the twenty year period. The initial lake level was well below z_{eq} of case 1 (> 60 m) so that even moderate runoff years caused lake level increases which prolonged meromixis. The twenty-one year meromictic episode from years 38 to 58 was initiated by a rapid lake level increase of 0.6 m yr^{-1} from years 38 to 43. Meromixis from years 1 to 20 was maintained by long-term lake level rise over the twenty year period, whereas for years 38 to 58 meromixis was maintained and prolonged by an abrupt lake level increase of *ca.* 3 m from years 42 to 46. By year 92 the lake level was so high (z_{max}>58 m) that only a seven year period of meromixis resulted, one third the duration of the event initiated on year 38.

A summary of predicted meromictic periods of all the cases is given in figure 10. The stability during meromictic years were classified as strong if the annual minimum difference between the mixed-layer salinity and salinity at 15 m relative to the maximum depth was greater than 4 g kg^{-1}. Meromictic events with annual minimum salinity differences between 2 and 4 g kg^{-1} were classified as moderately stable, and meromictic years with salinity differences less than 2 g kg^{-1} were classified as weakly stable.

Greater inputs of freshwater led to a greater frequency and duration of meromictic events. Whereas the case 1 simulation predicted twenty years of meromixis during the first twenty-one years, case 2 predicted only a six year event and no event was predicted for case 3. Cases 1, 2, and 3 all had multi-year meromictic events for the cluster of wet years (water years 1982, 1983, 1984 and 1986) from years 42 to 47 and 92 to 96, but the period of meromixis became shorter as freshwater inputs decreased. As the lake level increased, the stability associated with the meromictic events lessened. For example, meromixis from years 92 to 97 in case 2 was not as strong as the event from years 42 to 47 at a lake level 3 m higher.

Comparison of case 4 with case 2 and case 5 with case 3 provide insight into the effects of greater interannual variability of freshwater inputs on persistence of meromixis and the strength of associated stability. For example, the stability of meromixis was greater in years 1 to 8 and the meromixis period which began in year 42 persisted longer in case 4 than in case 2. Similarly, meromictic events were more frequent and lasted longer in case 5 than case 3.

Discussion

Exceptionally wet years consistently initiated meromixis. For instance, meromixis was initiated when inflows were high such as water year 1969 (simulation years 29 and 79) and sequential large water years 1982 and 1983 (simulation years 42, 43, 92 and 93). Further, if lake levels are well below the equilibrium lake level of the regional climate, moderately wet years could initiate meromixis as in cases 1, 2, and 4 on simulation year 1.

High lake levels decreased the stability and duration of meromixis. For example, cases 1, 4, and 5 had approximately equivalent inputs of freshwater from years 92 to 96 with lake levels on year 92 of 58 (case 1), 52.5 (case 4) and 46 m (case 5). Case 1 predicted a shorter duration of meromixis with lower stability than the other two cases. Smaller lake level rises and less dilution of the mixolimnion result from a constant input of freshwater at higher lake levels than at lower lake levels. Further, high salinities at lower lake levels result in greater salinity differences between the mixolimnion and monimolimnion during the onset of meromixis as the volume of the mixolimnion at low lake levels is less than the volume at higher lake levels.

A higher frequency and duration of meromixis was simulated when the eight wettest years had no reductions in freshwater inputs (cases 4 and 5 vs cases 2 and 3). These results suggest that if climate change results in a drier climate with high interannual hydrological variability (cases 4 and 5), the occurrence of meromixis in saline lakes will increase. For example, in a small saline lake in Victoria, Australia, meromixis was established when lake shrinkage and solute concentration during a prolonged drought was followed by flooding with freshwater during abnormally high rains (Timms 1972).

Generally, meromixis results in increased chemical stability (MacIntyre and Melack 1982) and significantly lower eddy diffusivities across the chemocline (Jellison and Melack, 1993*a*) relative to monomictic conditions. With the elimination of seasonal holomixis, mixolimnetic nutrient concentrations are depleted and accumulate in the monimolimnion (MacIntyre and Melack 1982, Jellison *et al.* 1993). During the breakdown of meromixis a large nutrient pulse results as the nutrient-rich monimolimnetic water is mixed throughout the water column.

During meromixis, prolonged periods of low mixolimnetic nutrient concentrations will likely lead to changes in algal biomass, primary productivity, and the composition of algal communities. In N-limited Pyramid Lake, during high runoff years the set up of temporary winter chemical stratification or meromixis led to a N-limiting condition and N-fixing blue-green algae blooms (Galat *et al.* 1990). In Mono Lake, algal biomass in spring and autumn decreased following the onset of meromixis, and annual photosynthetic production was reduced compared to monomictic conditions (Jellison and Melack 1993*b*). Annual production was greatest in 1988 following the breakdown of meromixis. In summary, greater interannual variability in vertical mixing, mixolimnetic and monimolimnetic nutrient concentrations, algal biomass, and algal production is predicted with a higher incidence of meromixis.

Present regional hydrology models predict a more strongly seasonal streamflow hydrology regime with characteristics of increased peak runoff, earlier snowmelt and lower base flows (Lettenmaier and Gan 1990, Cooley 1990, Pupacko 1993). If winter peak discharge increases substantially as a result of earlier and more rapid snowmelt, the likelihood of the development of a stronger and earlier winter seasonal chemocline during monomictic years will increase.

An earlier onset of stratification will likely affect productivity at several trophic levels. In many temperate lakes, nutrient limitation increases and becomes pronounced following the onset of seasonal thermal stratification as nutrients are exported across the thermocline via particle settling. In Lake Tahoe, differences in the spring mixing depth, and presumably its effect on nutrient fluxes, explain much of the interannual variation in primary production (Goldman *et al.* 1989). Temporary winter chemical stratification resulted in N-limiting conditions and the occurrence of N-fixing algal blooms in Pyramid Lake (Galat *et al.* 1990). Early onset of thermal stratification in N-limited Mono Lake is also expected to shift the seasonal pattern of nutrient availability and thus primary production. Temporal changes in primary production will affect *Artemia*, the only macrozooplankton in Mono Lake. *Artemia* are absent during the winter but following hatching of over-wintering cysts in March reach high densities and support large populations of breeding and migratory birds throughout much of the remainder of the year. Thus, several direct and indirect effects of temporal changes in stratification are expected.

Other climatic changes that directly affect the lake need to be investigated. Changes in the wind, temperature and vapor pressure regimes would effect evaporation rates and lake levels. Hostetler and Benson (1990) simulated evaporation and lake levels to investigate the paleoclimate of Lake Lahontan and found that increased cloud cover in conjunction with increased precipitation could account for the water budget of the Pleistocene lake. Mixed-layer deepening would be effected by changes in the wind regime as well. The use of lake-basin scale hydrological models coupled with regional climate models produced reasonably good predictions of surface temperature and evaporation for Pyramid Lake (Hostetler and Giorgi 1993). Synthetic streamflow and climate changes derived from coupled hydrological and regional climate models for the Mono Basin should be incorporated as hydrological and meteorological inputs to the lake model to improve prediction of vertical mixing regimes for climate change scenarios.

References

Cooley, K.R. 1990. Effects of CO_2-induced climatic changes on snowpack and streamflow. Hydrol. Sci. J. 35:511-522.

Galat, D.L., J.P. Verdin, and L.L. Simis. 1990. Large-scale patterns of *Nodularia spumigena* blooms in Pyramid lake, Nevada, determined from Landsat imagery: 1972-1986. Hydrobiologia 197:147-164.

Gill, A.E. 1982. Atmosphere-Ocean Dynamics. International Geophysics Series. Vol. 30, Academic Press, New York.

Gloor, M., A. Wüest, and M. Münnich. 1994. Benthic boundary mixing and resuspension by internal seiches. Hydrobiologia 284:59-68.

Goldman, C.R., A. Jassby, and T. Powell. 1989. Interannual fluctuations in primary production: meteorological forcing of two subalpine lakes. Limnol. Oceanogr. 34:310-323.

Granger, O. 1977. Increasing variability in California precipitation. Ann. Assoc. Amer. Geogr. 69:533-543.

Graumlich, L.J. 1993. A 1000-year record of temperature and precipitation in the Sierra Nevada. Quat. Res. 39:249-255.

Hammer, U.T. 1986. Saline lake ecosystems of the world. Junk.

Hostetler, S. and L.V. Benson. 1990. Paleoclimatic implications of the high stand of Lake Lahontan derived from models of evaporation and lake level. Climate Dynamics 4:207-217.

Hostetler, S.W. and F. Giorgi. 1993. Use of output from high-resolution atmospheric models in landscape-scale hydrologic models: an assessment. Wat. Resour. Res. 29:1685-1695.

Houghton, J.G. 1969. Characteristics of rainfall in the Great Basin. Ph.D. thesis, Univ. Oregon, Eugene. 292 p.

Imberger, J. and G.N. Ivey. 1993. Boundary mixing in stratified reservoirs. J. Fluid Mech. 248:477-491.

Imberger, J. and J.C. Patterson. 1981. A dynamic reservoir simulation model, DYRESM: 5. *In:* Transport Models for Inland and Coastal Waters. Ed. H. B. Fischer, pp. 310-361, Academic Press, New York.

Imberger, J. and J.C. Patterson, 1990. Physical Limnology. Adv. Appl. Mech. 27:303-475.

Jassby, A.D., T.M. Powell, and C.R. Goldman. 1990. Interannual fluctuations in primary production: direct physical effects and tropic cascade at Castle Lake, California. Limnol. Oceanogr. 35:1021-1038.

Jellison, R. and J.M. Melack. 1993*a*. Meromixis in hypersaline Mono Lake, California. 1. Stratification and vertical mixing during the onset, persistence, and breakdown of meromixis. Limnol. Oceanogr. 38:1008-1019.

Jellison, R. and J.M. Melack, 1993*b*. Algal photosynthetic activity and its response to meromixis in hypersaline Mono Lake, California. Limnol. Oceanogr. 38:818-837.

Jellison, R., L.G. Miller, J.M. Melack, and G.L. Dana. 1993. Meromixis in hypersaline Mono Lake, California. 2: Nitrogen fluxes. Limnol. Oceanogr. 38:1020-1039.

Kattelmann, R. 1992. Historical floods in the eastern Sierra Nevada, p. 74-86. *In* C.A. Hall, V. Doyle-Jones, and B. Widawski [eds.], The history of water in the Eastern Sierra Nevada, Owens Vally and White Mountains. University of California Press.

Lettenmaier, D.P. and T.Y. Gan. 1990. Hydrologic sensitivities of the Sacramento-San Joaquin River basin, California, to global warming. Wat. Resour. Res. 26:69-86.

Lin, A. 1976. The meromictic Great Salt Lake. J. Great Lake Res. 2:375-383.

MacIntyre, S and J.M. Melack. 1982. Meromixis in an equatorial African soda lake. Limnol. Oceanogr. 27:595-609.

Mason, D.T. 1967. Limnology of Mono Lake, California. Univ. Calif. Publ. Zool. 83:1-110.

Melack, J.M. 1983. Large, deep salt lakes: a comparative limnological analysis. Hydrobiologia 158:1-14.

Michaelson, J., L. Haston, and F.W. Davis. 1987. 400 years of central California precipitation variability reconstructed from tree rings. Water Resour. Bull. 23:809-818.

Münnich, M., A. Wüest, and D.M. Imboden. 1992. Observations of the second vertical mode of the internal seiche in an alpine lake. Limnol. Oceanogr. 37:1705-1719.

Patten, D.T., and others. 1987. The Mono Basin ecosystem, effects of changing lake level. National Academy Press, Washington, D.C.

Patterson, J.C., P.F. Hamblin, and J. Imberger. 1984. Classification and dynamic simulation of the vertical density structure of lakes. Limnol. Oceanogr. 29:845-861.

Pupacko, A. 1993. Variations in northern Sierra Nevada streamflow: implications of climate change. Water Resour. Bull. 29:283-290.

Roden, G.I. 1989. Analysis and interpretation of long-term climatic variability along the west coast of North America, p. 93-111. *In* D.H. Peterson [ed.], Aspects of climatic variability in the Pacific and western Americas. Geophysical Monogr. Ser. 55.

Steinhorn, I. 1991. On the concept of evaporation from fresh and saline water bodies. Wat. Resour. Res. 27:645-648.

Stine, S. 1994. Extreme and persistent drought in California and Patagonia during medieval time. Nature 369:546-549.

Timms, B.V. 1972. A meromictic lake in Australia. Limnol. Oceanogr. 17:918-922.

Vorster, P. 1985. A water balance forecast model for Mono Lake. Calif. Water Resour. Monogr. 10. U.S. Dep. Agric. Forest Serv. Region 5.

Weinstock. 1981. Vertical turbulence diffusivity for weak or strong stable stratification. J. Geophys. Res. 86:9925-9928.

Table 1. Description of hydrology scenarios simulated during 100 year simulations.

Case	Percentage of Historical Hydrology	Eight largest runoff years reduced
1	100	no
2	87.5	yes
3	75	yes
4	87.5	no
5	75	no

Table 2. Equilibrium lake level predictions from LAAMP/DYRESM, Vorster (1985) and LADWP monthly water balance models. LADWP and Vorster model results from Patten *et al.* (1987). The LADWP and Vorster models used synthetic freshwater inputs generated from forty years of historical hydrology.

Model		Average Yearly Runoff ($Mm^3 yr^{-1}$)	Evaporation ($m\ yr^{-1}$)	Equilibrium Lake Depth (m)
LAAMP/DYRESM				
	case 1	131.25	1.01	53
	case 2	112.5	1.01	46-46.5
Vorster		122.0	1.07	52.5-53
		91.5	1.07	45.5-46
LADWP		122.0	1.07	54
		91.5	1.07	48.5-49

Figure 1. Bathymetry of Mono Lake with sampling stations (●) and the Paoha Island meteorology station (◆). The direction relative to the lake is given for the near lake meteorology station.

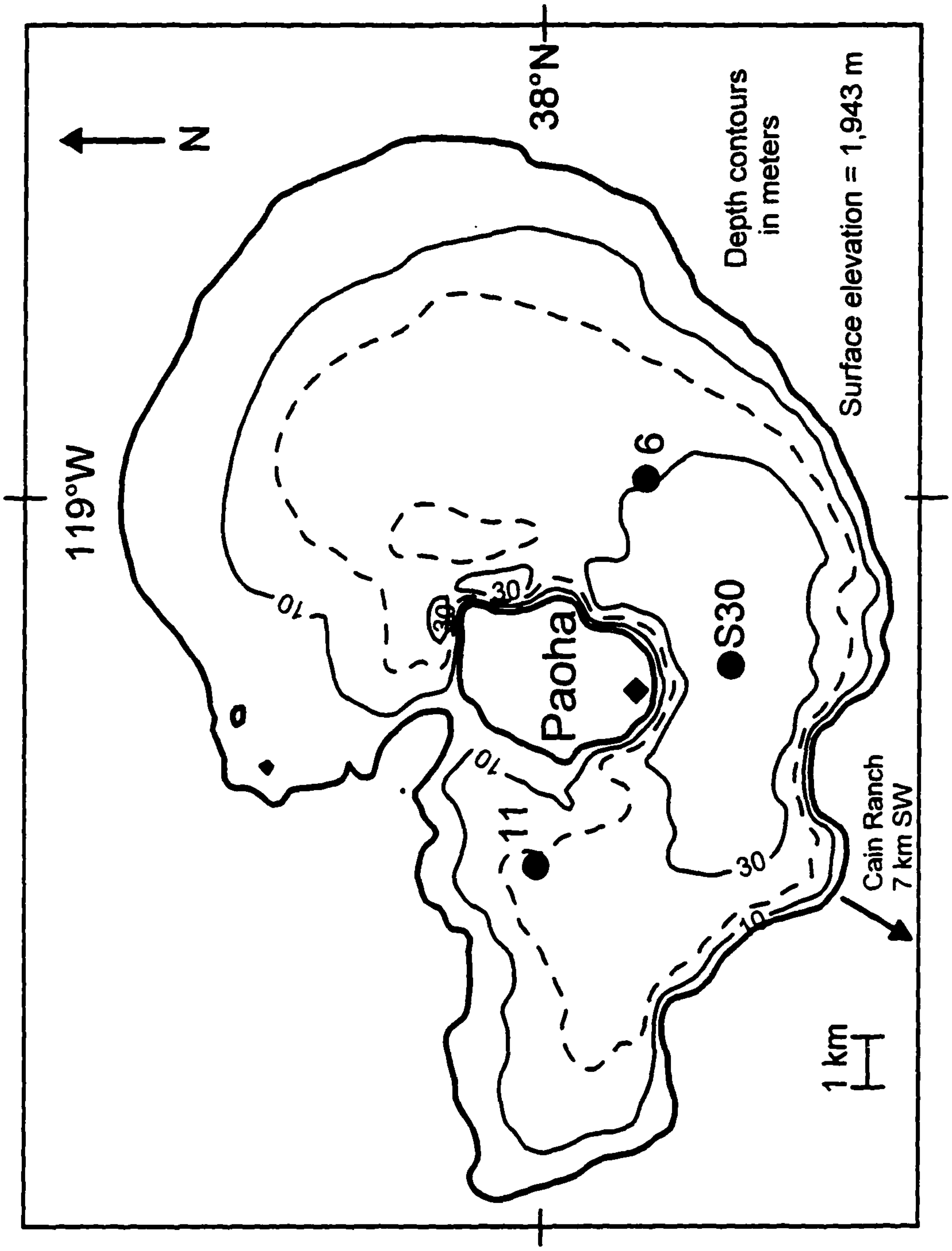

38°N
119°W
N
Depth contours
in meters
Surface elevation = 1,943 m
6
S30
Paoha
11
10
30
Cain Ranch
7 km SW
1 km

Figure 2. 1992 and 1993 daily simulation inputs - (A) incoming shortwave radiation (SW) and underwater attenuation coefficient based on PAR (Atten) (B) air temperature (Air T) and long wave radiation (LW) (C) wind speed (Wind) and vapor pressure (VP) (D) daily gauged discharge (Inflow) and maximum lake depth (Depth).

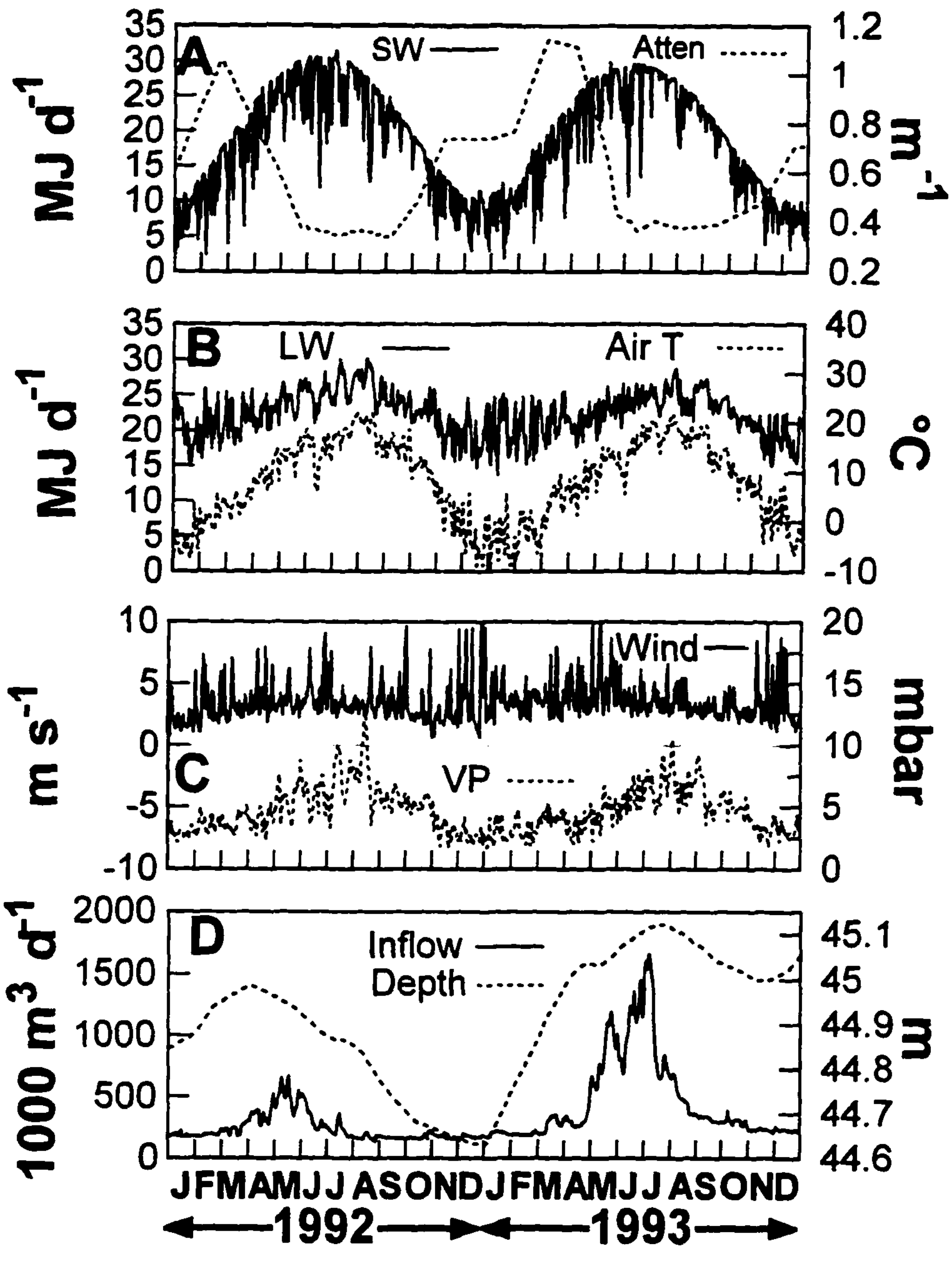

A
SW
Atten
MJ d-1
m-1
B
LW
Air T
°C
C
Wind
VP
m s-1
mbar
D
Inflow
Depth
1000 m3 d-1
m
JFMAMJJASONDJFMAMJJASOND
1992
1993

Figure 3. Maximum lake depth from 1982 to 1990.

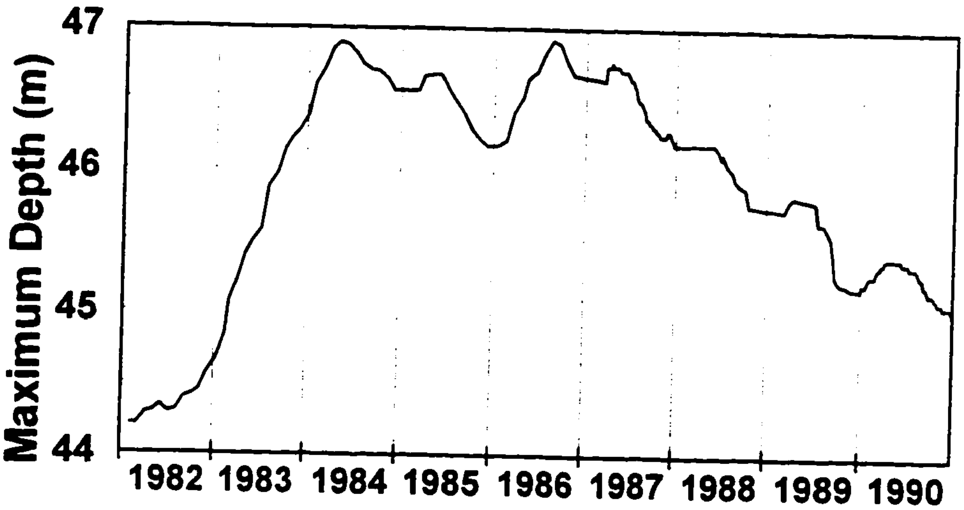

Maximum Depth (m)
47
46
45
44
1982 1983 1984 1985 1986 1987 1988 1989 1990

Figure 4. Hydrology from 1940 to 1990 - (A) total annual precipitation (B) total annual stream discharge (C) monthly maximum lake depth (D) total monthly stream discharge.

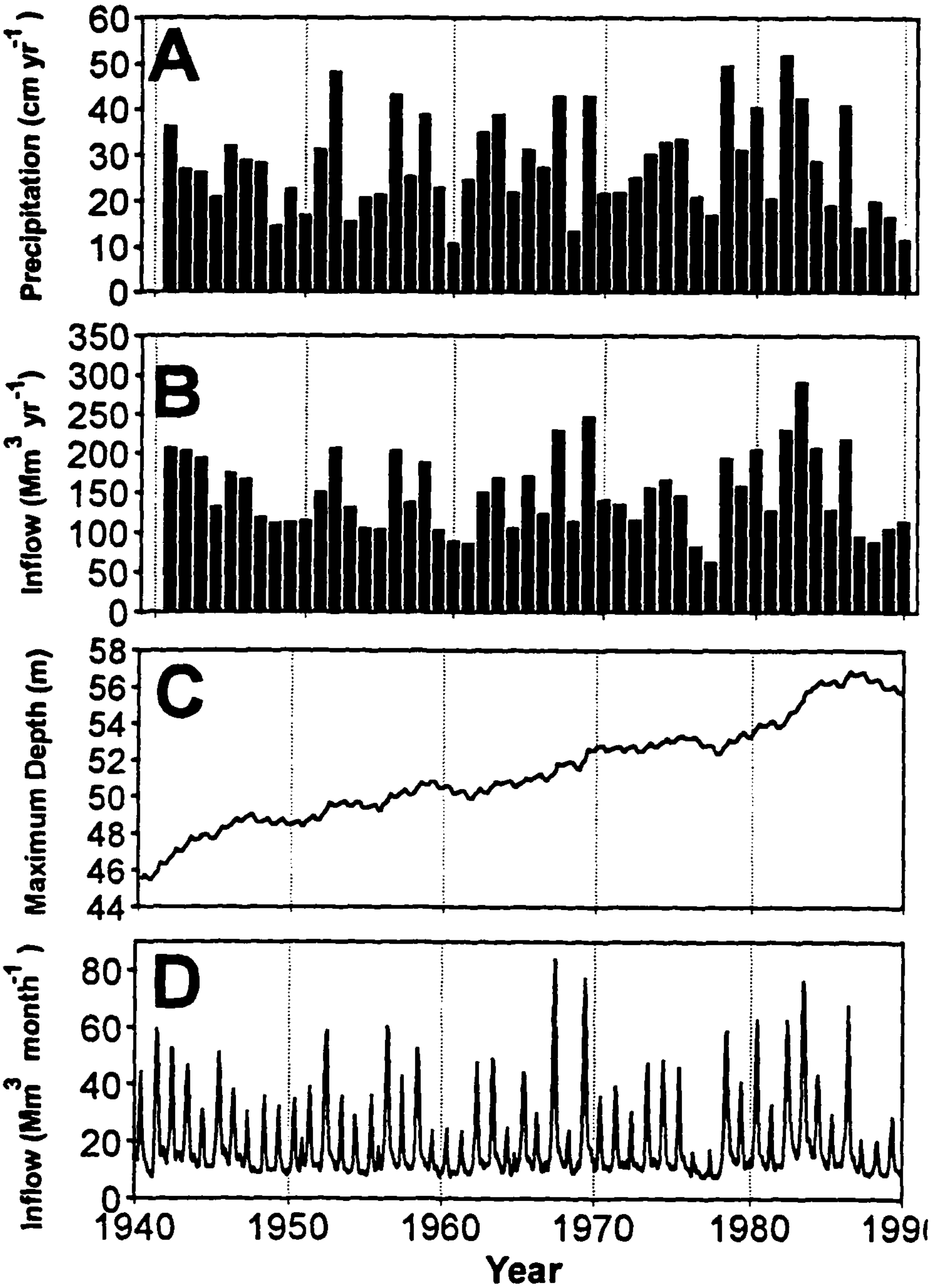

A
B
C
D
Precipitation (cm yr^{-1})
Inflow (Mm^3 yr^{-1})
Maximum Depth (m)
Inflow (Mm^3 month^{-1})
Year
1940
1950
1960
1970
1980
1990

Figure 5. Profiles of (A) measured temperature (°C) (B) measured salinity ($g\ kg^{-1}$) (C) modeled temperature (°C) (D) modeled salinity ($g\ kg^{-1}$) from 1992 to 1993.

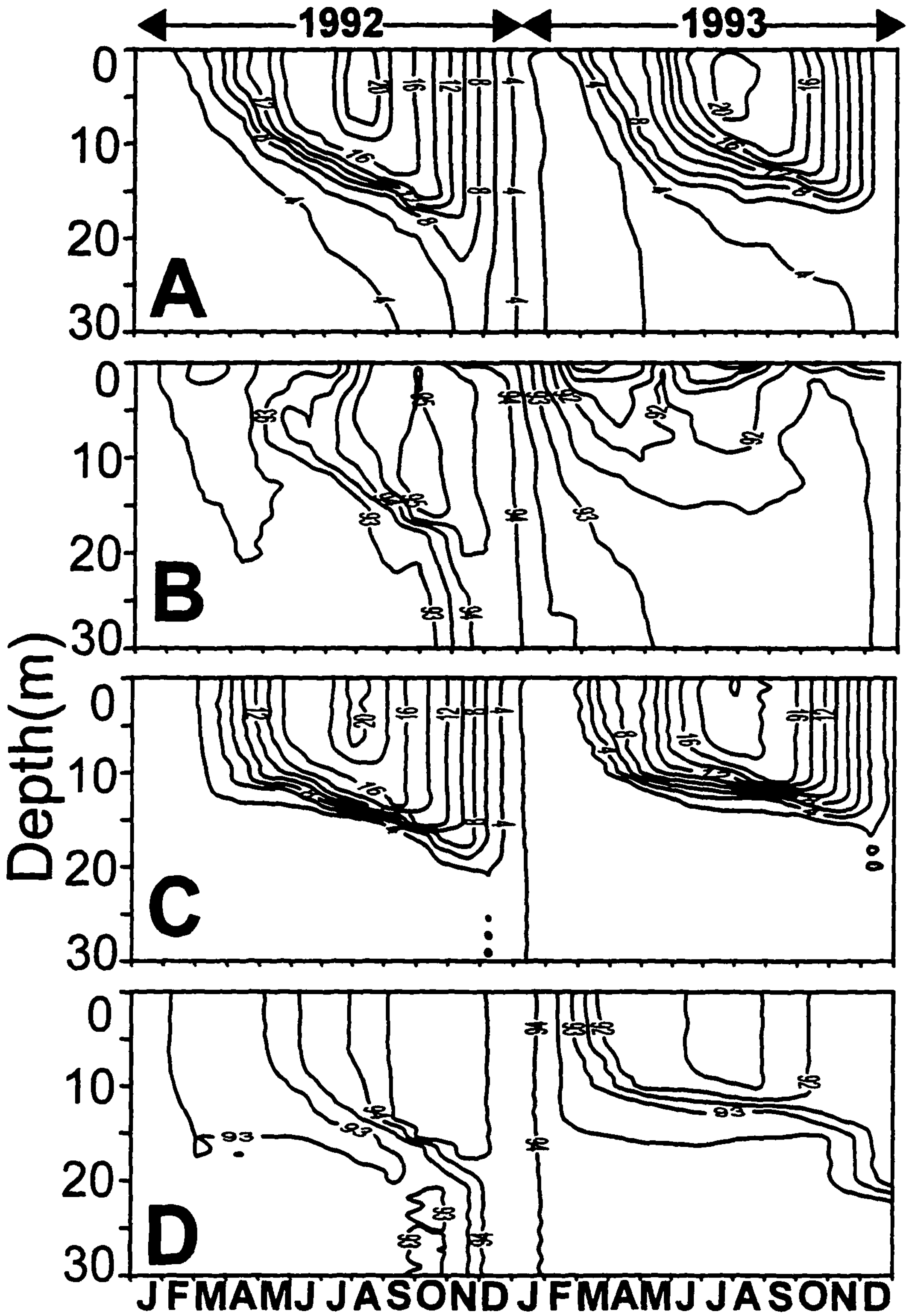
1992
1993
Depth(m)
A
B
C
D
0
10
20
30
J F M A M J J A S O N D J F M A M J J A S O N D
93

Figure 6. Simulation for 1992 and 1993 with modified vertical diffusivity parameterization - (A) temperature (°C) (B) salinity (g kg^{-1}).

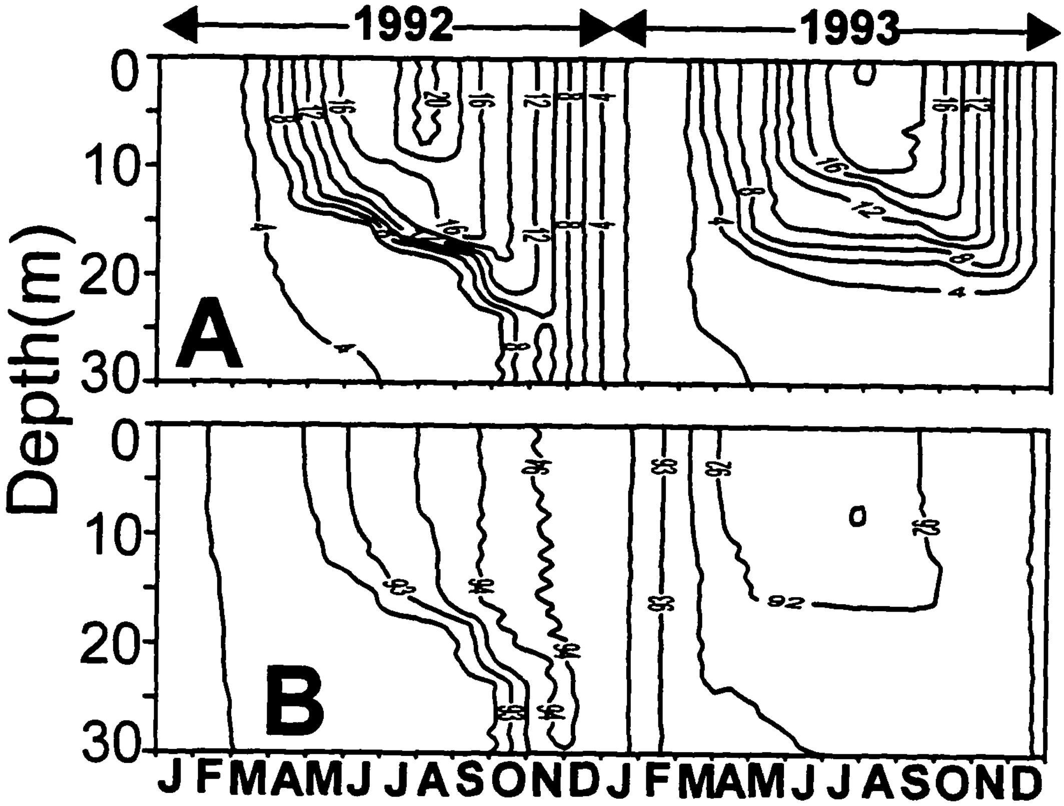
1992
1993
0
10
20
30
Depth(m)
A
B
J F M A M J J A S O N D J F M A M J J A S O N D
92

Figure 7. Salinity (g kg^{-1}) profiles from 1982 to 1990 - (A) measured (B) modeled.

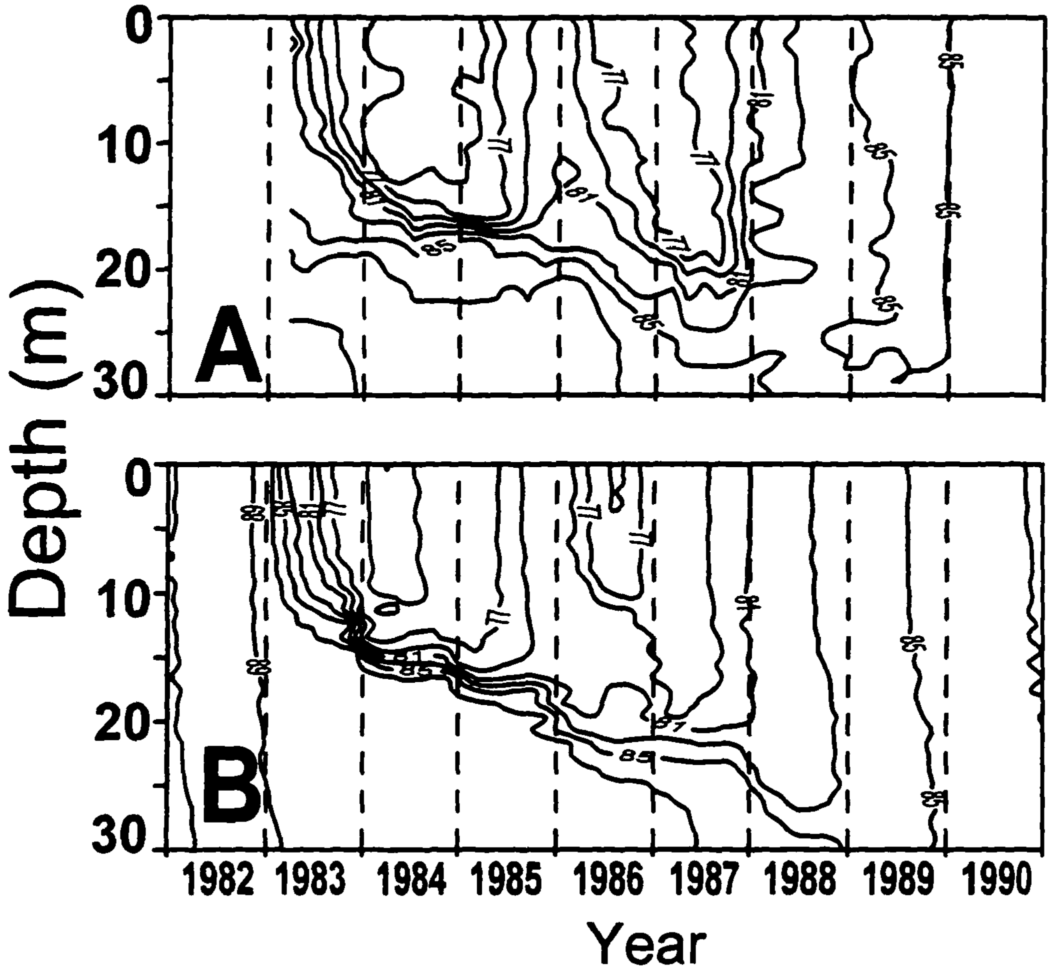
Depth (m)
A
B
Year
1982
1983
1984
1985
1986
1987
1988
1989
1990

Figure 8. Simulated lake levels for cases 1-5.

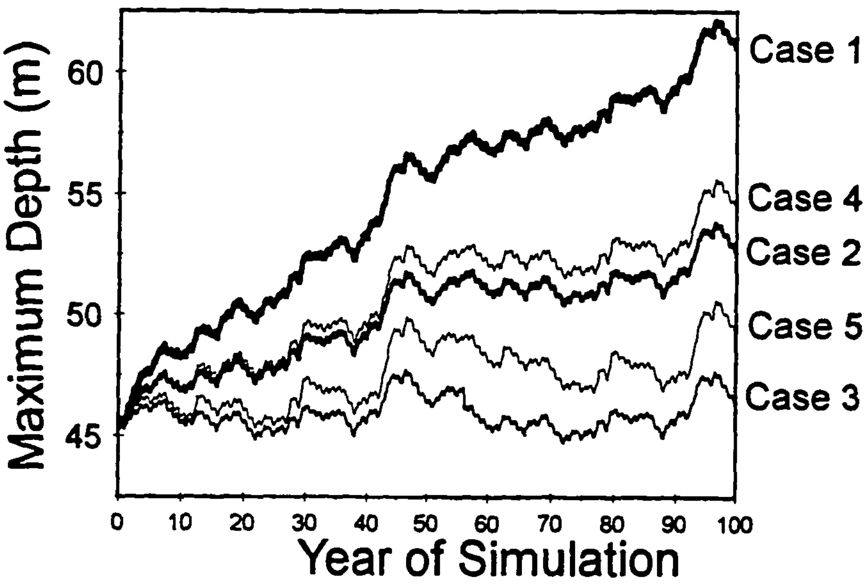
Maximum Depth (m)
60
55
50
45
Case 1
Case 4
Case 2
Case 5
Case 3
0
10
20
30
40
50
60
70
80
90
100
Year of Simulation

Figure 9. Two week averages of mixed-layer salinity (thick) and salinity 15 m relative to the maximum depth (thin) for case 1.

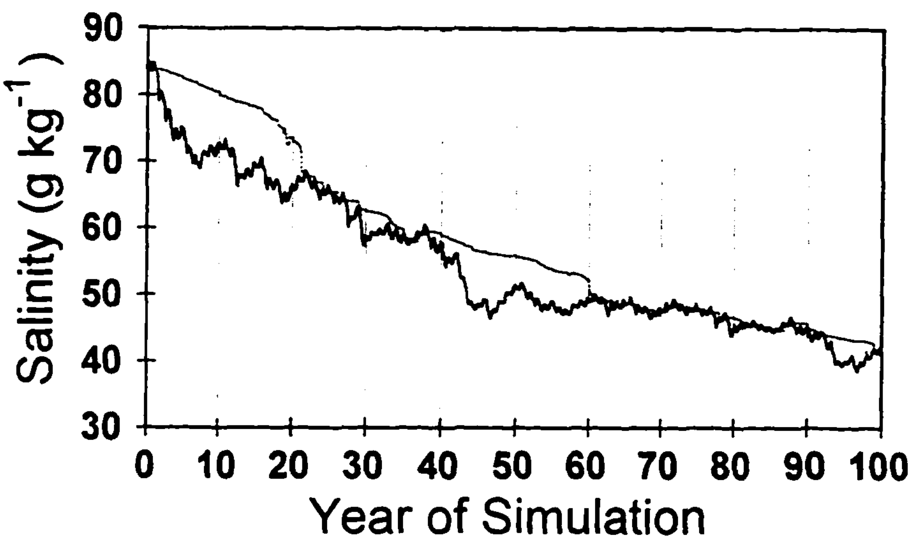
90
80
70
60
50
40
30
Salinity (g kg^{-1})
0
10
20
30
40
50
60
70
80
90
100
Year of Simulation

Figure 10. Summary of strong (black bars), moderate (dotted bars) and weak (clear bars) stability during meromictic years for cases 1-5. A year without a bar is monomictic. A * indicates meromixis had not terminated by the end of the simulation.

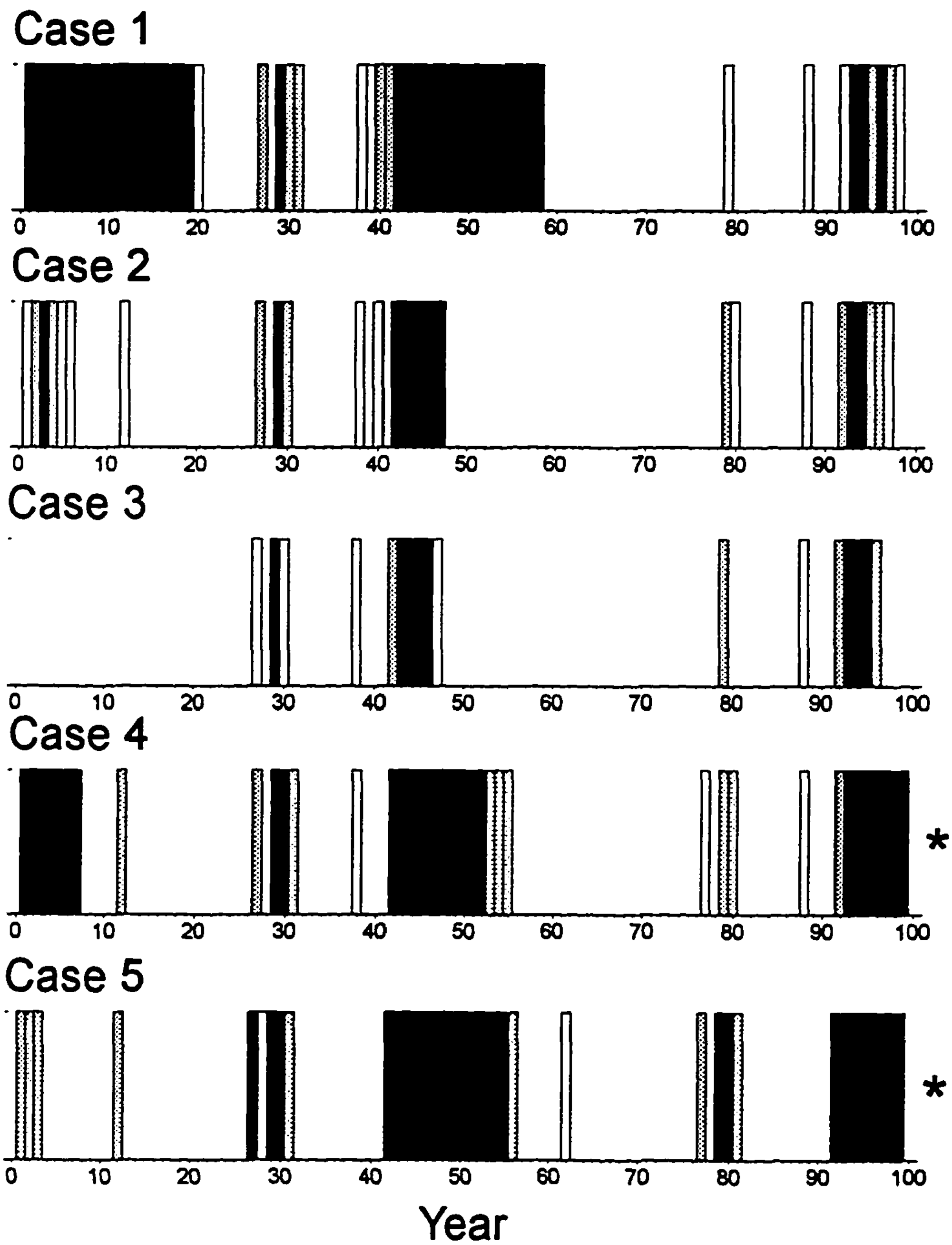
Case 1
0 10 20 30 40 50 60 70 80 90 100
Case 2
0 10 20 30 40 50 60 70 80 90 100
Case 3
0 10 20 30 40 50 60 70 80 90 100
Case 4
*
0 10 20 30 40 50 60 70 80 90 100
Case 5
*
0 10 20 30 40 50 60 70 80 90 100
Year

CHAPTER 3

Effect of Hydrologic Variations on Stratification and Upward Ammonia Flux in Hypersaline Mono Lake

Introduction

Saline lakes are generally located in semi-arid climates which are characterized by high seasonal and interannual variability in precipitation and stream inputs. In addition, stream discharge into many saline lakes is diverted for anthropogenic uses which have led to falling lake level and increased salinities. Examples include the Aral Sea (Micklin 1988), Dead Sea (Steinhorn 1985), Walker (Cooper and Koch 1990) and Mono (Jellison and Melack 1993*a*). In saline lakes, hydrological variations, whether natural or anthropogenic, can strongly influence vertical mixing dynamics due to the linkage between salinity stratification and the water flux at the surface (evaporation, precipitation, and stream discharge).

In freshwater bodies variations in the quantity and quality of riverine inputs can affect the average vertical water structure. In relatively arid regions, riverine inflows into reservoirs can be significantly more saline than the lake water which can result in the build-up of a saline water mass at the base of the dam (Imberger *et al.* 1978; Imberger 1982), a condition often alleviated by selective withdrawal (Imberger 1982) or a destratification technique such as bubble plumes (Schladow 1992, 1993). The effect of large riverine inflows during wet years into reservoirs and small lakes results in a lower retention time, increased advection, and a delay in the onset of thermal stratification. Thus, variations in stream discharge in freshwater bodies generally affect the thermal stratification dynamics with the caveat that in arid regions salinity stratification may be caused by saline riverine inputs.

In saline lakes, stream and precipitation inputs are always more dilute than the surface water and enter as surface overflows. Thus salinity stratification depends on the balance between freshwater inputs (precipitation and stream discharge) and evaporation. If freshwater inputs are greater than evaporation then the lake level rises, the mixed-layer salinity decreases, and stable salinity stratification results. Conversely, if freshwater inputs are less than evaporation, lake level decreases, mixed-layer salinity increases, and unstable salinity stratification results. Unlike most freshwater bodies, in saline lakes the vertical density structure undergoes large variations in water column stability depending on whether stable (rising lake level) or unstable (falling lake level) salinity stratification has developed over the thermally stratified period.

Several physical limnological investigations of saline lakes have documented the occurrence of ectogenic meromixis, a condition of persistent chemical stratification with incomplete mixing over the course of a year caused by large influxes of freshwater. The Dead Sea was meromictic for over a 100 years until falling lake level from the onset of stream diversions in the 1960s led to nearly equivalent mixolimnetic and monimolimnetic salinities prior to complete turnover in 1979 (Steinhorn 1985). Ectogenic meromixis in several North American Great Basin saline lakes such as Mono Lake (Jellison and Melack 1993*a*) resulted after exceptionally wet years which caused rapid large increases in lake level. The effect of meromixis on the nitrogen budget (Jellison *et al.* 1993) and primary productivity (Jellison and Melack 1993*b*) was documented for six years (1983-1988) of meromixis and the following two years of monomixis (e.g. one period of complete mixing per year) in Mono Lake. However, with the exception of the Dead Sea (Anati and Stiller 1991) few long-term studies have examined the physical limnology of saline lakes during periods of monomixis.

In this paper we describe the physical limnology of Mono Lake during six years of monomixis (1989-1994). Linkages between freshwater inputs (precipitation and runoff), evaporation, and seasonal stratification dynamics are described. Estimates of vertical diffusivities from the heat flux gradient method corrected for solar heating were calculated. The influence of hydrological inputs and wind forcing on the stratification and vertical transport dynamics are discussed. Ammonia is the primary form of nitrogen in N-limited Mono Lake (Jellison and Melack 1993*b*). Diffusivities were used to estimate seasonal and interannual upward ammonia fluxes to evaluate the effect on algal nutrient supply.

Study Site

Mono Lake lies in a closed basin with an area of 1800 km^2 located on the western edge of the North American Great Basin just east of the Sierra Nevada, California (38°N, 119°W) (Fig. 1). At an elevation of 1943 m above sea level Mono Lake has a 160 km^2 surface area, a 17 m mean depth, a 45 m maximum depth, and salinity of *ca.* 94 g L^{-1}.

The pH of Mono Lake is ≈10. Sodium is the major cation, and chloride and carbonate are the major anions; sulfate, borate, and silicate concentrations are also high (Jellison and Melack 1993*a*). Soluble reactive phosphorus was >300 μM throughout the water column from 1989-1994. Mono Lake is

N-limited and at the pH of 9.8, $[NH_3] = 5 \times [NH_4^+]$; concentrations of nitrate and nitrite are less than 1 μM (Jellison *et al.* 1993).

Most of the precipitation in the Mono Basin falls in the high elevations of the Sierra Nevada as snow (Patten *et al.* 1987). Stream discharge is the major hydrologic input to Mono Lake and is derived largely from snowmelt in the spring and summer. The five major streams that drain the high Sierran escarpment to the west of the lake are gauged.

The lake level declined 14 m (1956 to 1942 m surface elevation) from 1947 to 1982 because of diversion of freshwater inflow from the lake with the extension of the Los Angeles Aqueduct into the Mono Basin in 1941. The lake was monomictic when it was studied in the early 1960s (Mason 1967) and late 1970s through early 1980s (Melack 1983). In 1982 a large influx of freshwater from an abnormally high Sierra snowpack resulted in a 2.6 m rise in lake surface (Fig. 2) and the onset of 6 years of meromixis (Jellison and Melack 1993*a*). Meromixis persisted until 1988 and was characterized by a marked decrease in vertical mixing (Jellison and Melack 1993*a*) and nutrient transport across the pycnocline (Jellison *et al.* 1993) which resulted in diminished algal productivity (Jellison and Melack 1993*b*). A relatively stable lake level (*ca.* 1943 ± 0.5 m) occurred from 1990 to 1994. Another exceptionally wet year in 1995 led to a 1.0 m lake level rise and the onset of meromixis.

Methods and Numerical Analysis

Meteorology and Hydrology

Hourly averages of 1 s measurements of photosynthetically available radiation (PAR, 400 to 700 nm) from 1989 to 1994 were recorded at the Cain Ranch (CR) meteorological station 7 km southwest of the lake. Beginning in

October, 1991, hourly averages of shortwave radiation (SW, 280 to 2800 nm) were recorded at CR and PAR at the Paoha Island (PI) meteorological station near the center of the lake (Fig. 1). Daily averages of PAR measured at PI were 94.9% of those at CR (SE=47 μE m^{-2} s^{-1}, r^2=0.93, n=1104). CR PAR was used to estimate PAR over the lake from January, 1989 to September, 1991 and other PI PAR gaps. Daily average PAR was 45.5% of SW (SE=3.9 W m^{-2}, r^2=0.99, n=1095) assuming a conversion of 4.57 μEinst = 1 joule (McCree 1972).

Ten minute averages of 1 s measurements of wind speeds were recorded at PI (sensor height *ca.* 4 m above lake), and hourly wind speed averages were recorded at Lee Vining (LV) and Simis Ranch (SR) meteorological stations (sensor heights 10 m above ground) from 1991 to 1994 (Fig. 1). Linear regressions between PI and the SR and LV daily average wind speeds from 1990 to 1993, WS_{Paoha}=1.08WS_{Simis} (SE=0.70 m s^{-1}, r^2=0.77, n=1415), WS_{Paoha}=1.06$WS_{Lee\ Vining}$ (SE=0.86 m s^{-1}, r^2=0.65, n=1513), were used to fill in gaps in the PI wind speed record. SR is located to the north of the lake and often records wind speeds which are predominantly from the southwest after crossing the south to north fetch of the lake.

Ten minute averages of 1 s measurements of air temperature and relative humidity were measured at PI from 1992 to 1994. Relative humidity, RH (%), is defined as $RH = r/r_s \times 100$, where r and r_s are the measured and saturated air mixing ratios. The mixing ratio, r, is defined as the ratio of the water vapor density in the air, ρ_w (kg m^{-3}), to the density of dry air, ρ_D (kg m^{-3}) and may be computed from the relationship,

$$r = \frac{0.62197 f_w e}{(p - f_w e)}$$

derived from the ideal gas law (e.g. PV=nRT) where p is the atmospheric pressure (mbar), e is the vapor pressure (mbar), and f_w is a correction factor for the departure of the mixture of air and water vapor from ideal gas laws (assumed equal to 1). The saturation vapor pressure, e^*, is a function of air temperature and was calculated with Lowe's (1977) empirical relationship at sea level pressure (p=1013.5 mbar). The saturation mixing ratio, r_s, can be computed with the above equation, and the mixing ratio, r, can then be computed from the relative humidity. Solving for e in the above equation yields, $e = rp/(r+0.62197)$ and direct computation of the vapor pressure can be made with p equal to the Mono Lake surface pressure of 800 mbar at 1943 m. The approximation $e=RH_D \times e^* \times c_{elev}$, where c_{elev} is the elevation pressure correction (=0.79) and RH_D is the daily average relative humidity, is a good approximation.

Hourly totals of precipitation were recorded continuously from 1988 to 1994 at SR. Total daily CR precipitation was recorded prior to October, 1991. Average annual CR precipitation from 1940 to 1990 was 28 cm yr^{-1}. Vorster (1985) estimated annual precipitation over the lake to be 20 cm yr^{-1} (based on isohyetal maps of the Mono Basin), about 73% of CR precipitation. Approximately 75% of the annual precipitation onto the lake surface occurs between October and March (Vorster 1985). SR precipitation was 64% of CR from October to March during 1988 to 1991 (SE = 0.55 cm $month^{-1}$, r^2=0.87, n=21). The 1989 to 1994 Mono Lake monthly precipitation totals were derived from Simis Ranch values by multiplying by 1.14 (73%/64%).

Lake surface elevations were recorded weekly to monthly from staff gauges. Daily lake surface elevations were computed by interpolation between measurements. The daily total discharge of the five major perennial streams in the Mono Basin were recorded at gauges approximately 5 to 7 km upstream of the lake.

Temperature, Conductivity, Salinity, and Density

The 1989 and 1990 temperature profiles were measured at 1 m depth intervals at stations 6, 11, and S30 (Fig. 1) with a thermistor (Yellow Springs Instr. 701) and Wheatstone bridge circuit (Cole-Parmer model 8502-25) with an accuracy of 0.05 °C (Jellison and Melack 1993*a*). The 1989 and 1990 conductivity profiles were collected at stations 6 and 11 (Fig. 1) at monthly intervals with a van Dorn water sampler and were almost always sampled at 7 depths (2, 8, 12, 16, and 20 m at both stations and 24 and 28 m at station 6 only). Conductivity samples were filtered immediately through ≈1 μm pore size Gelman A/E glass-fiber filters and stored at 4 °C. Conductivity of samples were measured in the laboratory in a 1-cm cell (Lab-line) between 24 and 26 °C and corrected to 25 °C. Replicate readings indicated a measurement uncertainty of 0.4 mS cm^{-1} (Jellison and Melack 1993*a*).

Beginning in January, 1991, vertical profiles of temperature and conductivity at stations 6, 11, and S30 (Fig. 1) were made with a conductivity-temperature-depth profiler (CTD) (Sea-Bird Electronics, model Seacat SBE 19). The CTD is a free-falling instrument which samples at 2 Hz. Addition of customized buoyancy to the CTD resulted in descent rates of *ca. 0.25* m s^{-1} yielding approximately a 0.13 m vertical resolution.

Monthly CTD profiles were made from September to February for all years and all of 1991. Bi-weekly CTD profiles were made from March to August for 1992, 1993, and 1994 except for a gap in July, 1993. On most field dates, two CTD profiles were made at stations S30, 6, and 11.

The nominal thermistor response time (*ca.* 0.5 s) is slower than the conductivity sensor response time (*ca.* 0.2 s) on the Seacat CTD. The mismatch in the temperature and conductivity response times and differences in the vertical placement of sensors on the CTD results in 'spikes' in the derived salinity (or conductivity corrected to a standard temperature) profile. A 0.5 s low pass filter was applied to the conductivity profile to match the sensor response times (i.e. conductivity signal smoothed to 0.5 s response time of the thermistor).

The conductivity measured by a cell is a volume-weighted integral of the instantaneous and spatial distribution of conductivity in the sensitive volume of the cell and is governed by 1) the initial flushing of the cell, 2) the thermal and haline boundary layers on the wall of the cell, and 3) the heat stored in the wall of the cell (Lueck 1990). The initial flushing of the cell should be constant for all profiles since the CTD is equipped with a pump which provides a constant flow. The second factor, the thermal and haline boundary layer mismatch within the cell, should be relatively unimportant because the pumped flow in the cell is fully turbulent (N. Larson, Sea-Bird, *pers. comm.*). The third factor, the thermal inertia of the conductivity cell, requires correction. Lueck (1990) describes thermal inertia correction theory and Lueck and Picklo (1990) determined an algorithm to correct the effect of thermal inertia of Sea-Bird conductivity cells which was applied to the CTD profiles here.

The conductivity and pressure sensors were assumed to measure instantaneously, whereas the temperature of a water parcel sampled by the CTD lags in time as a result of longer response time and a boundary layer time constant. The slower response temperature profiles were shifted back in time to match the conductivity and pressure profiles.

The relation to compute conductivity at 25 °C, C_{25}, was determined from CTD measurements of Mono Lake water (C_{25}=86.6 mS cm^{-1}) over a temperature range of 3 to 28 °C. C_{25} was computed as:

$$C_{25} = C_T(1+2.05\times10^{-2}(25-T)+3.52\times10^{-4}(25-T)^2+8.5\times10^{-6}(25-T)^3)$$

where C_i is the conductivity (mS cm^{-1}) at temperature i (°C) and T is the temperature at which the raw conductivity measurement was made. Corrected conductivity was computed and plotted for a range of alignment time constants for each CTD profile (0.5 to 1.5 s). The alignment constant which minimized spiking in the corrected conductivity profile was chosen. The profile with the least spiking was used at each station. Most alignment times ranged from 0.7 to 1.0 s with an average of 0.8 s.

The density of Mono Lake water, ρ_w (kg m^{-3}) as a function of temperature, T (°C), and conductivity at 25 °C, C_{25} (mS cm^{-1}), is given by,

$$\rho_w = c_1 + c_2 T + c_3 T^2 + c_4 C_{25} + c_5 C_{25}^2 + c_6 T C_{25}$$

where c_1 = 1003.40, c_2 = 1.335x10^{-2}, c_3 = -6.20x10^{-3}, c_4 = 4.897x10^{-1}, c_5 = 4.23x10^{-3}, and c_6 = -1.35x10^{-3} (R. Jellison *unpub. data*). After CTD processing, conductivity and density profiles had 1 m resolution and temperature profiles had 0.1 to 0.2 m resolution depending on the descent rate.

Total dissolved solids, TDS, (g l^{-1}) was computed as:

$$TDS = 8.0629 + 0.3792 \times C_{25} + \times 0.006322 \times C_{25}{}^2$$

(R. Jellison *unpub. data)*. The salinity, S (g L^{-1}), and TDS were assumed to be equivalent. The salinity in units of g kg^{-1} was derived by dividing S in g L^{-1} by the local density. The linear expansion coefficients of heat, $\alpha=\rho_0^{-1}\partial\rho/\partial T$, and salt, $\beta=\rho_0^{-1}\partial\rho/\partial S$, are -2.5×10^{-4} ($^{\circ}C^{-1}$) and 8.8×10^{-4} ($g\ kg^{-1})^{-1}$, respectively.

Light, Ammonium, and Dissolved Oxygen

Attenuation of PAR in the water column was measured monthly at 0.5 m intervals with a submersible quantum sensor at two stations (6 and 11) from 1989 to 1993 and at station 30 in 1994. Dissolved oxygen was measured at two stations (6 and 11) with a temperature-oxygen meter (YSI, model 58) and polarographic probe (YSI, model 5739). The oxygen electrode is calibrated against Miller titrations of Mono Lake water (Walker *et al.* 1970).

Monthly vertical profiles of ammonia at 2, 8, 12, 16, and 20 m were made at stations 6 and 11 from 1989 to 1993 and at station 30 during 1994. At deeper station 6 (or station 30 in 1994) additional samples at 24 and 28 m were made. The samples were collected with an opaque Van Dorn water sampler and immediately filtered through a 25-mm Gelman A/E glass-fiber filters (pore size, 1 μm). Ammonia concentrations were measured with the indophenol blue method (Strickland and Parsons 1972). The molar extinction coefficient in Mono Lake water is smaller than that for distilled-deionized water with indophenol blue method. Therefore, molar extinction coefficients were determined for a series of dilutions of Mono Lake water and used to correct the reagent blank.

Numerical Procedures

Eddy diffusivities were calculated with flux-gradient heat method modified for solar heating (Jassby and Powell 1975),

$$K_z = \frac{1}{\delta T/\delta z}\left[\frac{1}{A_z}\frac{d}{dt}\int_z^{z_m} A_u T_u du - \frac{1}{\rho c}R_z\right]$$

where K_z is the coefficient of vertical eddy diffusivity at depth z, z_m is the maximum depth of the lake, A_z is the area at depth z, T is temperature, ρ is density, c is thermal capacity, and t is time. Temperature gradients were estimated as 2-m central differences. Depths, areas, and volumes were changed to correspond to changes in lake level. The heat integral was evaluated at 1-m intervals with lakewide mean temperatures and area-capacity curves (Pelagos Corp. *unpub. data*). Computed eddy diffusivities were corrected for thermal molecular diffusivity (1.4×10^{-7} m^2 s^{-1}).

Internal waves and other water movements often necessitate sampling of multiple stations to reduce errors in lakewide mean temperature profiles in moderately sized lakes. Sampling was most often done during calm to low wind conditions from early to midday, however thermocline profiles were vertically displaced up to 2 m relative to each other on a number of field days suggesting internal wave activity similar to the observations of Jellison and Melack (1993*a*).

Lakewide mean temperatures derived from sigmoidal temperature profiles taken from various stations are displaced relative to each other due to internal seiches, and the conventional mean will smear the vertical temperature gradient over the range of isotherm displacement (Sweers 1968). Instead, the Sweer's 'inverse algorithm', where depths of isotherms are averaged and used to construct a mean temperature profile, was used whenever the temperature was monotonically decreasing with depth (generally March to October). Temperatures derived from three stations (S30, 6, and 11) were used throughout the analysis. Lakewide average conductivity profiles from stations S30, 6, and 11 were computed as averages at a particular depth.

Errors in the estimates of heat content arising from internal water movements are potentially much larger than those due to instrument error alone (*cf.* Stauffer 1992). Several field dates from June to August in 1993 and June to October 1994 had 8 to 10 stations sampled (Fig. 1). Two additional lakewide mean temperature profiles were derived with the Sweers algorithm from all the stations and the stations 4, 8 and 9 (Fig. 1). Jellison and Melack (1993*a*) found that the lakewide heat content error was reduced if a 3 profile Sweers temporally moving average was applied to the data. The averages were compiled with the Sweers algorithm in the same manner as with individual profiles of a field day.

Solar heating was estimated from hourly measurements of incident PAR at Paoha Island. PAR was converted to SW with the ratio 45.5% calculated from the two sensors at CR. Hourly albedoes assumed a flat foamless lake. Attenuation in the water column was divided into seven wavelength bands (*see* Jassby and Powell 1975), six with assumed constant attenuation coefficients (Jellison and Melack 1993*a*) and a temporally varying PAR attenuation coefficient. Generally, from May to August light attenuation was greater through the thermocline and hypolimnion than the mixed-layer. During these periods two attenuation coefficients (below and above upper boundary of seasonal thermocline) were computed from the light profiles. PAR attenuation coefficients were linearly interpolated between sampling dates.

The upward flux of ammonia through the thermocline was estimated using a Fickian diffusion equation during the heating season. If we assume that eddy diffusivities derived from the heat-flux gradient method corrected for thermal diffusivity (1.4 x 10^{-7} m^2 s^{-1}) approximate eddy diffusivities for ammonia, then

$$J_N = -K_Z \frac{\partial N}{\partial z}$$

where J_N is the upward flux of ammonia in mol m^{-2} s^{-1}, K_z is the eddy diffusivity for ammonia in m^2 s^{-1}, and $\partial N/\partial z$ the ammonia gradient in mol m^{-4}. Since the spatial resolution of ammonia measurements was coarse (*ca.* 4 m), the ammonia gradient was determined as the difference between adjacent measurements divided by the distance between samples. Eddy diffusivities used to determine the ammonia flux were calculated at the midpoint between ammonia samples at 4 m intervals. Lakewide average dissolved oxygen and ammonia profiles were constructed from the mean of measurements at stations 6 and 11, except in 1994 when only station 30 was sampled.

Results

Hydrology

An evaporation rate of 93 to 95 cm yr^{-1} was estimated from measured daily averages of wind speed and vapor pressure; and sub-daily water surface temperatures predicted with the one-dimensional vertical mixing model DYRESM (Chapter 4). A mass transfer equation was used in the simulation where,

$$E = C_E \Delta P_V \cdot v_w$$

where E is evaporation (kg s^{-1}), ΔP_V is the daily average vapor pressure (mbar), v_w is the daily average wind speed (m s^{-1}), C_E is the Stanton constant ($=L_E/(\rho c)$), L_E is the latent heat of evaporation ($\approx 2.5 \times 10^6$ J kg^{-1} in Mono Lake),

ρ is the density of the lake water at the air-water interface, and c is the specific heat of Mono Lake water ($\approx$3860 J kg^{-1} °C) (Brutsaert 1982). The saturation vapor pressure over saline lakes is lower than freshwater bodies and required a 5% reduction for the salinity of Mono Lake (Salhotra *et al.* 1985). The lake level decrease from evaporation with constant temperature throughout the evaporation process, Z_E, was calculated as:

$$Z_E = \frac{(1+\gamma S')E}{\rho'}$$

where $\gamma = \rho^{-1}(\partial\rho/\partial S)\,|_T$, S' is the new salinity (g kg^{-1}), and ρ' is the new density (Steinhorn 1991) which accounts for losses of volume from evaporation (E/ρ') and volume shrinkage from increased salinity ($\gamma S' E/\rho'$).

Annual evaporation estimates for Mono lake derived from water budget, energy budget, mass transfer, and pan evaporation studies range from 95-200 cm yr^{-1} (Vorster 1985). The DYRESM estimate is at the lower range of most annual evaporation estimates (95-120 cm yr^{-1}). During 1992 monthly evaporation ranged from 2.0 cm month^{-1} (January) to 14.8 cm month^{-1} (August) (Table 1).

Annual precipitation totals were computed from November to October which roughly coincides with the beginning of holomixis and the high precipitation period. Total annual precipitation over Mono Lake ranged from 26 cm (1993) to 8 cm (1989). Precipitation in 1990 and 1992 was 12-13 cm and in 1991 and 1994 annual precipitation was 17-19 cm. The 1993 total precipitation was the only year to exceed the 20 cm yr^{-1} 50-year average (1941-1990). Virtually no rain fell at Simis Ranch from April-October, 1989, which was the lowest rainfall period during the six years (Fig. 3). The highest precipitation occurred during the four month period of December, 1992 to

March, 1993 (4.2 to 6.2 cm month^{-1}, total 21.6 cm). March, 1991 (6.3 cm) and May, 1994 (5.3 cm) were also exceptionally wet months.

Monthly stream discharge was divided by the average lake surface area at the beginning and end of each month, yielding potential lake level rise from stream inputs. Stream caused lake level increases are presented here to emphasize the influence of discharge on lake level fluctuations. The highest yearly total discharge occurred during 1993 (100.4 cm yr^{-1}) and was approximately equal to evaporation. The lowest yearly discharge occurred during 1989 (22.0 cm yr^{-1}). Stream discharge of the remaining years ranged from 46.4 cm yr^{-1} (1991) to 66.2 cm yr^{-1} (1990). Low monthly stream discharge occurred from October to March each year and coincided with the period of snowpack accumulation in the Sierra Nevada (Fig. 3). The six year trend of increasing winter base flows from 1 cm month^{-1} in 1989 to 4 cm month^{-1} in 1994 reflected the end of a drought, decreases in groundwater recharge, and reductions in winter diversions. Peak discharge occurred between May and July each year. Four of the five highest monthly discharge totals occurred from May to July, 1993, equivalent to a 0.6 m lake level increase from stream discharge.

Lake levels fluctuated within a 1.25 m range during the 6 years (Fig. 3), an exceptionally stable period compared to the past 50 years (1970-1994 shown in Fig. 2). Lake levels increased from December to March each year from a combination of low evaporation (Table 1) and maximum annual precipitation (Fig. 3). Larger winter lake level rises resulted from high winter precipitation in 1993 and high winter stream discharge in 1994. Falling lake level occurred by April or May from 1989 to 1992 as evaporation increased and freshwater inputs were low. Lake levels increased through August, 1993, from high stream discharge and then fell only 0.1 m by December as discharge nearly balanced evaporation. Lake levels increased through June, 1994, which coincided with peak discharge and then decreased rapidly with reductions in stream inputs, no summer precipitation, and high evaporation.

Temperature, Conductivity, and Density Stratification

The 1991 to 1994 conductivities corrected to 25 °C ranged from 88-92 mS cm^{-1} (Fig. 4). Winter lake level rises (Fig. 3) during low evaporation resulted in dilution of the upper water column and weak stable salinity stratification for 1-2 months in 1991 (March) and 1992 (February-March). The 1991 and 1992 conductivity dynamics were similar (Fig. 4), and only 1992 is discussed in detail. By May 27 inverse salinity stratification (e.g. mixed-layer salinity > hypolimnetic salinity) had developed with a 0.7 mS cm^{-1} conductivity difference across a sharp unstable chemocline at 8-11 m. Even though the chemocline had deepened ≈5 m by July 21, evaporative concentration of the mixed-layer increased the conductivity difference across the chemocline by 0.5 mS cm^{-1} from a 0.15 m fall in lake level. The salinity had increased above the chemocline since the total mass of salt above 15 m remained constant (May 27 and July 21 conductivity profiles nearly equivalent below 15 m) but the volume decreased. By September 7, a 0.3 m lake level decrease since April 1 resulted in nearly a 1.5 mS cm^{-1} conductivity difference across the chemocline with a 0.2-0.5 mS cm^{-1} hypolimnetic conductivity increase. By November 11 just prior to turnover, the conductivity step across the chemocline had weakened to 0.7 mS cm^{-1} from entrainment of the less saline hypolimnion just prior to holomixis.

Four consecutive months of high precipitation beginning in December, 1992, led to a 0.5 m lake level increase and resulted in a stable chemocline at 10-15 m with a gradient of 0.1 mS cm^{-1} m^{-1} on April 25, 1993 (Fig. 4). Dilution of the upper 5 m of the lake by June 24 resulted from high snowmelt discharge (May-July). High autumn base flows (September-December) maintained salinity stratification through October 12 (Fig. 4). By the next sampling date (December 16) the lake was holomictic. The hypolimnetic conductivity remained at approximately 90.5 mS cm^{-1} from April-October.

During 1994 weak stable chemical stratification was sampled as late as May 25 (Fig. 4) as high stream discharge in May (12 cm) matched evaporative losses. Falling lake level after June 1 led to an unstable chemocline at 10 m (0.5 mS cm^{-1} conductivity difference) on July 22. An exceptionally large lake level drop in August (*ca.* 0.15 m) led to a 1.4 mS cm^{-1} conductivity decrease across the chemocline (12-14 m) only a month later on August 25. By October 19 the chemocline had deepened to 17 m and the conductivity step across the chemocline had decreased to 1 mS cm^{-1} from hypolimnetic entrainment similar to 1992. The average hypolimnetic conductivity increased only slightly from May 25 to August 25, but increased 0.3 mS cm^{-1} the next two months indicative of a downward salt flux in September.

During the six year period mixed-layer temperatures were lowest in February (2-3 °C) and highest in July or August (> 20 °C). Hypolimnetic temperatures were lowest in February (2-3 °C) and increased 1-4 °C by September of each year. Representative temperature profiles from late April to mid-November from 1989 to 1994 (Fig. 5) reveal substantial differences in the thermal dynamics between years. The largest seasonal hypolimnetic temperature increase (4°C, May 4-September 12), earliest turnover date (late

October/early November), and lowest thermocline temperature gradients during the six years characterized the 1989 thermal dynamics.

The 1990 and 1991 thermal dynamics were characterized by a 2-3°C hypolimnetic temperature rise from early May to mid-October and almost equivalent downward seasonal thermocline migration with respect to time and depth from June to October. The early May, 1990, profile had the shallowest May mixed-layer depth (*ca.* 5 m) of the six years. The 1992 temperature dynamics were similar to 1990 and 1991 except the seasonal thermocline established at a lower depth in the spring with less thermocline deepening afterwards. The early May profile in 1991 had weak thermal stratification from high wind forcing throughout the spring. Vertical temperature profiles in 1993 and 1994 were similar from May to October prior to turnover characterized by low rates of hypolimnetic heating (1-2°C).

The 1991-1994 density profiles reveal the interplay between significant differences in interannual conductivity dynamics (Fig. 4) and the repetitive low interannual variance in seasonal temperature dynamics (Fig. 5) on seasonal water column stability. Density throughout the water column over the 4 years varied from 1071-1078 kg m^{-3} from 1991-1994 (Fig. 6).

Only a 1 to 2 kg m^{-3} density difference was measured across the pycnocline in 1991 and 1992 during summer stratification. Falling lake level by early May during both years resulted in unstable chemical stratification and a gradual increase in the mixed-layer conductivity through the summer as discussed earlier. Even though temperature differences across the thermocline were greater than 10°C (5-15°C, density change of 3 kg m^{-3}) from June to September, the density difference across the pycnocline was small (1 kg m^{-3} in September). Within the range of conductivities considered here, a 1 mS cm^{-1}

change in conductivity is equivalent to a 1.5 kg m^{-3} density change. By September 7, the mixed-layer was 1.3 mS cm^{-1} more saline than the hypolimnion (2 kg m^{-3} decrease across pycnocline) resulting in a 1 kg m^{-3} density difference across the pycnocline.

A 2 kg m^{-3} density difference across the pycnocline on the April 25, 1993, profile (Fig. 6) was as large as any profile measured in 1992. Strong density stratification so early in the year resulted from a 1 kg m^{-3} increase across the pycnocline from stable salinity stratification. As late as October 12 (Fig. 6) a 3 kg m^{-3} density difference was measured in 1993.

Moderately strong density stratification (> 2 kg m^{-3}) at the end of May, 1994, (Fig. 6) had setup with weak stable salinity stratification. High mixed-layer temperatures (>20°C) in July increased the density difference to about 3 kg m^{-3} on July 25 (Fig. 5). Even though the August 25 (Fig. 5) temperature profile was nearly equivalent to July 25, a 1 kg m^{-3} decrease in density across the pycnocline resulted from an $\approx$1 mS cm^{-1} increase in mixed-layer conductivity.

Seasonal and interannual differences in the stability of the water column reflect differences in the timing and amount of freshwater inputs (Fig. 7). Thermal stability was similar for all four years, but salinity stability differed between years and caused large variations in total stability. Maximum stability in 1993 was twice as great as 1991 and 1992, and a factor of 1.5 greater than 1994. Total water column stability in 1991 and 1992 was similar. Greater stability from February to March in 1992 resulted from higher winter freshwater inputs (i.e. weak stable salinity stratification). In 1991, high March precipitation and high June stream discharge led to greater summer stability from less evaporative concentration of the mixed-layer. The large 1993 winter precipitation total led to total stability similar to the 1991 and 1992 maximums by March. Total stability in 1994 was intermediate between 1991-1992 and 1993.

During years with unstable salinity stratification, maximum stability did not always coincide with maximum thermal stability. For example, maximum stability in June, 1992 was nearly equivalent to August even though thermal stability was lower. The effect of inverse salinity stratification in August was sufficient to decrease total water column stability to similar values estimated during less thermally stratified June. In 1994, the stability maximum occurred during July, a month prior to maximum thermal stability. Maximum water column stability in 1993 coincided with maximum thermal stability as salinity stratification persisted throughout the year.

The 1989-1990 conductivity measurement accuracy was not sufficient to interpret the salinity and density dynamics as precisely as in 1991-1994. However, insights into the 1989-1990 salinity and density dynamics can be inferred if the 5 m (average of 2 and 8 m) and 26 m (average of 24 and 28 m) conductivity measurements and density estimates are compared to the 1991-1994 CTD measurements (Fig. 8).

The rapid lake level drop beginning in April, 1989 (*ca.* 10 cm month^{-1}) caused a higher rate of mixed-layer volume shrinkage and earlier onset of inverse salinity stratification (April) than the other years. Inverse conductivity stratification contributed to the weakest density steps across the pycnocline during summer stratification (estimated $\approx$1 kg m^{-3}) of all the years. Larger hypolimnetic temperature increases during stratification in 1989 coupled with the low inputs of freshwater support the inference of higher vertical mixing rates across the pycnocline resulting from lower water column stability relative to the other years (Fig. 8).

The 1990 conductivity dynamics were likely to have been similar to those in 1994 if the hydrology of both years is considered. Both years had high October-June stream discharge (*ca.* 4-8 cm month^{-1}) and similar lake levels. During both years the 5 and 26 m conductivity followed the same trend of prolonged weak stable salinity stratification through April followed by evaporative concentration of the mixed-layer during the summer. The 1990 spring lake level rise and summer lake level decrease were less than 1994. Hence, it is likely the spring, 1990, salinity stratification was weaker than 1994 (i.e. less freshwater dilution) but stronger in the summer (i.e. less evaporative concentration).

In summary, 1989 and 1993 represent the two extremes of the effect of hydrology on stratification dynamics during monomixis in Mono Lake. Salinity stratification throughout 1993 resulted from a positive water balance where freshwater inputs exceeded evaporation. Salinity stratification resulted in strong stability throughout stratification until turnover in late November to early December. During drought conditions in 1989, a large decrease in lake level resulted from low freshwater inputs. During thermal stratification, evaporative concentration of the mixed-layer resulted in inverse salinity stratification, weak density stratification, and a large downward heat flux. The other four years were intermediate cases between these two extremes. Stable salinity stratification in the spring persisted for a longer duration in 1990 and 1994 than 1991 and 1992 from greater precipitation and stream discharge inputs. However, all these years had unstable salinity profiles by mid-summer.

Double Diffusive Salt Fingering

Except for 1993, a negative water balance resulted in falling lake levels through the stratified period which led to inverse salinity stratification by June. These conditions are sufficient to promote double diffusive salt fingering. Salt fingering occurs when temperature stabilizes the water column and salinity is destabilizing, precisely the conditions measured over five of the six years in this study. Since the temperature stability has to be greater than the destabilizing influence of salinity in order for the density profile to be stable, the stability ratio, R_ρ, must be greater than 1 which is defined as,

$$R_\rho = -\frac{\alpha\, \partial T/\partial z}{\beta\, \partial S/\partial z}$$

where α and β are the coefficients of expansion of heat and salt and $\partial T/\partial z$ and $\partial S/\partial z$ the temperature and salinity gradients across the interface in question. As R_ρ approaches 1 (neutral stability) the destabilizing effect of unstable salinity stratification results in a larger downward salt flux via salt fingering.

Initially, the potential of double diffusive salt fingering was evaluated from the temperature and salinity steps across the seasonal pycnocline following the methods of Anati and Stiller (1991) in their analysis of the Dead Sea. In Figure 9, the seasonal pycnocline temperature and salinity steps for 1991, 1992, and 1994 from June/July to October/November are shown where $\partial T/\partial z$ and $\partial S/\partial z$ were computed over 3 m intervals. Stability ratios equal to 1 and 2 over the range of temperature and salinity steps measured across the pycnocline are plotted to indicate periods when salt fingering is likely to be significant. From Figure 9, circumstantial evidence suggests that salt fingering occurred from at least August to holomixis for all three years.

Step-like structure in temperature and salinity have been reported in active regions of double diffusive salt fingering in various oceans (Tait and Howe 1971, Lambert and Sturges 1977, Miller and Browning 1974). October temperature profiles from 1991 and 1994 reveal staircase structures below the thermocline which may indicate that salt fingering was occurring at the time of sampling (Fig. 10). The convective layers have length scales of 2-3 m separated by interfaces with thickness of *ca.* 0.5 m and temperature steps of 0.2-0.6 °C. Salinity steps (not shown) were estimated as 0.03-0.1 g kg^{-1}. Staircase structures were sampled at a number of locations during the October sampling dates in 1991 and 1994 which suggests basin scale layering within the hypolimnion driven by salt fingering.

The salt finger phenomena is not evident in the October, 1992 profile. However, several isothermal regions in the profiles (25-27 m, 22 m) are suggestive of 'relict' or 'fossil' regions of prior salt fingering. With the onset of salt fingering, the downward salt flux broadened the interface until R_ρ increased and salt fingering ceased (or diminished). Selected August and September profiles also show a number of nearly isothermal regions throughout the hypolimnion which are suggestive of prior salt fingering (Fig. 10). However, 'fossil' salt fingering signatures in these profiles are not basin scale and suggest spatial and temporal variability in this double diffusive phenomena during August-September. Perhaps the 1991 and 1994 October profiles maintained basin wide salt finger layering from rapid mixed-layer deepening driven by surface cooling which maintained a sharp inverse conductivity interface at the pycnocline on a basin wide scale. A number of profiles during 1989 and 1990 with 1 m resolution also indicate salt fingering occurred. The 1989 profiles suggest fingering may have occurred as early as May.

Estimates of heat and salt fluxes from salt fingering can be made from the following equations:

$$R_f^* = \frac{\alpha F_T}{\beta F_S}$$

$$R_f^* = \frac{0.44}{(R_\rho - 0.6)^{0.5}} \qquad \text{for } 1.2 < R_\rho < 2 \quad \text{(McDougall and Taylor 1984)}$$

$$R_f^* = 0.56 \qquad \text{for } R_\rho > 2 \quad \text{(Turner 1967)}$$

$$F_S = \frac{0.19}{(R_\rho - 0.5)}(gK_T)^{1/3}\beta^{1/3}\Delta S^{4/3} \qquad \text{(Boyd and Perkins 1987)}$$

where R_ρ is the stability ratio as defined earlier, F_T is the vertical temperature flux (°C m s^{-1}), F_S is vertical salt flux (g of salt m s^{-1} kg^{-1} of lake water), R_F^* is the density flux ratio, K_T is the diffusivity of heat ($1.4\text{x}10^{-7}$ m^2 s^{-1}), and ΔS is the salinity step across the interface (*see* Imboden and Wüest 1995). Salt finger eddy diffusivity estimates can be made with the equations,

$$K_z^S = \frac{F_S}{\partial S/\partial z}$$

$$K_z^T = \frac{F_T}{\partial T/\partial z}$$

from several profiles which had salt fingering.

Fast response temperature and conductivity sensors are required to accurately estimate interface thickness, salinity steps, and temperature steps. Our CTD had low sampling frequency (2 Hz), slow response sensors (T≈0.5 s, C≈0.2 s), and coarse spatial resolution (≈0.125 m). Further, conductivity measurement accuracy was only about 0.05-0.1 mS cm^{-1} resulting in crude estimates. Kunze (1987) showed that the above flux equations based on stability theory are valid only if the interface is thin enough (≈30 cm) that individual fingers extend through it. For thicker interfaces salt finger fluxes are less than the estimates derived from the above empirical equations and depend on the interface thickness.

We estimated salinity and temperature steps from profiles in Figure 10 assuming that the temperature and salinity steps were equivalent to the two isothermal (or isohaline) regions separating an interface. For example, in the September 21, 1994 profile, the two isothermal regions at 21.5 (4.7 °C) and 23-24 m (4.45 °C) were used to estimate the temperature step across the 'presumed' interface at 22 m. In many cases, the inaccuracy of the conductivity measurements precluded direct determination of salinity steps. In these cases salinity steps were estimated that maintained a stable density profile. We also assumed that the interfaces were 0.3 m thick at the time of salt fingering so that the empirical equations are valid. With these assumptions the heat and salt flux calculations are considered maximum estimates.

R_ρ values ranged from 2 to 4, F_T ranged from 1×10^{-6} to 1×10^{-5} °C m s^{-1}, and F_S ranged from 1×10^{-6} to 1×10^{-5} g m s^{-1} kg^{-1}. The ratio of F_T:F_S generally ranged from 1.5 to 2. The diffusivity of salt, K_z^S, (5×10^{-6} to 2×10^{-5} m^2 s^{-1}) was 3-8X greater than the diffusivity of heat, K_z^T, (1×10^{-6} to 5×10^{-6} m^2 s^{-1}).

Eddy Diffusivities

Only diffusivities at the thermocline are reported here since errors in heat content below the thermocline increased with depth. The relative error in lakewide heat content and diffusivity estimates below the maximum temperature gradient depth from field dates in 1993 and 1994 with 8-12 stations sampled are summarized in Table 2. Even though the three profile moving average reduced errors, eddy diffusivities at the maximum temperature gradient without the moving average are reported here to more clearly elucidate the temporal linkages between vertical mixing and hydrology.

A number of hypolimnetic heating and mixing mechanisms have been previously evaluated. Methane bubbles (Chapter 1), geothermal heat flux (Jellison *et al.* 1993, Chapter 1), and sediment heat flux (Jellison *et al.* 1993; Chapter 1) do not significantly contribute to the hypolimnetic heating or mixing. The significance of salt fingering is addressed in the discussion.

We hypothesize that thermocline tilting and internal waves could account for some of the heat transfer across the thermocline through a sediment heat transfer mechanism as proposed by Dutton and Bryson (1964). Assume the seiche is such that the thermocline surface remains a plane, but tilts with respect to the horizontal. During half the seiche period the cold hypolimnetic water overlies the warm epilimnetic sediments at one end of the lake and epilimnetic water overlies cool hypolimnetic sediments. The heat content transferred from the warm epilimnetic sediments to the cool hypolimnetic water can be calculated as,

$$Q / A = k \Delta T (2P / \pi \alpha)^{1/2}$$

where Q is the heat content transferred during a seiche period P, A is sediment area, ΔT is the temperature difference between the epilimnetic sediments and the hypolimnetic water, k is thermal conductivity, and α is thermal diffusivity ($\alpha = k\rho/c$, where ρ is density and c is specific heat).

The epilimnetic sediment temperature at depth z, T_z^S, was assumed to equal the temperature of the Sweers profile at z. Internal wave amplitudes of 1-2 m during calmer periods and 2-3 m during windy days with periods varying from 8-24 hrs were measured with thermistor chains in 1995, a period of strong stratification during the onset of meromixis (Romero and MacIntyre, *unpubl. data*). We calculated the heat flux 'around' the thermocline with an assumed amplitude of 2 m for the entire season and a period of 24 hours for the metalimnion. We assumed that during the first half of the seiche period, half of the metalimnetic perimeter is on average in contact with sediments 1 m above. Over a full internal wave period all of the sediments will on average be in contact with the sediment 1 m above the equilibrium depth for half the period. Hence, ΔT equals the temperature difference between the sediment temperature 1 m above (i.e. the water temperature of Sweers profile 1 m above) and the water temperature at the equilibrium depth. Sediment area, A, was estimated as the difference in areas between the equilibrium depth and 1 m above.

The mechanism accounted for <5% of the heat flux across the thermocline from March-May. Approximately 5-10% of the heat flux from July-September was attributed to the mechanism during 1990-1991 and 1993-1994. The high heat flux across the thermocline in 1989 and 1992 decreased the relative importance of the mechanism. Eddy diffusivities reported here are only corrected for solar heating, but calculations of heat transfer across the thermocline via the mechanism proposed by Dutton and Bryson (1964) suggests further investigation.

Solar heating below the thermocline was low in the winter and early spring due to low seasonal insolation and high water turbidity with PAR extinction coefficients ≈1 m^{-1}. With the onset of thermal stratification, water clarity increased (≈0.3 m^{-1}) from zooplankton grazing. A higher percent of incident PAR penetration below the thermocline resulted in significant solar heating from June-August for most years (i.e. >10%). Solar heating accounted for a smaller proportion of heating below the thermocline in 1992 (*ca.* 4%) because the mixed-layer depth was greater throughout the season. Solar heating accounted for an average of 19% of the 1982-1990 heat flux below the maximum temperature gradient (Jellison and Melack 1993*a*). The higher solar heating contribution in 1982-1990 was caused by a combination of relatively shallow mixed-layer depths and low heat content changes below the thermocline during the 6 year period of meromixis (1983-1988). Hence, the relative importance of solar heating was greater during meromixis.

Minimum diffusivities generally occurred at or just below the thermocline and ranged from >1.0×10^{-5} to 2.3×10^{-7} $m^2\ s^{-1}$ at the thermocline from April-September over the six years (Fig. 11). Maximum seasonal diffusivities at the thermocline occurred during weaker stratification and shallow thermocline depths during the spring (April-May). Minimum seasonal diffusivities from July-September generally corresponded to the period of strong thermal stratification. An interannual comparison of the seasonal trends in diffusivities can be partly explained by seasonal wind speed (Fig. 11), conductivity dynamics, and water column stability. The seasonal wind speed is the average of daily wind speeds over the central difference interval of the eddy diffusivity estimate.

The highest rates of summer vertical mixing occurred during 1989 (4.19×10^{-6} $m^2\ s^{-1}$, SE=1.87×10^{-6}) from the rapid onset and persistence of inverse chemical stratification from drought conditions which resulted in the lowest water column stability of the six years (estimated ≈1 kg m^{-3} density difference across pycnocline). Low wind speeds from March-April, 1990 led to the development of strong thermal stratification by May, 1990. Low diffusivity estimates through mid-June (<3.0×10^{-6} m^2 s^{-1}) were calculated though wind speeds were high in May. The low 1990 summer vertical mixing estimates (1.06×10^{-6} m^2 s^{-1}, SE=9.27×10^{-7} June-September) resulted primarily from a persistent sharp thermocline that deepened <2 m during June-July. June-July had high discharge (>7 cm $month^{-1}$) which led to only a 5 cm drop in lake level and a low rate of mixed-layer evaporative concentration. Hence, density stratification during June-July, 1990 was likely strong as inverse salinity stratification had not significantly decreased the density difference across the pycnocline. Similarly, in 1991 only a 5 cm lake level drop from the April annual maximum delayed significant evaporative concentration of the mixed-layer until August which resulted in a moderately low average summer diffusivity estimate (1.41×10^{-6} m^2 s^{-1}, SE=9.44×10^{-7}). The coarse temporal resolution of the 1991 profiles in March-April likely overestimated the average spring diffusivity (8.11×10^{-6} m^2 s^{-1}, SE=1.77×10^{-6}) during a period of substantial thermocline deepening; however, wind speeds were high.

Low wind speeds in April-May, 1992 resulted in relatively low average spring vertical mixing estimates by mid-May (4.16×10^{-6} m^2 s^{-1}, SE =2.07×10^{-6}). The early onset of unstable salinity profiles in April, 1992, led to weak stratification (June-September) with higher summer vertical mixing rates (1.67×10^{-6} m^2 s^{-1}, SE=7.90×10^{-7}) than 1991. The lowest diffusivity estimate over the six years was calculated in early August, 1992 which coincided with low wind speeds over the central difference time interval. During April-May, 1993, wind speeds were high and resulted in relatively high spring vertical mixing estimates (5.65×10^{-6} m^2 s^{-1}, SE=2.45×10^{-6}) even though the lake was strongly stratified from stable salinity stratification. The 1993 average summer diffusivity (9.53×10^{-7} m^2 s^{-1}, SE = 4.75×10^{-7}) across the thermocline from June-September was slightly lower than 1990 with a lower variance. An increase in the mid-August, 1993 diffusivity coincided with higher wind speeds. Compared to other years, the 1994 spring wind speeds were low and diffusivities were low in the spring (3.40×10^{-6} m^2 s^{-1}, SE=1.03×10^{-6}). The 1994 average summer diffusivity (1.63×10^{-6} m^2 s^{-1}, SE=6.54×10^{-7}) was nearly equivalent to 1992 even though average wind speeds over the central difference intervals were lower.

Mean diffusivities during the summer (June-September) were compared across years with *t*-tests because the Kolmogorov-Smirnov test detected no departures from normality within individual summers. Mean summer thermocline diffusivity in 1989 was significantly ($P<0.05$) higher than all other years. The mean for 1993 was significantly lower than 1992 ($P < 0.1$) and 1994 ($P<0.05$). No significant differences in mean summer diffusivities were detected between years 1990, 1991, 1992, and 1994.

Eddy diffusivities at the thermocline during strong stratification ($N^2>1.6 \times 10^{-3}$ s^{-2}, mainly from May-September) were compared to the Brunt-Väisälä frequency N, where $N^2 = (g\,\rho^{-1})(\delta\rho\;\delta z^{-1})$. The log-log regression of diffusivities on N^2 was

$$K_Z = 4.0x10^{-8}(N^2)^{-0.68}, \qquad r^2=0.27,\ n = 35.$$

If average wind speed over the central difference interval is added as an independent variable the log-log regression was

$$K_Z = 8.9x10^{-9}(WS)^{0.89}(N^2)^{-0.75}, \qquad r^2=0.44,\ n = 35.$$

Dissolved Oxygen, Ammonia, and Upward Ammonia Flux

Except for 1989 the seasonal oxygen dynamics were similar each year with hypolimnetic anoxia within a month of the onset of seasonal stratification and an entirely oxygenated water column during holomixis (Fig. 12). The winter 1989 dissolved oxygen remained near zero following the breakdown of 6 years of meromixis when a large reservoir of reduced solutes that accumulated during meromixis were mixed throughout the water column. Maximum seasonal mixed-layer dissolved oxygen (> 7 mg L^{-1}) corresponded with cool spring temperatures and the spring algal bloom. Temperature increases and zooplankton accumulation resulted in low summer mixed-layer oxygen (<4 mg L^{-1}). During the fall, dissolved oxygen increased as mixed-layer temperatures decreased and fall algal blooms occurred.

During winter holomixis, the highest ammonia values 45-50 μM were measured in the 1988-1989 winter after the breakdown of meromixis (Fig. 12). Ammonia was also high (25-30 μM) during the 1989-1990 holomictic period. Ammonia was <10 μM during the last four holomictic periods which indicates the influence of meromixis on the ammonia dynamics had ended after two years of monomixis.

The 1989 epilimnetic ammonia concentrations decreased temporarily from April-June (<10 μM) during a period of high algal production, but then increased through the summer as the brine shrimp, *Artemia*, converted algal particulate nitrogen via grazing and excretion (Jellison *et al.* 1993). Ammonia concentrations increased to 30 μM by December. The 1990 ammonia dynamics were similar to 1989 with lower concentrations.

The 1991-1994 ammonia dynamics were no longer influenced by the 1983-1988 meromictic event and were similar to each other. December-February ammonia concentrations were nearly equivalent throughout the water column except in 1993 where the onset of seasonal salinity stratification in January resulted in an earlier accumulation of ammonia. Mixed-layer ammonia concentrations decreased to <2 μM at the onset of thermal stratification each year which coincided with the spring algal bloom. Mixed-layer ammonia concentrations increased to 6-15 μM in May after the spring bloom. The 1991-1992 mixed-layer ammonia concentrations remained greater than 5 μM from June-September whereas the 1993-1994 concentrations were less than 5 μM. Hypolimnetic ammonia concentrations increased with the onset of strong stratification until August to October, depending on the year. Maximum hypolimnetic ammonia concentrations ranged from 35 μM in 1991 to 60 μM in 1994 at 26 m (average of 24 and 28 m samples).

The ammonia flux from March-May (spring) and June-September (summer) ranged over a hundred fold through the six years (Fig. 13). During the spring and summer of 1989 high vertical mixing rates and large ammonia gradients resulted in the largest upward ammonia flux of the six years. Spring flux estimates were relatively large in 1992 and 1993 primarily from high eddy diffusivities. Even though the 1991 spring diffusivities were large, the 1991 spring flux estimate was low from low ammonia gradients. High spring wind speeds delayed the onset of strong thermal stratification with a subsequent lag in the buildup of hypolimnetic ammonia. The lowest ammonia flux estimate occurred during the spring, 1994, primarily from low to negative ammonia gradients across the seasonal pycnocline.

The largest summer flux estimates in 1990 and 1992 were primarily caused by large ammonia gradients. Higher 1990 ammonia concentrations relative to 1991 to 1994 suggest a lingering influence of the six year meromictic episode (1983-1988). The lowest summer flux estimate in 1993 was primarily from low eddy diffusivity estimates. In summary, over the six years, ammonia fluxes varied from 10.3 mmol m^{-2} day^{-1} (1989) to 0.045 mmol m^{-2} day^{-1} (1994) in the spring and from 2.2 mmol m^{-2} day^{-1} (1989) to 0.12 mmol m^{-2} day^{-1} (1993) in the summer.

Discussion

Ectogenic meromixis from 1982-1988 and the present event initiated in 1995 appear to be rare events in Mono Lake. The low lake elevations and high salinities prior to the onset of meromixis resulted in larger lake level increases and greater dilution of the near surface water column than at higher lake levels for equivalent freshwater inputs (Jellison and Melack 1993*a*). Simulations with a one-dimensional vertical mixing model with a range of hydrology scenarios derived from a fifty year hydrological record verified that low lake levels are more likely to result in ectogenic meromixis during anomalously wet years (Chapter 2).

Monomixis has been documented in Mono Lake in the mid-1960s (Mason 1967) and from 1976-1982 (Winkler 1977, Lenz 1982, Melack 1983). Consistently falling lake level since 1947 (*ca.* 0.4 m yr^{-1}) implies that the lake has been monomictic over the past 50 years except for 1982-1988 and the ongoing meromictic events. The 1989-1994 period of monomixis will likely represent the lowest 'modern' lake levels as the implementation of a new water policy for the Mono Basin will maintain the minimum lake level *ca.* 5 m higher than the average surface elevation over this study period. Hence, it is likely the 1989-1994 period will have had the highest 'modern' salinities.

Even though Mono Lake's surface elevation fluctuated over a small 1.25 m range from 1989-1994, the bathymetry and high salinity of Mono Lake (*ca.* 94 g L^{-1}) resulted in strong linkages between freshwater inputs (Fig. 3), salinity dynamics (Fig. 4), and seasonal vertical water column stability (Fig. 7). Suppose at a lake elevation of 1943 m the lake level decreases by 20 cm while the mixed-layer depth remains fixed at 1933 m (an initial 10 m mixed-layer depth). The mixed-layer volume would decrease 2.8% which would increase the salinity by 2.5 g L^{-1}; a 15 m initial mixed-layer would decrease the mixed-layer volume by 1.7%. Hence, relatively small lake level fluctuations during the stratified period can cause large variations in the mixed-layer salinity and total water column stability. The conductivity difference between the mixed-layer (C_{ML}) and hypolimnion (C_H) ranged from unstable stratification (C_{ML}-1.5=C_H mS cm^{-1}) to moderately stable stratification (C_{ML}+0.7= C_H mS cm^{-1}) over the six years of monomixis. Salinity stratification varied the density difference across the pycnocline over a 3 kg m^{-3} range (-2.0 to 1.0 kg m^{-3}) nearly equivalent to the 3-4 kg m^{-3} maximum density increase across the thermocline from temperature during strong thermal stratification from July to September. Variations in mixed-layer salinity dynamics were primarily a function of lake level fluctuations driven by the water flux at the surface.

Anati and Stiller (1991) provided evidence for salt fingering in the Dead Sea during the late summer and early winter. Conditions were similar to those observed in Mono Lake and calculations suggest salt fingering to be a likely phenomena. In Mono Lake, salt fingering appears to be variable in time and space throughout most of the period when salt fingering is likely (August-

September). However, in October and November, basin scale layers formed by salt fingers are likely since mixed-layer deepening maintains a sharp thin interface across the entire pycnocline. Diffusivity estimates (1×10^{-6} to 1×10^{-5} $m^2\ s^{-1}$) derived from simple assumptions indicate that salt fingering may be a significant hypolimnetic mixing mechanism from August to holomixis.

Salt fingering has been documented in various regions throughout the world's oceans; examples include the northwestern Pacific (Miyake *et al.* 1995), the equatorial Pacific (Miller and Browning 1974), the northeastern Atlantic (Tait and Howe 1971), the Atlantic in the Sargasso Sea near Bermuda (Cooper and Stommel 1968), and the Caribbean Sea (Lambert and Sturges 1977). Average temperature and salinity steps across salt finger interfaces are remarkably similar throughout the world's oceans, 0.2-0.5 °C and 0.02-0.10 g kg^{-1}. In Mono Lake, the range of estimated temperature and salinity steps was similar to oceanographic cases, 0.2-0.7 °C and 0.03-0.1 g kg^{-1}. However, homogeneous convective layers between interfaces are >10 m thick in oceans, whereas in Mono Lake they are <5 m. Interface thickness in oceans are ≈5 m, much larger than the interface thickness observed in the 1991 and 1994 October profiles in Mono Lake (≈0.5-1 m). Estimated salt finger effective diffusivities in oceans used gradients calculated over the interface thickness (Boyd and Perkins 1987, Miyake *et al.* 1995) with values of $K_S^Z = 1.1\text{-}1.7\times10^{-3}$ $m^2\ s^{-1}$ and $K_T^Z = 4\text{-}7\times10^{-3}\ m^2\ s^{-1}$ which are a factor of 1000 greater than the Mono Lake estimates. However, we assumed a 0.3 m interface thickness during presumed periods of active salt finger mixing when the empirical flux equations are valid. For 2-5 m thick interfaces that are typical of ocean thermohaline staircases, Kunze (1987) showed that fluxes depend on interface thickness and are at least an order of magnitude smaller than the empirical flux equations used here. The ratio of oceanic salt:heat effective diffusivities is ≈3, slightly lower than the range we calculated for Mono Lake of 3-8.

Monomictic average summer diffusivities at the thermocline excluding 1991 calculated in the same manner as Jellison and Melack (1993*a*) with a 3 point moving Sweers temporal average ranged from 1.1×10^{-6} (1990, 1993) to 4.0×10^{-6} m^2 s^{-1} (1989). During meromictic years with high stability (1982-1984, 1986-1987), average summer (June-September) diffusivities at the thermocline ranged from 2×10^{-7} to 7×10^{-7} m^2 s^{-1} (Jellison and Melack 1993*a*). Conductivity differences between 2 and 28 m during meromixis varied from ≈5 to >10 mS cm^{-1} and density differences were > 5 kg m^{-3}, much greater than during monomixis.

Comparison of the 1991-1994 and the 1983-1990 estimates of the theoretical relationship between eddy diffusivity and Brunt-Väisälä frequency in the form, $K_z = a(N^2)^m$, where a is a measure of the general magnitude of turbulence and m depends on mode of turbulence generation, support the conclusions of Jellison and Melack (1993*a*). Comparisons of the general magnitude of turbulence, m, for the two periods was evaluated by setting $m = -0.58$ which resulted in $a = 7.0 \times 10^{-8}$ (r^2=0.27, n=35). Higher water column stability during meromixis resulted in a lower magnitude of turbulence from 1983-1990 (a=4.9×10^{-8}) than 1991-1994. Both periods also indicate that the dominant mode of turbulence generation at the thermocline is from local shear since m lies closer to -0.5 (-0.58 (1983-1990), -0.68 (1991-1994)) than -1 when turbulence is generated by large-scale horizontal eddies cascading down to smaller eddies (Welander 1968).

A significant linkage between salinity stratification and summer vertical mixing occurred only for drought conditions in 1989 and above average hydrological inputs in 1993. In 1989 a falling lake level throughout the year likely led to the early onset of unstable salinity stratification by May and the highest vertical mixing rates of the six years. Stable salinity stratification throughout 1993 resulted in significantly lower diffusivity estimates during the summer (June-September) than 1992 or 1994.

Not surprisingly, the explained variance increased with the addition of wind speed as an independent variable to the log-log regression of diffusivities on N^2. Shear induced mixing below the mixed-layer of most lakes is generally small (Munnich *et al.* 1992), however, the bathymetry of Mono Lake (large surface area to volume ratio) may result in significant shear-induced interior diapycnal mixing during periods of high winds and large amplitude internal waves. Further, internal waves can cause significant boundary mixing (Gloor *et al.* 1994). The vertical modal structure and amplitudes of internal waves and lake bathymetry (e.g. surface to volume ratio) are the primary determinants of the importance of boundary mixing in a particular lake (Wüest *et al.* 1994). As mentioned earlier in the evaluation of the Dutton and Bryson (1964) mechanism, internal waves of significant amplitude have been measured in Mono Lake. Further, the large surface to volume ratio suggests that boundary mixing is likely important in Mono Lake. Though the wind speed independent variable added to the Welander expression was an average over many days, it is a measure of high wind periods that may have caused significant internal wave activity.

The lake number, L_N, has been shown by Imberger and Patterson (1990) to be an indicator of mixing below the base of the mixed-layer and is defined as:

$$L_N = \frac{gS_t(1 - {z_t}/{H})}{\rho_0 u_*^2 A_0^{1.5}(1 - {z_g}/{H})}$$

where g is the gravitational acceleration, S_t is the lake stability, z_t the height to the center of the metalimnion, z_g is height to the center of volume of the lake, u_* is the shear velocity, and A_0 is the lake surface area. For large L_N (>>1), the bottom of pycnocline remains horizontal. For small L_N (<1), the entire pycnocline tilts with the generation of currents below the pycnocline which results in active hypolimnetic mixing and/or upwelling.

L_N from 1991 to 1994 calculated from daily average wind speeds (Fig. 14A) were low (<5) during the majority of every winter and spring except in 1993 (Fig. 14B). Further, several low L_N days resulted from high wind events during the period of strong thermal stratification in 1991, 1992, and 1994. In Figure 14C multi-day averages of L_N indicate that the effect of wind forcing can be significant. Though the 1991 total water column stability was lower than 1994 (Fig. 7), lower August wind speeds in 1991 resulted in higher L_N values.

The relation between K_Z and the average L_N over the central difference interval used to calculate K_Z (Fig. 14D) is,

$$K_Z = 1.5 \times 10^{-5} L_N^{-1.1} \qquad r^2=0.68, n=43,$$

excluding the spring, 1993 eddy diffusivity estimates. The relation derived here is similar to the relation used in Chapter 2 where eddy diffusivity was dependent on $L_N^{-0.8}$. The spring, 1993 eddy diffusivity estimates indicate that enhanced mixing resulted during periods of moderate L_N. Wind speeds during spring, 1993 were significantly higher than any other period during the four years and likely reflect the interaction between wind forcing, vertical water column density structure, and internal wave dynamics. Nearly linear stratification in the upper 10-15 m of density profiles during the winter and spring of 1993 was measured, unlike 1991, 1992, and 1994 which may have been a factor in the higher diffusivity estimates.

Comparison of the average annual upward ammonia flux during the thermally stratified period from 1983 to 1994 is given in Table 3. Except during 1983, average ammonia gradients were much larger during meromixis from the accumulation of ammonia in the monimolimnion. Eddy diffusivities from 1984 to 1987 were much lower than any monomictic years. However, only the 1986 ammonia flux estimate was substantially lower than any monomictic estimate. During meromixis large ammonia gradients relative to monomixis resulted in similar or greater flux estimates. Hence, the effect of lower rates of vertical mixing during meromixis is compensated by larger ammonia gradients which result in similar upward ammonia fluxes as monomictic periods.

The response of nutrient availability in hyposaline, large, and deep Pyramid Lake, Nevada has been evaluated over a range of climatic conditions. 'Temporary' meromixis in Pyramid Lake resulted in large algal blooms of N_2-fixing blue-greens during periods of above average fluvial discharge from incomplete winter mixing (Galat and Verdin 1988). During the 1990-1992 drought with low allochthonous nitrogen inputs into Pyramid Lake climatic variations were found to affect N availability by altering the timing of winter deep mixing, varying the potential for upwelling, and varying the rate of spring warming of surface waters (Lebo *et al.* 1994).

In Mono Lake the linkage between the upward nutrient flux and hydrologic variations during small variations in lake levels (*ca.* 1.25 m range over 6 years, 0.5 m maximum seasonal increase) produced a similar range of summer nutrient conditions that Pyramid Lake underwent for much larger variations (i.e. record high fluvial discharge to drought conditions). For example, dry 1992 resulted in higher summer vertical mixing and relatively large ammonia fluxes from the early onset of unstable salinity stratification, whereas during relatively wet 1993, persistent stable salinity stratification led to low summer ammonia fluxes across the thermocline. However, biological factors complicate the relation between vertical mixing and the upward ammonia flux. In 1994, low spring and low summer ammonia fluxes were estimated mainly from negative ammonia gradients in the pycnocline region throughout stratification. Negative ammonia gradients were likely caused by a large metalimnetic population of photosynthetic bacteria. Further, elevated ammonia concentrations after the breakdown of meromictic events as in 1990 can cause large upward fluxes even during low vertical mixing periods from large ammonia gradients.

References

Anati, D.A. and M. Stiller. 1991. The post-1979 thermohaline structure of the Dead Sea and the role of double-diffusive mixing. Limnol. Oceanogr. 36:342-354.

Boyd, J.D. and H. Perkins. 1987. Characteristics of the thermohaline steps off the northeast coast of South America, July 1983. Deep-Sea Res. 34:337-364.

Brutsaert, W. 1982. Evaporation in the atmosphere. D. Reidel. Dordrecht.

Cooper, J.J. and D.L. Koch. 1984. Limnology of a desertic terminal lake, Walker Lake, Nevada, U.S.A. Hydrobiologia 118:275-292.

Cooper, J.W. and H. Stommel. 1968. Regularly space steps in the main thermocline near Bermuda. J. Geophys. Res. 73:5849-5854.

Dutton, A.D. and R.A. Bryson. 1964. Heat flux in Lake Mendota. Limnol. Oceanogr. 7:80-97.

Galat, D.L. and J.P. Verdin. 1988. Magnitude of blue-green algae algal blooms in a saline desert lake evaluated by remote sensing: evidence for nitrogen control. Can. J. Fish. Aquat. Sci. 45:1959-1967.

Gloor, M., A. Wüest, and M. Münnich. 1994. Benthic boundary mixing and resuspension induced by internal seiches. Hydrobiologia 284:59-68.

Imberger, J. 1982. Reservoir dynamics modelling, p. 223-248. *In* E.M. O'Loughlin and P. Cullen [ed.], Prediction in water quality. Australian Academy of Science.

Imberger, J. and J.C. Patterson. 1990. Physical limnology. Adv. Appl. Mech. 27:303-475.

Imberger, J., J.C. Patterson, B. Hebbert, and I. Loh. 1978. Dynamics of reservoir of medium size. ASCE Hydr. Div. 104:725-743.

Imboden, D.M. and A. Wüest. 1995. Mixing mechanisms in lakes, p. 83-135. *In.* A. Lerman, D.M. Imboden, and J.R. Gat [ed.], Physics and Chemistry of Lakes. Springer-Verlag.

Jassby, A. and T. Powell. 1975. Vertical patterns of eddy diffusion during stratification in Castle Lake, California. Limnol. Oceanogr. 20:530-543.

Jellison, R. and J.M. Melack. 1993*a*. Meromixis in hypersaline Mono Lake, California. 1. Stratification and vertical mixing during the onset, persistence, and breakdown of meromixis. Limnol. Oceanogr. 38:1008-1019.

Jellison, R. and J.M. Melack. 1993*b*. Algal photosynthetic activity and its response to meromixis in hypersaline Mono Lake, California. Limnol. Oceanogr. 38:818-837.

Jellison, R., L.G. Miller, J.M. Melack, and G.L. Dana. 1993. Meromixis in hypersaline Mono Lake, California. 2: Nitrogen fluxes. Limnol. Oceanogr. 38:1020-1039.

Kunze, E. 1987. Limits on growing, finite length salt fingers: a Richardson number constraint. J. Mar. Res. 45:533-556.

Lambert, R.B. and W. Sturges. 1977. A thermohaline staircase and vertical mixing in the thermocline. Deep-Sea Res. 24:211-222.

Lebo, M.E., J.E. Reuter, C.R. Goldman, and C.L. Rhodes. 1994. Interannual variability of nitrogen limitation in a desert lake: influence of regional climate. Can. J. Fish. Aquat. Sci. 51:862-872.

Lenz, P.H. 1982. Population studies on *Artemia* in Mono Lake, California. Ph.D. thesis, Univ. California, Santa Barbara. 230p.

Lowe, P.R. 1977. An approximating polynomial for the computation of saturation vapor pressure. J. Appl. Meteorol. 16:100-103.

Lueck, R.G. 1990. Thermal inertia of conductivity cells: theory. J. Atmos. Ocean. Tech. 7:741-755.

Lueck, R.G. and J.J. Picklo. 1990. Thermal inertia of conductivity cells: observations with a Sea-Bird cell. J. Atmos. Ocean. Tech. 7:756-768.

Mason, D.T. 1967. Limnology of Mono Lake, California. Univ. Calif. Publ. Zool. 83:1-110.

McCree, K.J. 1972. Test of current definitions of photosynthetically active radiation against leaf photosynthesis data. Agric. Meteorol. 10:443-453.

McDougall, T.J. and J.R. Taylor. 1984. Flux measurements across a finger interface at low values of the stability ratio. J. Mar. Res. 42:1-14.

Melack, J.M. 1983. Large, deep salt lakes: a comparative limnological analysis. Hydrobiologia 158:1-14.

Micklin, P.P. 1988. Desiccation of the Aral Sea: a water management disaster in the Soviet Union. Science 241:1170-1176.

Miyake, H., S. Sasaki, H. Yamaguchi, K. Masuda, G. Amma, and Y. Kamei. 1995. Thermohaline staircases in the warm-core ring off Cape Erimo, Hokkaido and their fluxes due to salt finger. J. Ocean. 51:99-109.

Miller, R.R. and D.G. Browning. 1974. Thermal layering between Galapagos Islands and South America. Deep-Sea Res. 21:669-673.

Münnich, M., A. Wüest, and D.M. Imboden, 1992. Observations of the second vertical mode of the internal seiche in an alpine lake. Limnol. Oceanogr. 37:1705-1719.

Patten, D.T., and others. 1987. The Mono Basin ecosystem, effects of changing lake level. National Academy Press, Washington, D.C.

Salhotra, A.M., E.E. Adams, and D.F. Harleman. 1985. Effect of salinity and ionic composition on evaporation: analysis of Dead Sea evaporation pans. Wat. Resour. Res. 21:1336-1344.

Schladow, S.G. 1992. Bubble plume dynamics in a stratified medium and the implications for water quality amelioration in lakes. Wat. Resour. Res. 28:313-321.

Schladow, S.G. 1993. Lake destratification by bubble-plume systems: design methodology. J. Hydr. Engr. 119:350-368.

Stauffer, R.E. 1992. Efficient estimation of temperature distribution, heat storage, thermocline migration and vertical eddy conductivities in stratified lakes. Freshwat. Biol. 27:307-325.

Steinhorn, I. 1985. The disappearance of the long term meromictic stratification of the Dead Sea. Limnol. Oceanogr. 30:451-472.

Steinhorn, I. 1991. On the concept of evaporation from fresh and saline water bodies. Wat. Resour. Res. 27:645-648.

Strickland, J.D.H. and T.R. Parsons. 1972. A practical handbook of seawater analysis, 2nd ed. Bull. Fish. Res. Bd. Can. 167.

Sweers, H.E. 1968. Two methods of describing the "average" vertical temperature distribution of a lake. J. Fish. Res. Bd. Can. 25:1911-1922.

Tait, R.I. and M.R. Howe. 1971. Some observations of thermohaline stratification in the deep ocean. Deep-Sea Res. 15:275-280.

Turner, J.S. 1967. Salt fingers across a density interface. Deep-Sea Res. 14:599-611.

Vorster, P. 1985. A water balance forecast model for Mono Lake. Calif. Water. Resour. Monogr. 10. US Dep. Agric. Forest Serv. Region 5.

Walker, K.F., W.D. Williams, and U.T. Hammer. 1970. The Miller method for oxygen determination applied to saline lakes. Limnol. Oceanogr. 15:814-815.

Welander, P. 1968. Theoretical forms for the vertical exchange coefficients in a stratified fluid with application to lakes and seas. Acta. Regiae. Soc. Sci. Litt. Gothob. Geophys. 1:1-26.

Winkler, D. [Ed.]. 1977. An ecological study of Mono Lake, California. Inst. Ecol. 12. Univ. Calif. Davis.

Wüest, A., D.C. van Senden, J. Imberger, G. Pieplke, and M. Gloor. Diapycnal diffusivity measured by microstructure and tracer techniques: a comparison. Symp. on Turbulent flow, Grenoble. 8 pp.

Table 1. Average monthly Mono Lake evaporation estimates from a one-dimensional vertical mixing model, DYRESM, using the bulk aerodynamic formulae and daily values of wind speed, air temperature, and vapor pressure for the period 1992-1994.

Month	Evaporation rate (cm month^{-1})
January	2.0
February	2.1
March	3.3
April	7.5
May	10.5
June	13.3
July	14.4
August	14.8
September	11.1
October	6.8
November	5.6
December	3.7

Table 2. Relative errors in heat content and eddy diffusivity (K_Z) for profiles derived from the Sweers method (one sampling date and moving average of three sampling dates [3pt]) defined as /(A-B)÷A/ for the following three data sets: standard (stations 6, 30 and 11), three (stations 4, 8 and 9), and all (all stations). Values are percent.

A	B	Heat Content	3pt Heat Content	K_z	3pt K_z
all	standard	1.09	0.83	18.11	6.48
all	three	2.78	1.2	22.39	14.15
standard	three	2.8	1.53	29.90	21.45

Table 3. Comparison of eddy diffusivity, ammonia gradient, and upward ammonia flux during meromixis (from Jellison *et al.* 1993) and monomixis.

Meromixis (1983-1988) Period	Eddy Diffusivity ($m^2 s^{-1}$)	Ammonia Gradient ($mmol\ m^{-4}$)	Upward Ammonia Flux ($mmol\ m^{-2} day^{-1}$)*
23 Mar-14 Sep 83	1.0×10^{-6}	2.8	0.3
5 Apr-20 Oct 84	8.4×10^{-7}	24.4	1.8
22 Mar-23 Aug 85	2.3×10^{-7}	67.5	1.4
14 Mar-14 Oct 86	1.0×10^{-9}#	45.9	0.004
6 May- 14 Nov 87	1.0×10^{-8}	113.2	0.1
22 Apr- 22 Oct 88	2.3×10^{-6}	59.0	11.6

Monomixis (1989-1994) Period	Eddy Diffusivity ($m^2 s^{-1}$)	Ammonia Gradient ($mmol\ m^{-4}$)	Upward Ammonia Flux ($mmol\ m^{-2} day^{-1}$)†
19 Apr-18 Oct 89	8.5×10^{-6}	6.9	5.2
9 Apr-7 Sep 90	1.7×10^{-6}	3.7	0.4
14 Apr-21 Aug 91	5.0×10^{-6}	0.9	0.2
27 Mar-7 Sep 92	3.0×10^{-6}	2.1	0.7
22 Mar-12 Oct 93	3.9×10^{-6}	1.0	0.3
27 Mar-21 Sep 94	3.1×10^{-6}	0.6	0.1

† Ammonia flux calculated from average eddy diffusivity and ammonia gradient over period.

In 1986 no change in heat content was measured beneath the persistent chemocline, thus the estimated upward flux was based on the molecular diffusivity of ammonia (1×10^{-9} $m^2 s^{-1}$).

* Average eddy diffusivity, K_z, and ammonia gradient, $\delta N/\delta z$, shown over period, upward ammonia flux, J_{NH_4}, calculated as:

$$J_{NH_4} = \frac{\sum_{i=1}^{n} K_z t_i \delta N / \delta z}{\sum_{i=1}^{n} t_i}$$

where t_i is the time period between sampling dates.

Figure 1. Mono Lake bathymetry with regular sampling stations (●), secondary sampling stations (▲), and meteorology stations (+).

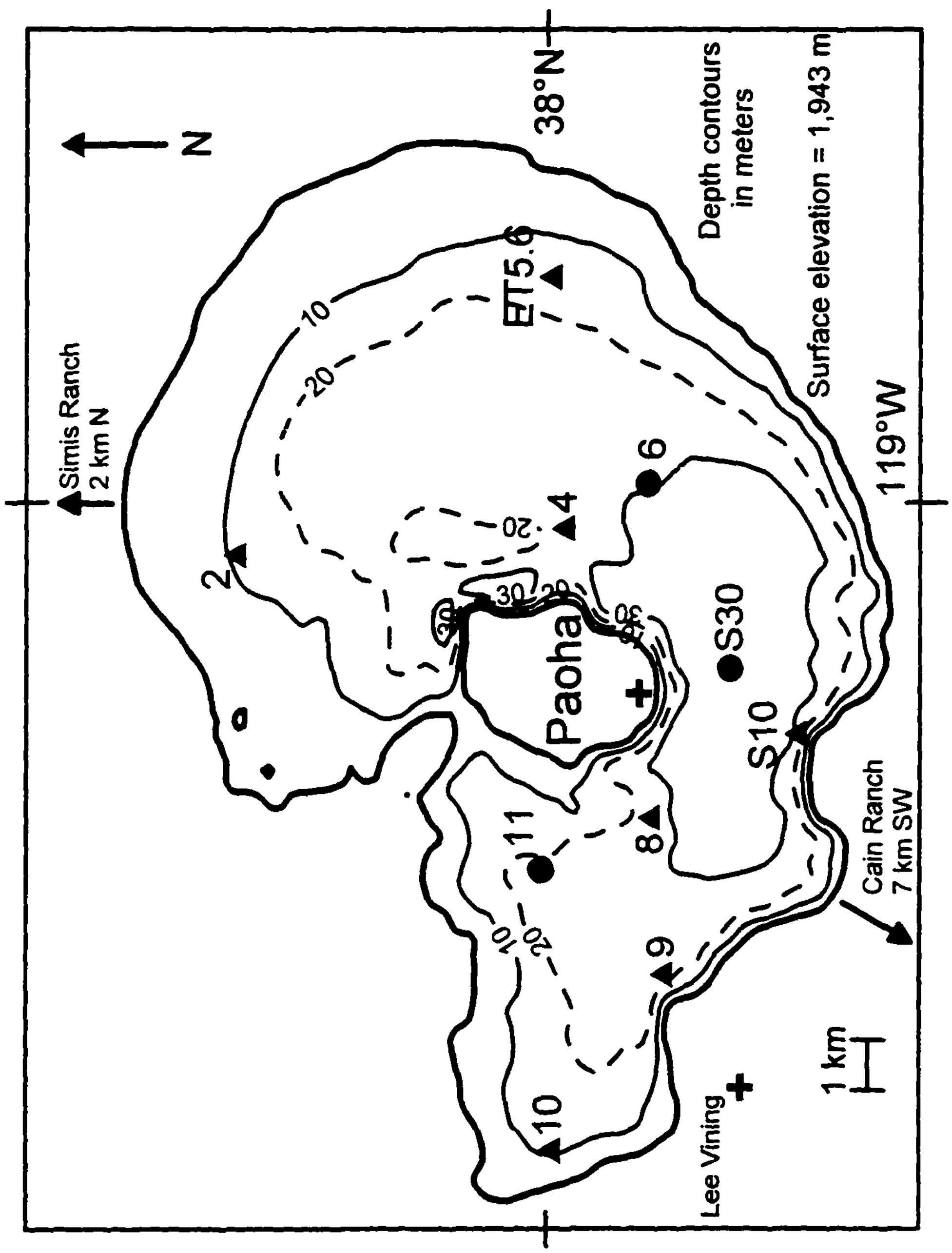
Simis Ranch
2 km N
N
38°N
Depth contours
in meters
Surface elevation = 1,943 m
119°W
ET5.6
10
20
4
6
2
30
Paoha
S30
S10
11
8
9
10
Cain Ranch
7 km SW
Lee Vining
1 km

Figure 2. Mono Lake surface elevation above sea level from January 1, 1970 to December 31, 1995. Vertical arrow indicates onset of meromixis in 1995.

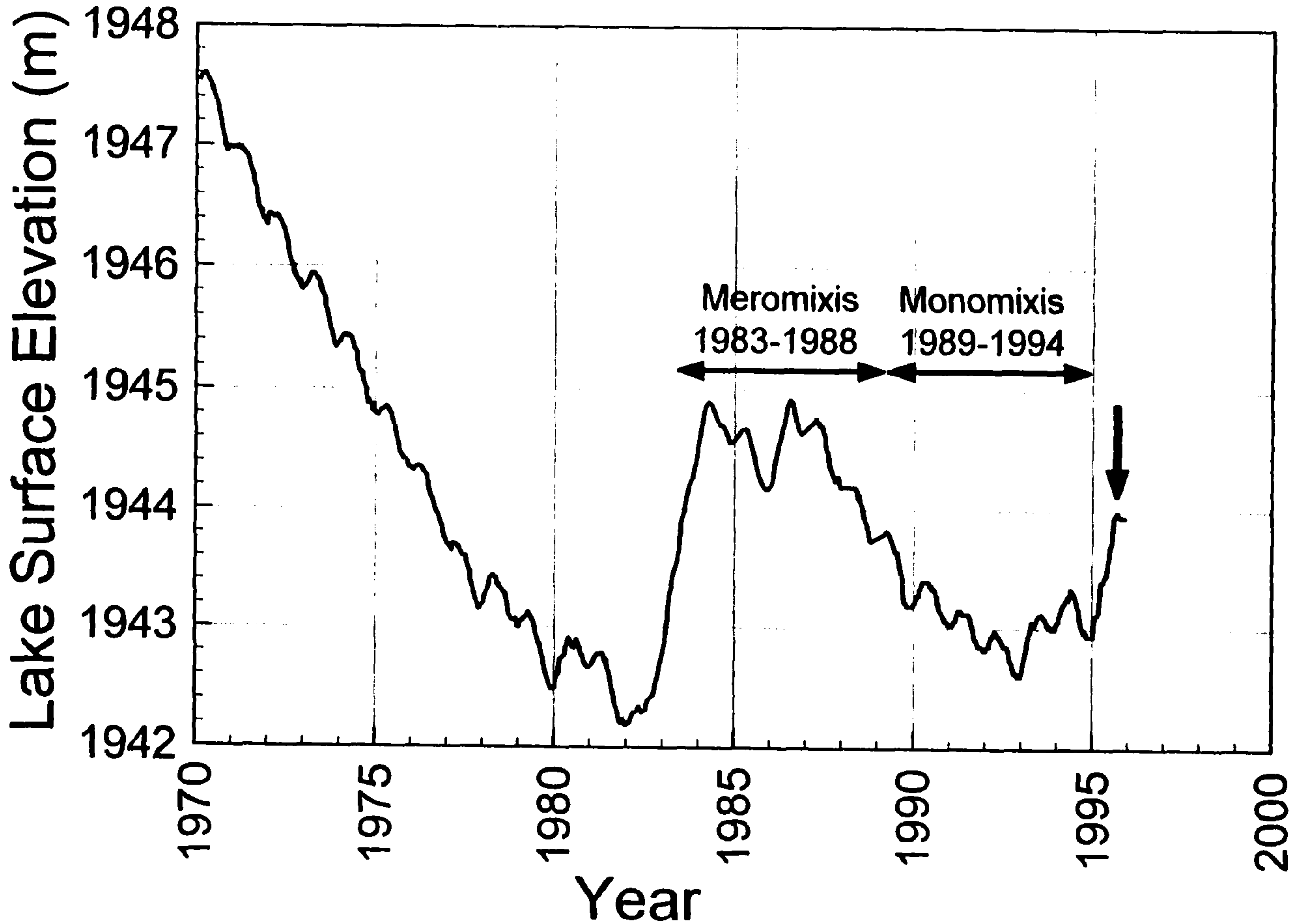
Lake Surface Elevation (m)
1948
1947
1946
1945
1944
1943
1942
1970
1975
1980
1985
1990
1995
2000
Year
Meromixis
1983-1988
Monomixis
1989-1994

Figure 3. January, 1989 to November, 1994 hydrology measurements. Monthly totals of precipitation onto the lake surface derived from Simis Ranch measurements (upper panel). Total monthly stream discharge below diversion points of the five major streams in the Mono Basin (middle panel). Mono Lake surface elevation on the 1st of the month (lower panel).

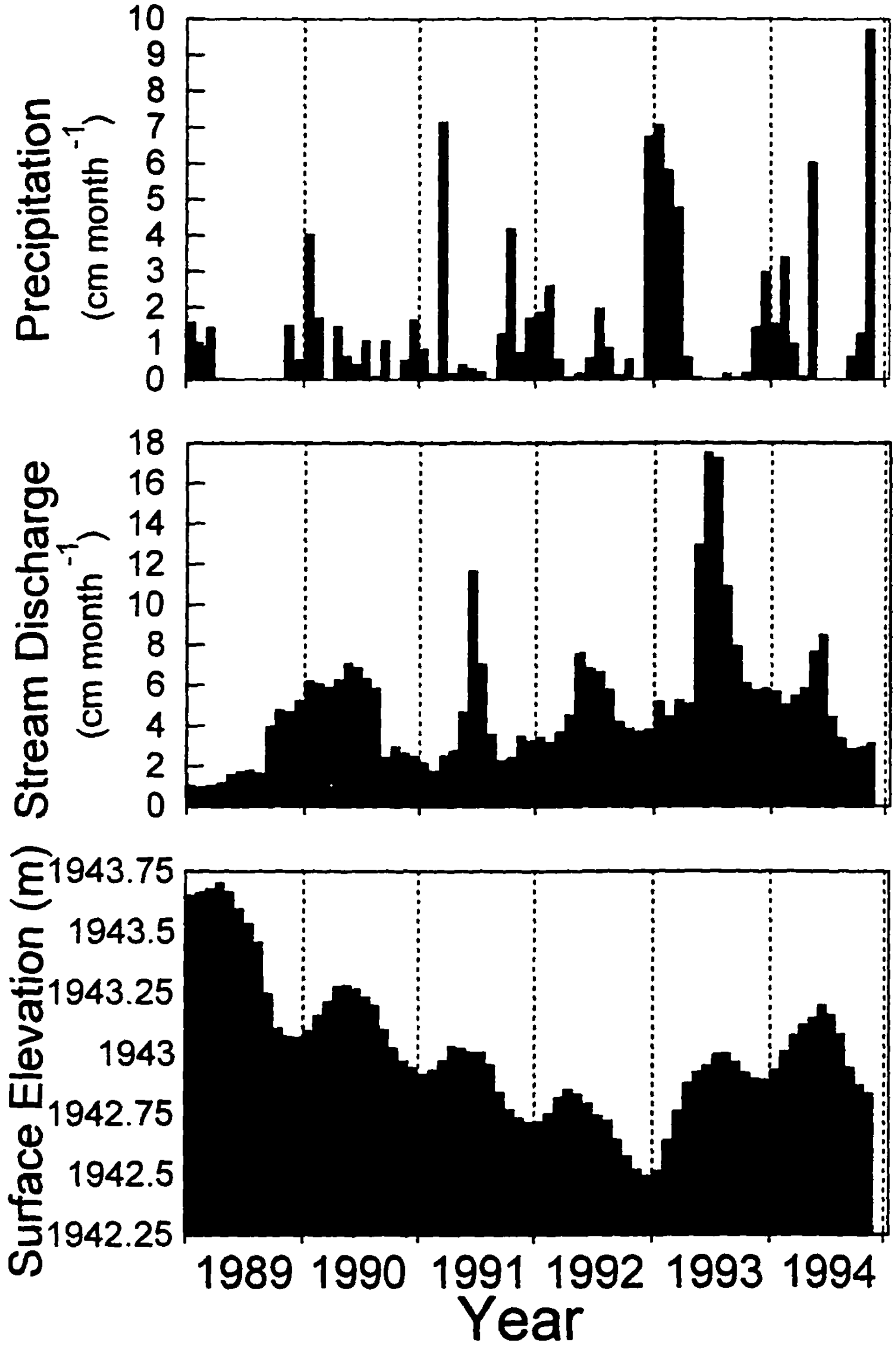

Precipitation (cm month^{-1})
10
9
8
7
6
5
4
3
2
1
0
Stream Discharge (cm month^{-1})
18
16
14
12
10
8
6
4
2
0
Surface Elevation (m)
1943.75
1943.5
1943.25
1943
1942.75
1942.5
1942.25
1989 1990 1991 1992 1993 1994
Year

Figure 4. Selected lake-wide average vertical profiles of conductivity corrected to 25°C from 1992, 1993, and 1994; and isopleths of conductivity from 1991-1994 with 0.3 mS cm^{-1} contour intervals.

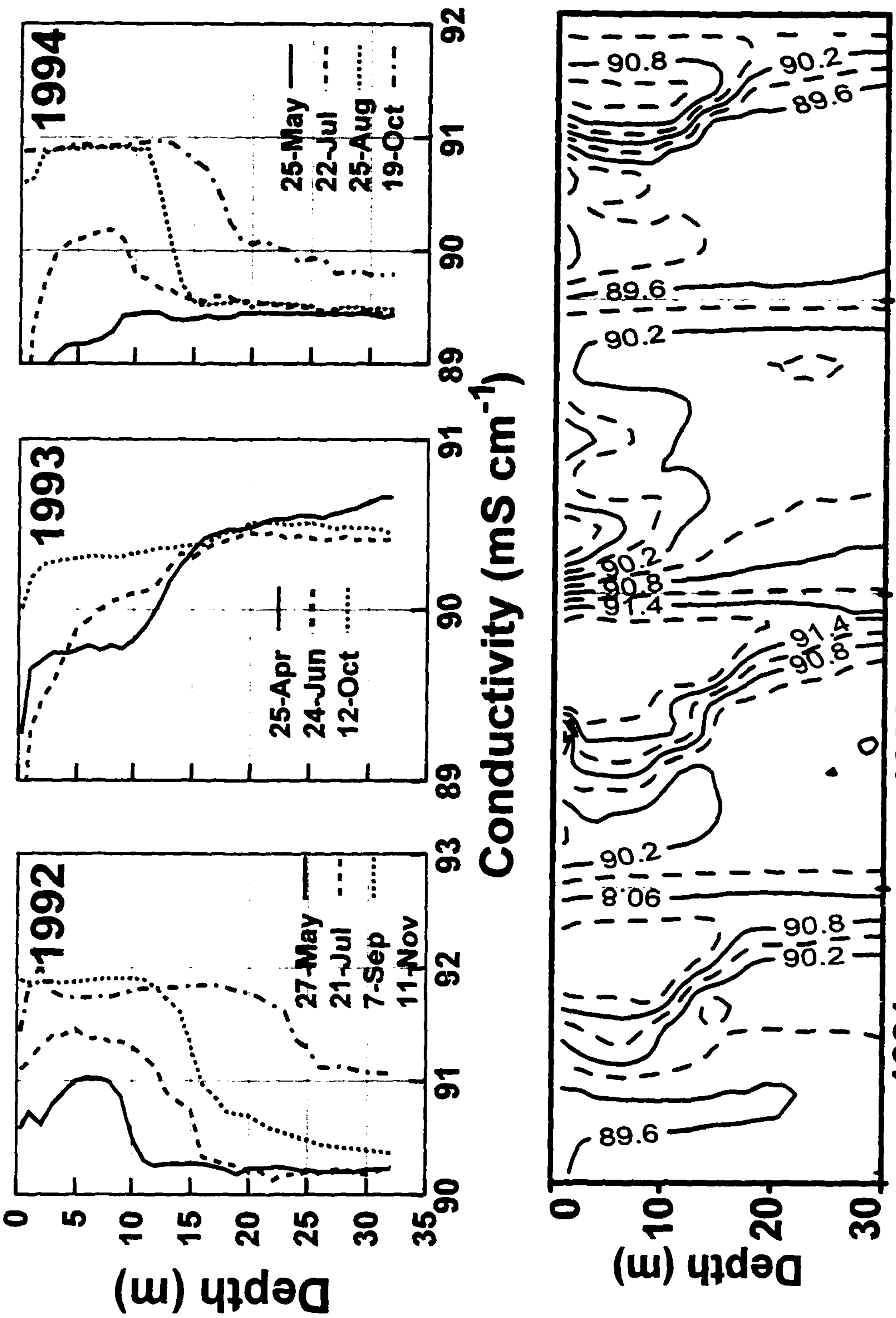
1992
27-May
21-Jul
7-Sep
11-Nov
1993
25-Apr
24-Jun
12-Oct
1994
25-May
22-Jul
25-Aug
19-Oct
Conductivity (mS cm^{-1})
Depth (m)
1991
1992
1993
1994
89.6
90.2
90.8
91.4

Figure 5. Selected lake-wide average vertical temperature (°C) profiles from 1989-1994.

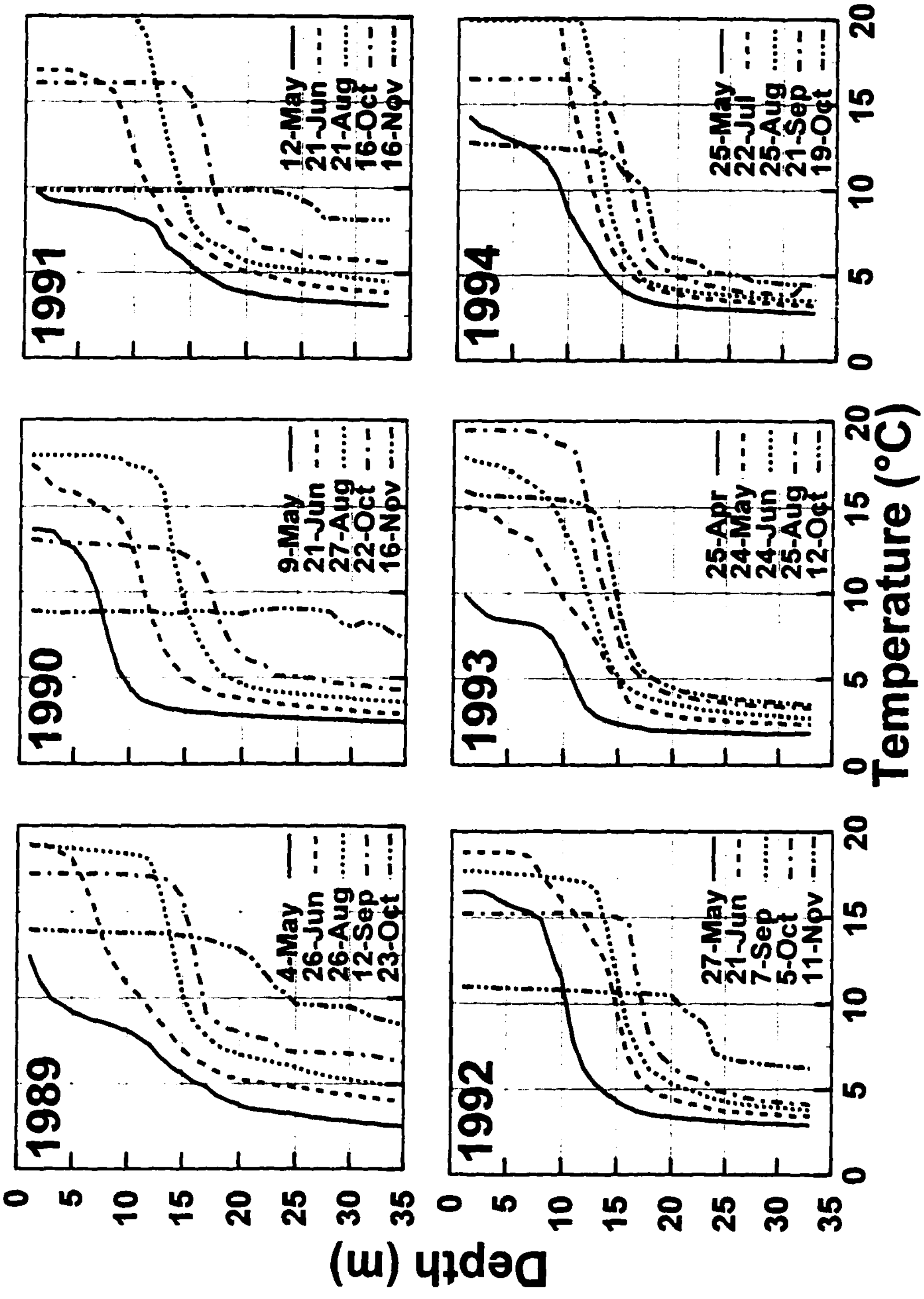
1989
4-May
26-Jun
26-Aug
12-Sep
23-Oct
1990
9-May
21-Jun
27-Aug
22-Oct
16-Nov
1991
12-May
21-Jun
21-Aug
16-Oct
16-Nov
1992
27-May
21-Jun
7-Sep
5-Oct
11-Nov
1993
25-Apr
24-May
24-Jun
25-Aug
12-Oct
1994
25-May
22-Jul
25-Aug
21-Sep
19-Oct
Depth (m)
Temperature (°C)

Figure 6. As Fig. 4 for density-1000 (kg m^{-3}). Isopycnal contour intervals 1 kg m^{-3}.

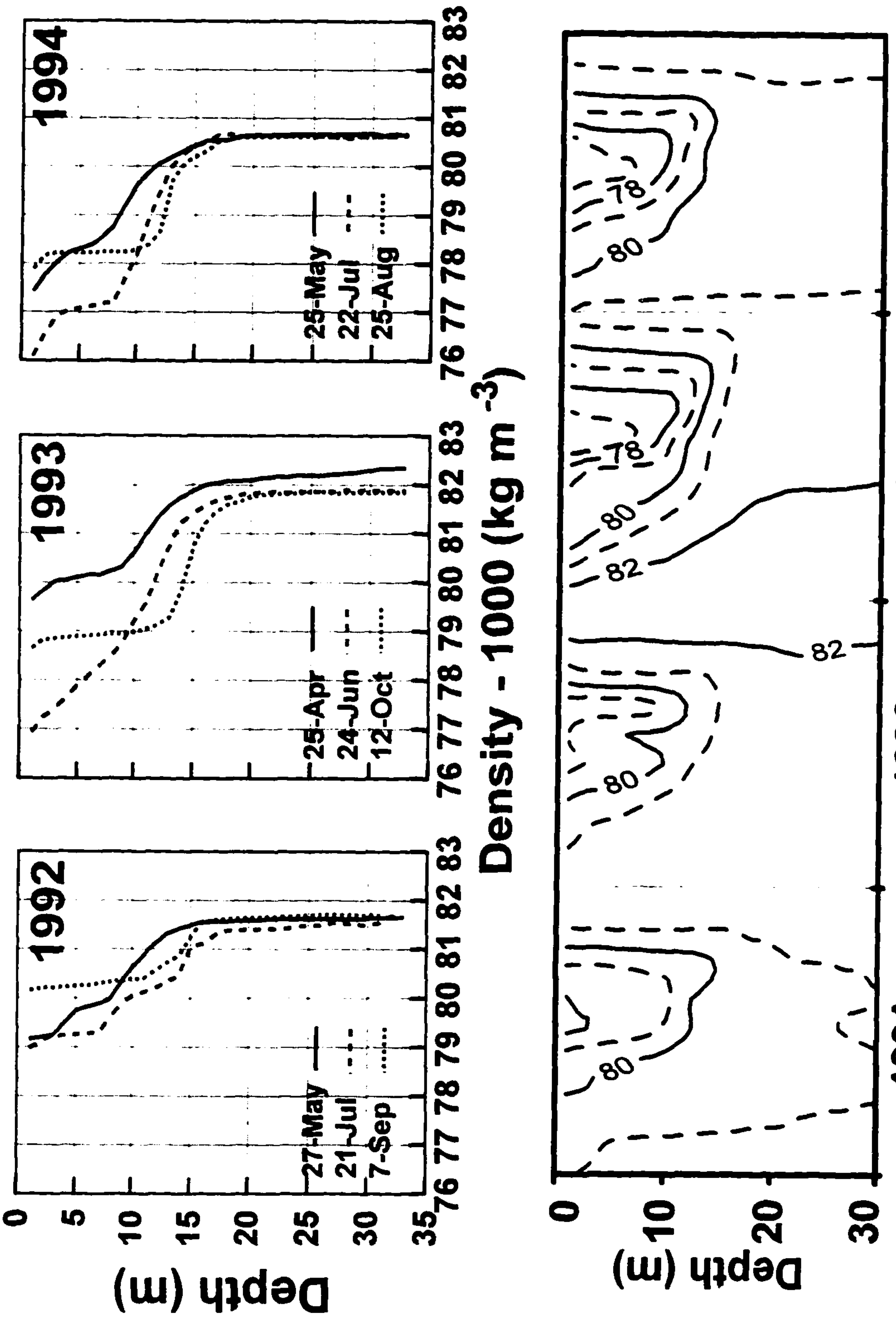
1992
1993
1994
27-May
21-Jul
7-Sep
25-Apr
24-Jun
12-Oct
25-May
22-Jul
25-Aug
76 77 78 79 80 81 82 83
Density - 1000 (kg m-3)
Depth (m)
0 5 10 15 20 25 30 35
80
78
82
1991
1992
1993
1994
0 10 20 30
Depth (m)

Figure 7. Total (•), thermal (□), and saline (◊) stability of the water column from 1991 to 1994. Stability, S_t, defined as the energy required to mix the entire water column against the potential energy of its stratification and calculated as:

$$S_t = \int_0^H (z - z_g) A(z) \rho(z) dz$$

where z is the vertical coordinate from the bottom of the lake, $A(z)$ is the area of the lake at height z, $\rho(z)$ is the water density at z, H is the water depth, and z_g is height to the center of volume of the lake defined as,

$$z_g = \frac{\int_0^H z A(z) dz}{\int_z^H A(z) dz}.$$

Thermal stability computed with 90 mS cm^{-1} isohaline profiles and saline stability computed with 15°C isothermal profiles.

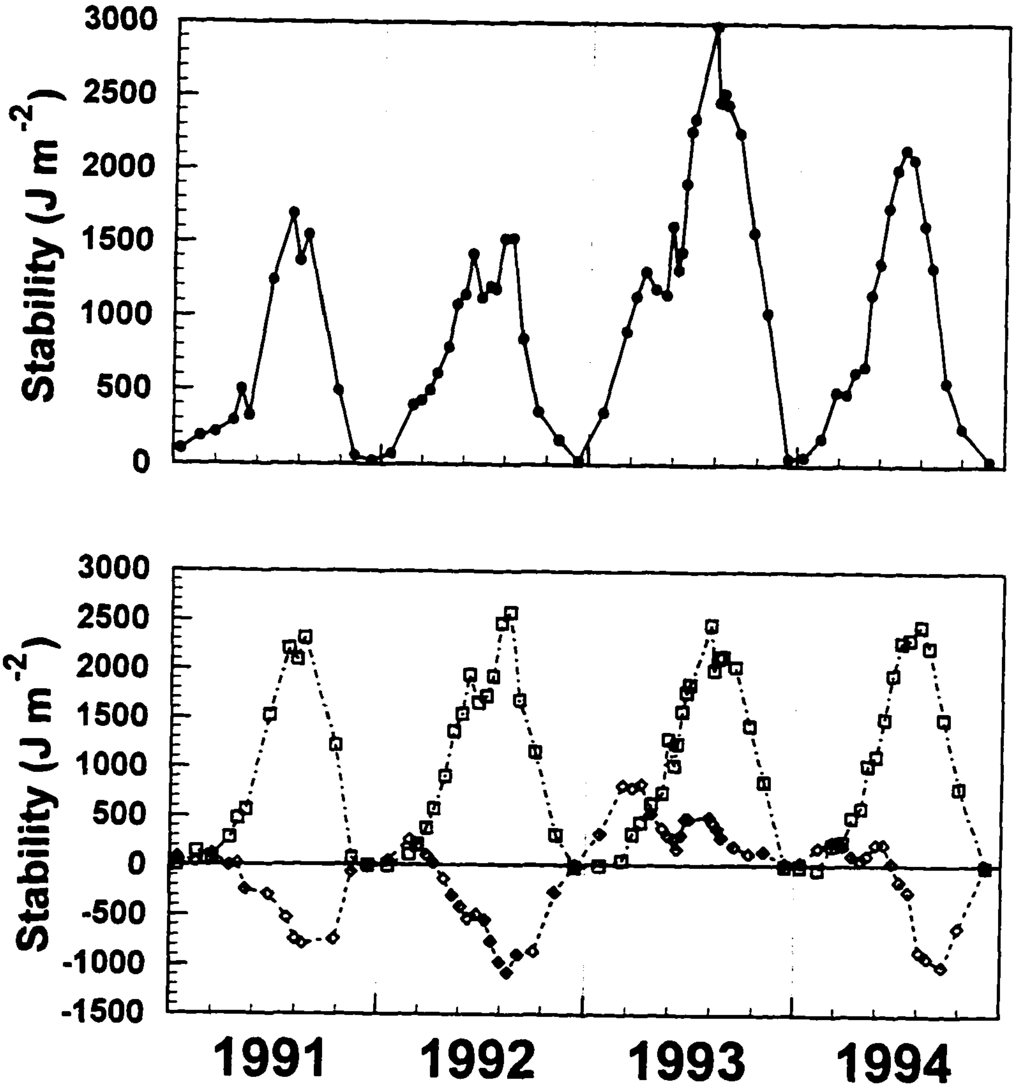

3000
2500
2000
1500
1000
500
0
Stability (J m^-2)
3000
2500
2000
1500
1000
500
0
-500
-1000
-1500
Stability (J m^-2)
1991
1992
1993
1994

Fig. 8. Measurements at 5 (solid line) and 26 m (dotted line) of temperature (°C), conductivity at 25°C (mS cm^{-1}), and density (kg m^{-3}). Conductivity and density values for 1989 and 1990 are averages of 2 and 8 m, and 24 and 28 m.

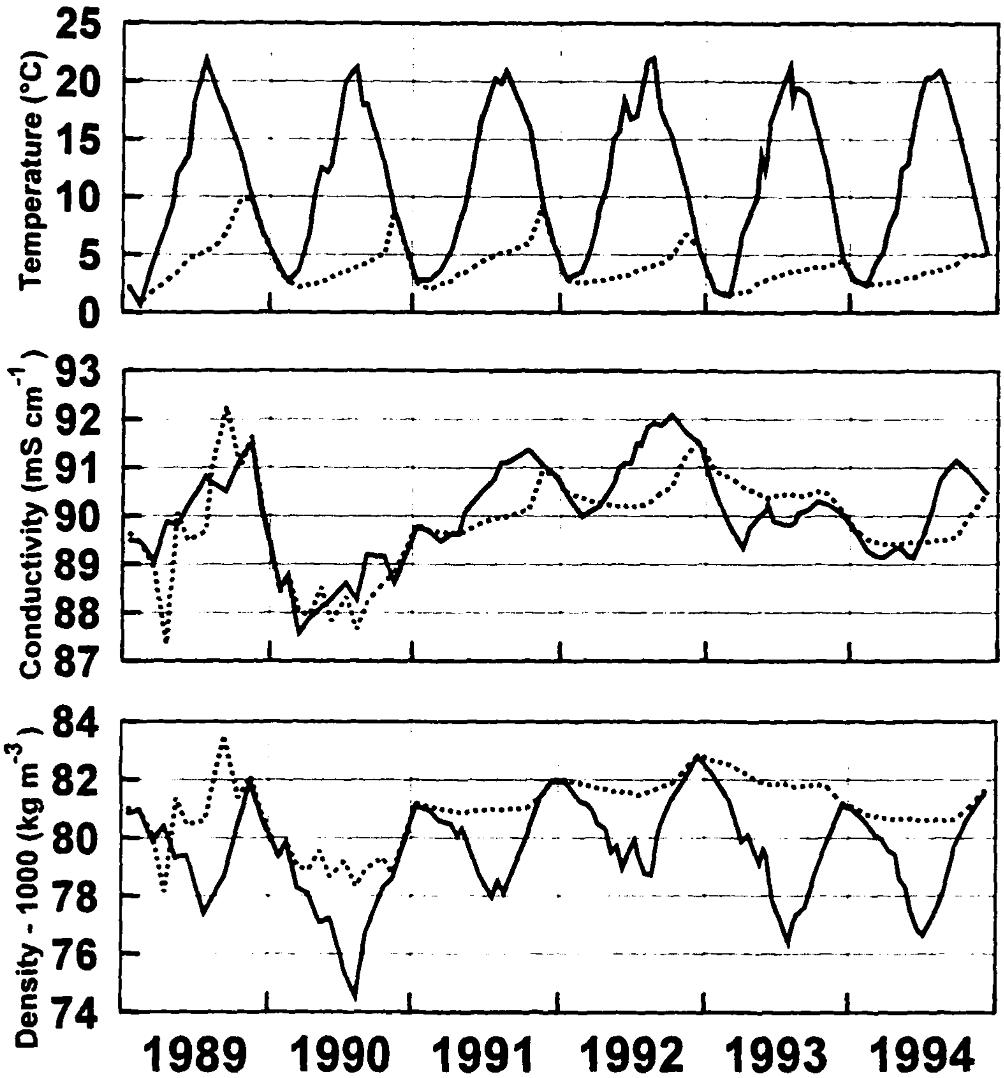
Temperature (°C)
25
20
15
10
5
0
Conductivity (mS cm-1)
93
92
91
90
89
88
87
Density - 1000 (kg m-3)
84
82
80
78
76
74
1989
1990
1991
1992
1993
1994

Figure 9. Temperature and salinity vertical steps across the pycnocline with $N^2=(g/\rho)(\partial\rho/\partial z)$ in $s^{-2} \times 10^{-3}$. Steps calculated over 3 m intervals.

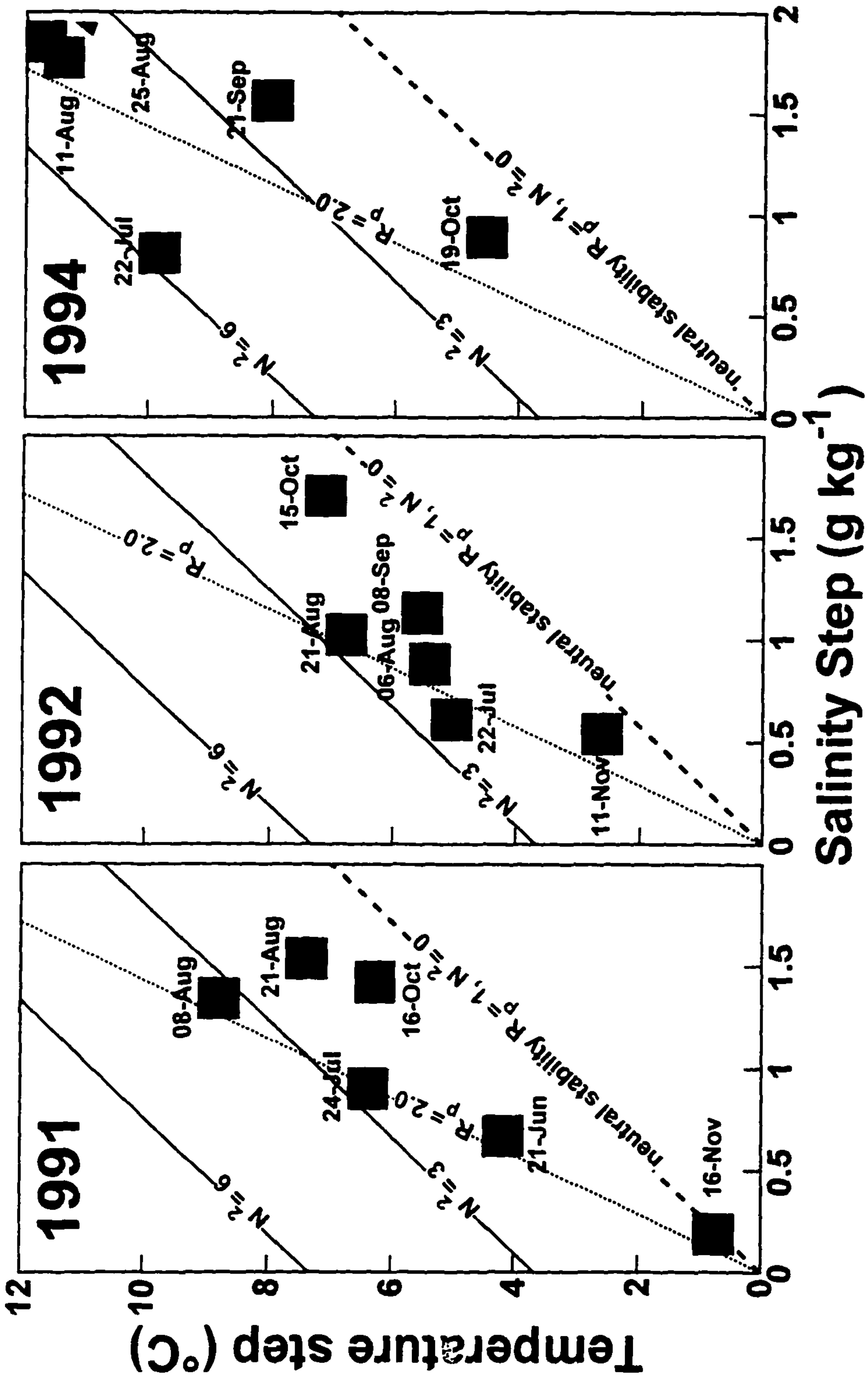
1991
1992
1994
Temperature step (°C)
Salinity Step (g kg^{-1})
$N^2 = 6$
$N^2 = 3$
$R_\rho = 2.0$
neutral stability $R_\rho = 1$, $N^2 = 0$
08-Aug
21-Aug
16-Oct
24-Jul
21-Jun
16-Nov
15-Oct
08-Sep
21-Aug
06-Aug
22-Jul
11-Nov
11-Aug
25-Aug
21-Sep
22-Jul
19-Oct

Figure 10. Selected profiles from August-October from 1991, 1992, and 1994. Asterisks indicate presumed 'fossil' isothermal regions from salt finger double diffusion.

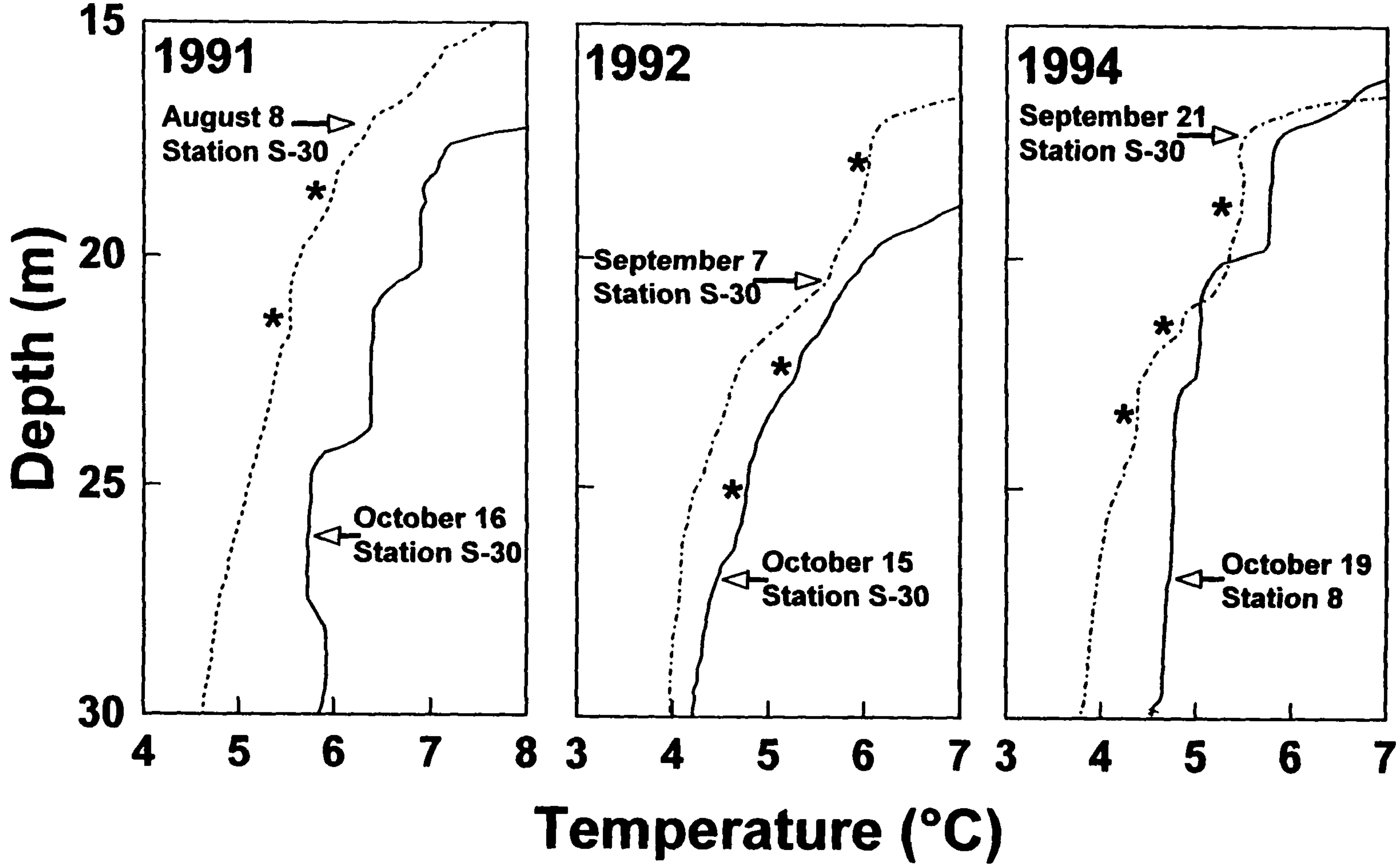
1991
August 8
Station S-30
October 16
Station S-30
1992
September 7
Station S-30
October 15
Station S-30
1994
September 21
Station S-30
October 19
Station 8
Depth (m)
15
20
25
30
4 5 6 7 8
3 4 5 6 7
3 4 5 6 7
Temperature (°C)

Figure 11. 1989-1994 K_z estimates at the thermocline (maximum temperature gradient) (□) and average wind speed over the central difference interval (◆)from April to September.

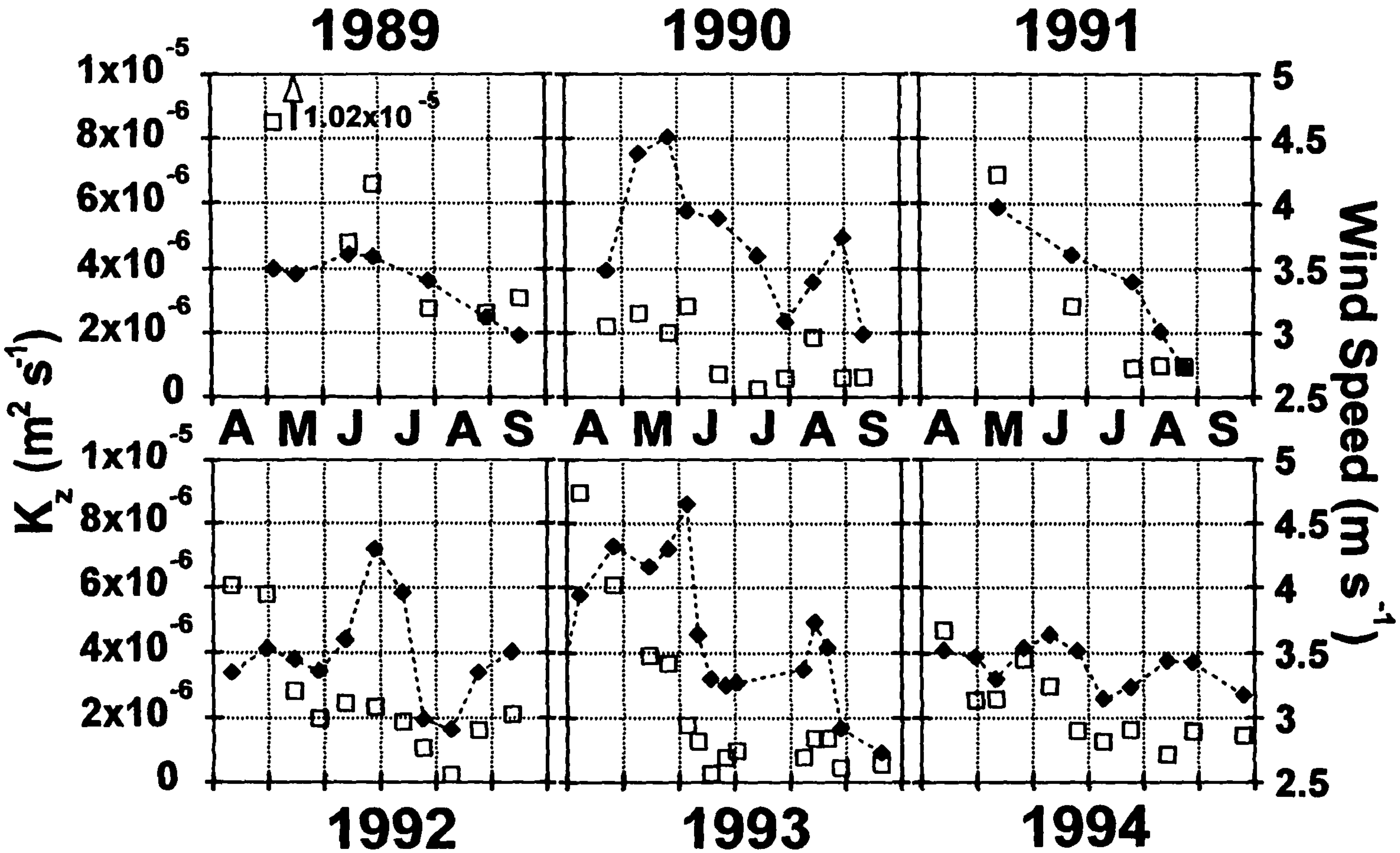

1989
1990
1991
1992
1993
1994
1.02x10^-5
A M J J A S
Kz (m² s⁻¹)
Wind Speed (m s⁻¹)
0
2x10^-6
4x10^-6
6x10^-6
8x10^-6
1x10^-5
2.5
3
3.5
4
4.5
5

Figure 12. Isopleth plots of dissolved oxygen (upper panel, mg L^{-1}) and ammonia (lower panel, μM) and from 1989 to 1994.

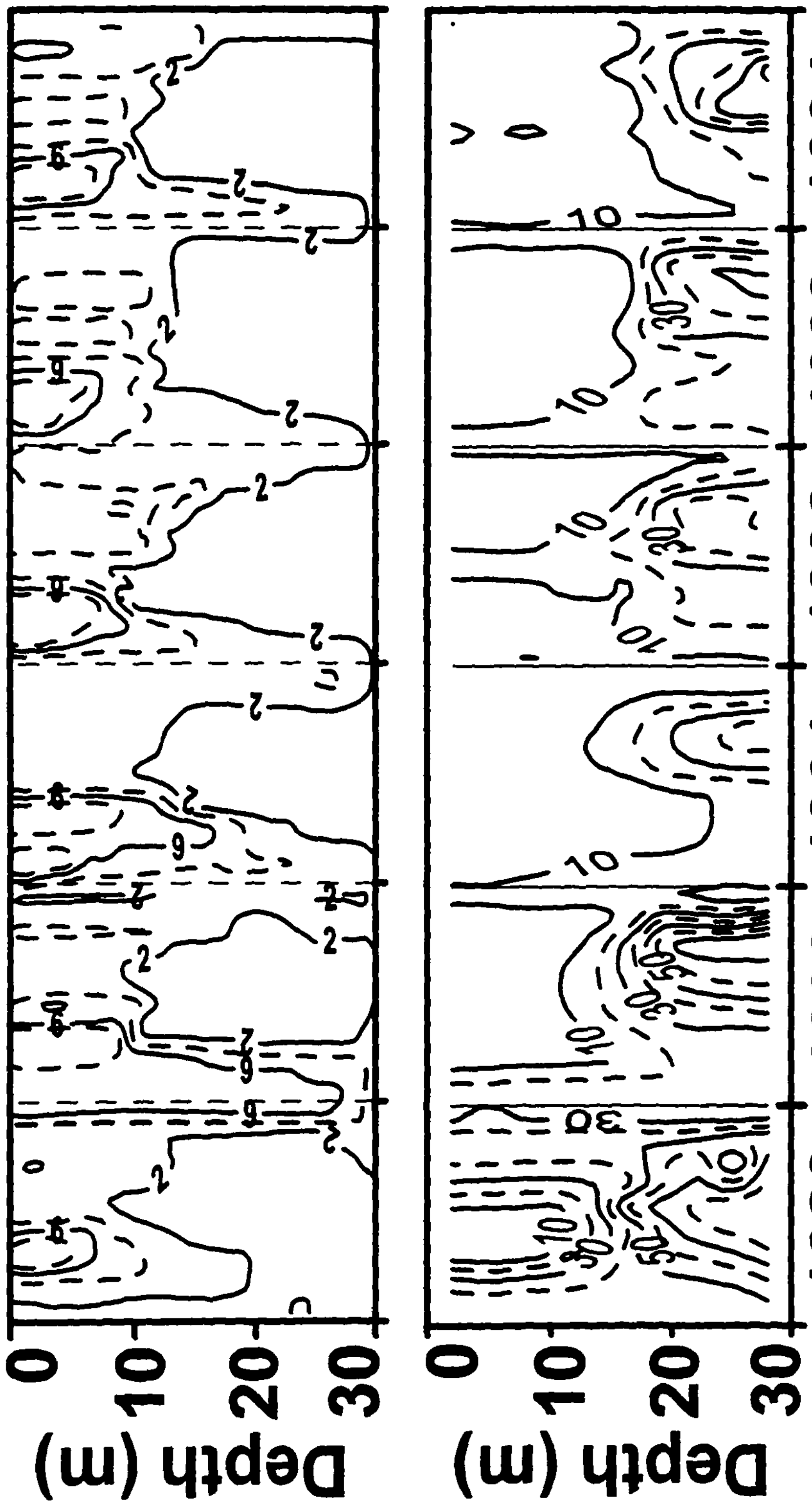

Depth (m)
0
10
20
30
Depth (m)
0
10
20
30
1989
1990
1991
1992
1993
1994

Figure 13. Spring (April-May) and summer (June-August) ammonia flux estimates.

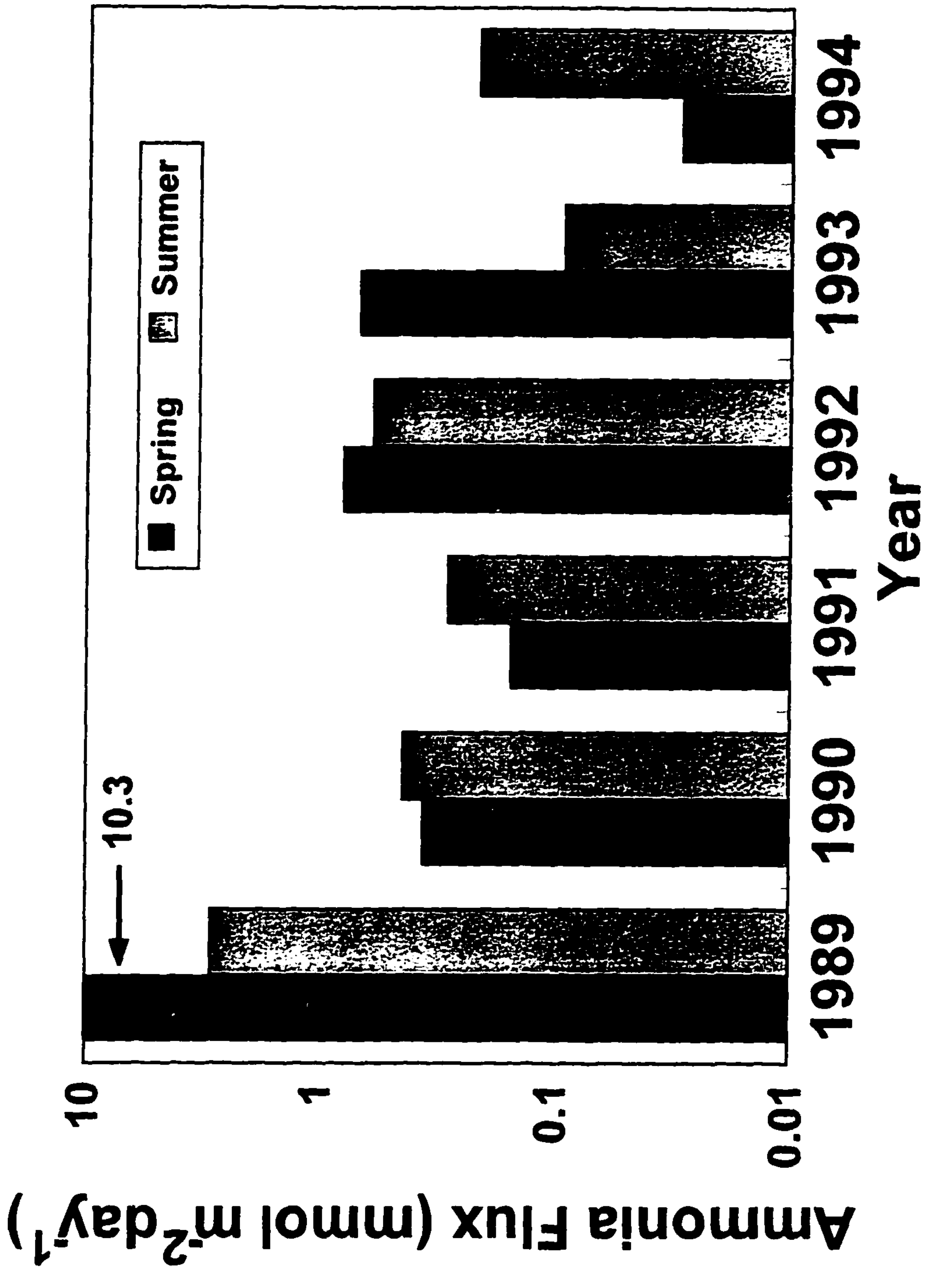

Spring
Summer
10.3
10
1
0.1
0.01
1989
1990
1991
1992
1993
1994
Year
Ammonia Flux (mmol m-2day-1)

Figure 14. (A) Average daily (dashed) and 31-point moving average (solid) wind speed. (B) Daily L_N estimated from daily average wind speeds and field profiles. (C) L_N computed from average wind speed over central difference interval (□) and 31-point moving average (solid). (D) L_N over central difference interval and K_z. Asterisks are three sampling dates in March-April, 1993 which have high K_z estimates during moderate L_N periods. Regression curve (solid line) computed without the March-April, 1993 estimates.

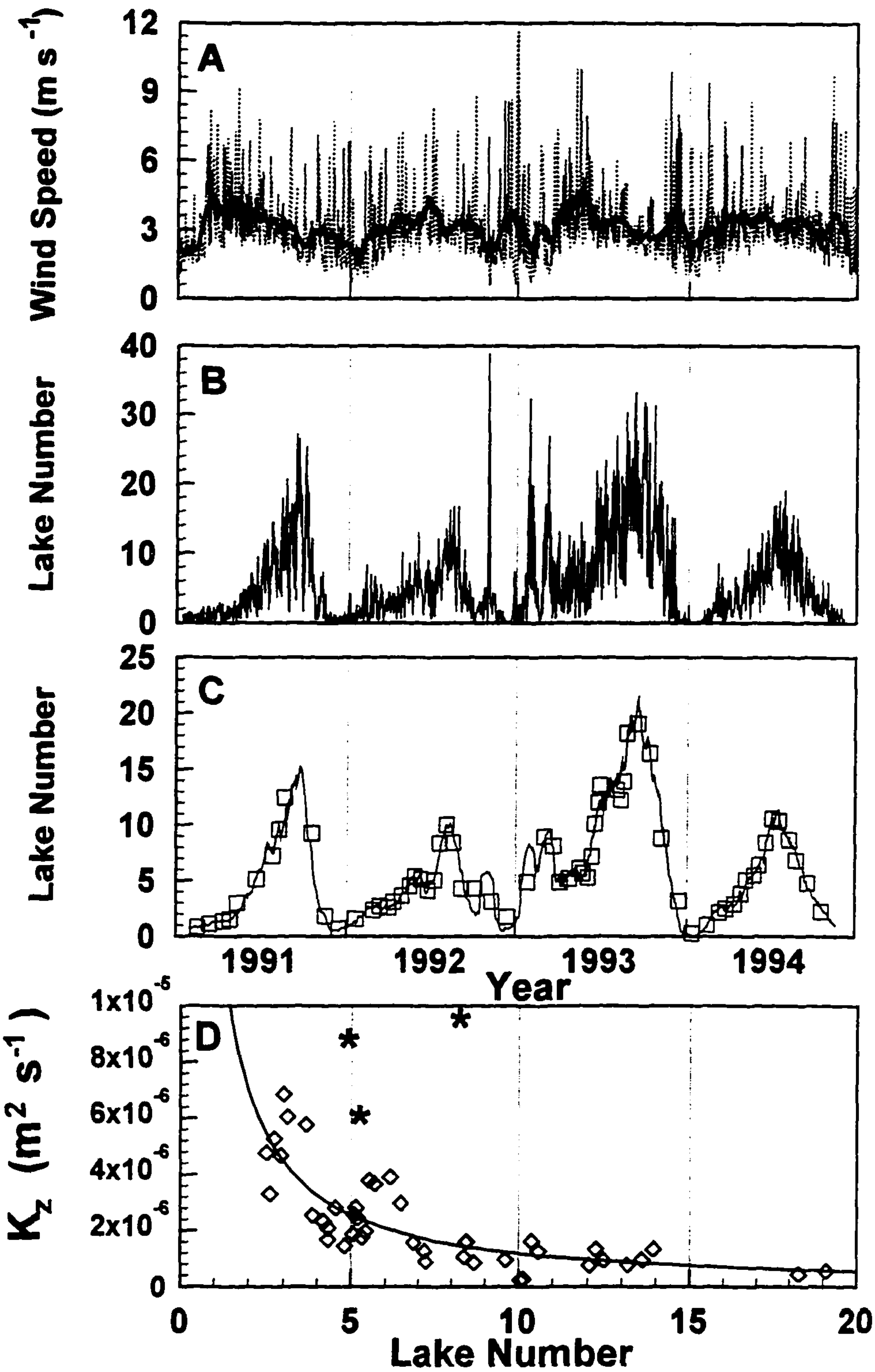

Wind Speed (m s-1)
A
B
Lake Number
C
Lake Number
1991
1992
1993
1994
Year
D
Kz (m2 s-1)
Lake Number

CHAPTER 4

Simulations of Vertical Mixing in a Hypersaline Lake

Introduction

Turbulent mixing influences the distribution of solutes and particles in lakes and must be incorporated into realistic ecosystem models. A number of one-dimensional (1D) vertical mixing models have been coupled to ecosystem models in lacustrine settings (Jewell 1995). Verification of such vertical mixing models is generally based on comparisons between field and simulated temperature profiles. Although vertical transport from the hypolimnion to epilimnion is often ecologically important, model validations that consider vertical mixing below the base of the mixed-layer have not been reported previously.

Application of stratification models to hypersaline lakes requires a thorough verification of vertical mixing parameterizations. Most vertical mixing models have been applied to the upper water column of marine settings (Price *et al.* 1986) or freshwater lakes (Patterson *et al.* 1984) where salinity stratification does not cause significant variations of the vertical density structure. Validation of a vertical mixing model in saline versus freshwater lacustrine settings is recommended for three reasons.

Firstly, the seasonal and interannual salinity dynamics of hypersaline lakes undergo large variations caused by freshwater dilution and evaporative concentration at the surface. During wet years with large freshwater inputs, salinity stratification results in density differences across the seasonal pycnocline which may lead to meromixis (condition of persistent chemical stratification) (Jellison and Melack 1993, Chapter 1). If evaporation exceeds freshwater inputs over the course of a year, falling lake level and inverse salinity stratification occurs. Inverse salinity stratification results from mixed-layer volume shrinkage after the onset of thermal stratification where mixed-layer salinity is greater than the hypolimnetic salinity (Chapter 1, Anati and Stiller 1990). Hence, a large range of density differences across the pycnocline occur as a function of the amount and timing of freshwater inputs into a saline lake.

Secondly, salinity is a conservative tracer of model performance whereas temperature is not. Heat input from radiation (Jassby and Powell 1974) and sediment-water heat exchange (Likens and Johnson 1969, Benoit and Hemond 1996) can be significant sources or losses of heat. Salinity changes throughout the metalimnion and hypolimnion are caused by turbulent mixing whereas solar insolation can be significant in metalimnetic heating.

Thirdly, vertical mixing below the mixed-layer in saline lakes is not influenced by inflow or outflow processes. Vertical transport arises solely from mechanisms such as shear-induced mixing (Münnich *et al.* 1992) and internal wave breaking in the interior of the lake, boundary mixing along the margins (Imberger and Ivey 1993, Gloor *et al.* 1993, Wüest *et al.* 1994), upwelling (Imberger and Patterson 1990), and double diffusion (Turner 1985). Incorporation of parameterizations of the various mixing mechanisms into a vertical mixing model can identify major mixing mechanisms below the base of the mixed-layer.

The application of the DYnamic Reservoir Simulation Model (DYRESM), a one-dimensional (1D) vertical mixing model, to hypersaline (*ca.* 94 g L^{-1}), moderately deep (*ca.* 45 m) Mono Lake, California (Fig. 1) is presented. A six year database of hydrological, meteorological, and physical limnological measurements during a period of monomixis (one period of complete mixing a year) were used as simulation inputs and verification data. Model validation includes comparisons between calculated and simulated eddy diffusivity estimates in the thermocline. Because the published version of the model underestimated vertical mixing below the base of the mixed-layer, several parameterizations of vertical mixing mechanisms were evaluated that increase metalimnetic and hypolimnetic transport.

Simulation Inputs and Model Description

DYRESM requires daily meteorological (longwave radiation, shortwave radiation, air temperature, air vapor pressure, and wind speed) and hydrological (stream discharge and precipitation) inputs. Additional inputs required by the model include the physical properties of Mono Lake water (kinematic viscosity, specific heat, and density) and a depth-area-volume table (Pelagos corp. *unpub. data*). A description of the simulation inputs and the vertical mixing model follow.

Fluxes of Momentum, Heat, and Water at the Air-water Interface

Four weather stations were used to compile daily meteorological data from January 1, 1989 to December 31, 1994. A six hour meteorological database was compiled from January 1, 1992 to December 31, 1994. The Paoha meteorological station is located at the southern tip of Paoha Island (Fig. 1). Three other stations around the perimeter of the lake (Cain Ranch, Lee Vining, Simis Ranch, Fig. 1) were used to fill gaps in the Paoha meteorology from March 15, 1990 to December 31, 1994. The January 1, 1989-March 14, 1990 meteorology was estimated entirely from the three lake perimeter stations.

Ten minute averages of readings made every second for wind speed, relative humidity, and air temperature were measured on Paoha Island beginning in mid-March, 1990. Wind run, maximum and minimum air temperature, total daily precipitation, and cloud cover (i.e. cloudy, partly cloudy, clear) were recorded at Cain Ranch from 1989 through 1991. Hourly measurements at Simis Ranch of air temperature and wind speed and at Lee Vining of wind speed were used to estimate Paoha meteorology when required from 1989 through 1994. Simis Ranch precipitation was used as the precipitation input from 1989 through 1994. Precipitation measurements are described below in more detail. Table 1 summarizes the relationships used to estimate the Paoha meteorology from stations around the lake perimeter.

The vapor pressure was calculated from temperature and relative humidity measurements from the Paoha weather station. Relative humidity, RH (%), is defined as $RH = r/r_s \times 100$, where r and r_s are the measured and saturated air mixing ratios. The mixing ratio, r, is defined as the ratio of the water vapor density in the air, ρ_w (kg m^{-3}), to the density of dry air, ρ_D (kg m^{-3}) and may be computed from the relation,

$$r = \frac{0.62197 f_w e}{(p - f_w e)} \tag{1}$$

derived from the ideal gas law (e.g. PV=nRT) where p is the atmospheric pressure (mbar), e is the vapor pressure (mbar), and f_w is a correction factor for the departure of the mixture of air and water vapor from ideal gas laws (assumed equal to 1). The saturation vapor pressure, e^*, is a function of air temperature and was calculated with Lowe's (1977) empirical relationship at sea level pressure (p=1013.5 mbar). The saturation mixing ratio, r_s, can be computed from (1), and the mixing ratio, r, can then be computed from the relative humidity. Solving for e in (1) yields, $e = rp/(r+0.62197)$ and direct computation of the vapor pressure can be made with p equal to the Mono Lake surface pressure of 800 mbar at 1943 m. The approximation $e=RH_D \times e^* \times c_{elev}$, where c_{elev} is the elevation pressure correction (=0.79) and RH_D is the daily average relative humidity, is a good approximation. Morton (1983) suggests average vapor pressure derived from relative humidity and temperature measurements be computed on a sub-daily time scale since saturation vapor pressure is a nonlinear function of temperature. Daily vapor pressure averages computed from 10-minute averages of relative humidity and air temperature were nearly equivalent to the approximation throughout the six years.

Daily and six hour averages of wind speed, air temperature, and vapor pressure are presented in Figures 2 and 3. The seasonality of the lower daily average wind speeds is caused by strong summer diurnal winds in the afternoon. Daily average air temperature ranges from -5 to 23°C, whereas six hour averages ranged from -10 to 30°C with a 5 to 10°C daily range. Since relative humidity from 1989 through July, 1991, was estimated from the air temperature (Table 1), the variability was lower. Daily fluctuations of six hour vapor pressures were *ca.* 1 mbar d^{-1}.

Hourly averaged measurements of photosynthetically available radiation (PAR, 400-700 nm) were recorded at the Cain Ranch meteorological station located 7 km southwest of the lake from 1989 through 1994 and at Paoha from August, 1991, through 1994. Hourly averages of shortwave and incoming longwave radiation were measured at Cain Ranch from August, 1991 through 1994. From January, 1989 through July, 1991, incoming longwave radiation, L_I, was estimated as,

$$L_I = \psi(1 + 0.17C^2)(273.15 + T_A)^6 \qquad (2)$$

where C is the percent cloud cover, ψ is a constant equal to $-5.18\text{x}10^{-13}$, and T_A is the air temperature (°C) (TVA 1972). A constant ψ equal to $-4.7\text{x}10^{-13}$ yielded longwave radiation estimates within the range of measured values, a lower emissivity of the atmosphere was required for the high lake surface elevation relative to sea level (Fig. 3). Longwave radiation emitted from the lake surface, L_O, was calculated by the model as:

$$L_O = \varepsilon\sigma(T_S + 273)^4 \qquad (3)$$

where ε is the surface emissivity (=0.97) and σ is the Stefan-Boltzmann constant.

Incoming shortwave radiation is absorbed by the water column and was computed by Beer's Law as:

$$Q_Z = A_S Q_0 \sum_{i=1}^{5} \lambda_i e^{-\eta_i z} \qquad (4)$$

where Q_Z is the amount of shortwave radiation absorbed at depth z, A_S is the shortwave albedo of the water surface, Q_0 is the incoming shortwave radiation, λ_i is the proportion of Q_0 in wavelength band i, and η_i is the attenuation coefficient of wavelength band i. Table 1 gives the extinction coefficients for wavelengths other than PAR. Incoming shortwave radiation from 1989 through July, 1991, was estimated from Cain Ranch PAR measurements (Table 1). The incoming shortwave radiation, Q_0, was corrected for albedo on an hourly basis assuming a flat foamless lake (*see* Jassby and Powell 1974). Calculated albedoes ranged from 4-14% from August, 1991, through 1994.

Shortwave inputs into the model accounted for A_S. Underwater PAR was measured with a submersible Li-Cor quantum sensor. PAR attenuation coefficients from 1989 through 1994 ranged from 0.3 to 1.3 m^{-1}. Daily values were estimated by interpolating between dates of field surveys. The total longwave and shortwave radiation simulation inputs and the PAR attenuation coefficients are shown in Figure 4.

The surface fluxes of momentum, sensible heat, and latent heat were estimated with the bulk mass transfer approach with the formulas:

$$\tau = \rho_A C_D U_{10}^2 \tag{5}$$

$$H = -\rho_A C_P C_H U_{10}(T_S - T_A) \tag{6}$$

$$E = -\frac{0.622}{p} \rho_A L C_W U_{10}(\chi e_S - e_A) \tag{7}$$

where the wind stress τ, the sensible heat transfer H, and the evaporative heat transfer E are estimated from the average air temperature T_A, sub-daily surface layer simulated temperature T_S, average vapor pressure of the air e_A, sub-daily saturation vapor pressure of the surface layer e_S, air density ρ_A (0.96 kg m^{-3}, 1943 m at 15°C), average wind speed at 10 m U_{10}, and the specific heat of air C_P (1005 J kg^{-1} °K); C_D (1.3×10^{-3}), C_H (1.9×10^{-3}), and C_E (1.9×10^{-3}) are the neutral momentum, sensible, and latent heat transfer coefficients referenced to 10 m. The activity of water in the saline solution, χ, is the ratio of the saturation vapor pressures of saline solution and freshwater both measured at the same temperature, and equals 0.95 for the range of salinities modeled here (Salhotra *et al.* 1985).

Wind speed measurements were standardized to a 10 m reference height, U_{10}, assuming a logarithmic profile, $U_{10}=U_z/[1-C_D^{0.5} \ln(10/z) / k]$, where U_z is the wind speed at the measurement height z and k is the von

Karman constant (=0.4) (Amorocho and DeVries 1980). Wind speed was measured approximately 4 m above the lake surface from 1990 to 1994, so that $U_{10}=1.09\ U_4$. A constant air density was assumed throughout the simulations so that equations (5) to (7) simplify to: $\tau = 1.47x10^{-6}\ U_{10}^2$, $H = -2.14\ U_{10}\ (T_A - T_S)$, and $E = -3.5\ U_{10}\ (0.95\ e_A - e_S)$.

Mono Lake Physical Properties - Measurement and Constants

The 1989 and 1990 temperature profiles were measured at 1 m depth intervals at stations 6, 11, and S30 (Fig. 1) with a thermistor (Yellow Springs Instr. 701) and Wheatstone bridge circuit (Cole-Parmer model 8502-25) with an accuracy of 0.05 °C (Jellison and Melack 1993). The 1989 and 1990 conductivity profiles were collected at stations 6 and 11 (Fig. 1) at monthly intervals with a van Dorn water sampler and were almost always sampled at 7 depths (2, 8, 12, 16, and 20 m at both stations and 24 and 28 m at station 6 only). Conductivity samples were filtered immediately through ≈1 μm pore size Gelman A/E glass-fiber filters and stored at 4 °C. Conductivity of samples were measured in the laboratory in a 1-cm cell (Lab-line) between 24 and 26 °C and corrected to 25 °C. Replicate readings indicated a measurement uncertainty of 0.4 mS cm^{-1} (Jellison and Melack 1993) but are likely higher as discussed below.

Beginning in January, 1991, vertical profiles of temperature and conductivity at stations 6, 11, and S30 (Fig. 1) were made with a conductivity-temperature-depth profiler (CTD) (Sea-Bird Electronics, model Seacat SBE 19). The CTD is a free-falling instrument which samples at 2 Hz. Addition of customized buoyancy to the CTD resulted in descent rates of 0.25-0.4 m s^{-1} yielding a 0.125-0.2 m vertical resolution. Monthly CTD profiles were made from September to February for all years and all of 1991. Bi-weekly CTD profiles were made from March to August for 1992, 1993, and 1994 except for a gap in July, 1993. On most dates, two CTD profiles were made at each station.

The conductivity and pressure sensors were assumed to measure instantaneously, whereas the temperature of a water parcel sampled by the CTD lags as a result of the slow thermistor response time (0.5 s slower than conductivity). The mismatch in the temperature and conductivity response times results in 'spikes' in the derived salinity (or conductivity corrected to a standard temperature) profile. The slower response temperature profiles were shifted back in time to match the conductivity profiles. Corrected conductivity was computed and plotted for a range of time constants for each CTD profile (0.5 to 1.5 s). The time constant which minimized spiking in the corrected conductivity profile was chosen. The best profile (e.g. least spiking) of the two CTD casts made at each station was used. The average time constant was 0.8 s.

Conductivity at 25 °C was computed as:

$$C_{25} = C_T(1+2.05\times10^{-2}(25-T)+3.52\times10^{-4}(25-T)^2+8.5\times10^{-6}(25-T)^3) \qquad (8)$$

where C_i is the conductivity (mS cm^{-1}) at temperature i (°C) and T is the temperature at which the raw conductivity measurement was made (R. Jellison *unpub. data*). The density of Mono Lake water (MLW), ρ_w (kg m^{-3}) as a function of temperature, T (°C), and conductivity at 25 °C, C_{25} (mS cm^{-1}), is given by,

$$\rho_w = c_1 + c_2T + c_3T^2 + c_4C_{25} + c_5C_{25}^2 + c_6TC_{25} \qquad (9)$$

where c_1 = 1003.40, c_2 = 1.335x10^{-2}, c_3 = -6.20x10^{-3}, c_4 = 4.897x10^{-1}, c_5 = 4.23x10^{-3}, and c_6 = 1.35x10^{-3} (R. Jellison *unpub. data*).

Total dissolved solids, *TDS*, (g L^{-1}) was computed as:

$$TDS = 8.0629 + 0.3792 \times C_{25} + \times 0.006322 \times C_{25}{}^{2} \qquad (10)$$

(R. Jellison *unpub. data*). The salinity, S (g L^{-1}), and *TDS* were assumed to be equivalent. The salinity in units of g kg^{-1} was derived by dividing S in g L^{-1} by the local density. The linear expansion coefficients of heat, $\alpha=\rho_0^{-1}\partial\rho/\partial T$, and salt, $\beta=\rho_0^{-1}\partial\rho/\partial S$, are -2.50x10^{-4} (°C^{-1}) and 8.75x10^{-4} (g kg^{-1})$^{-1}$, respectively. Calculation of lake level fluctuations from precipitation, stream discharge, and evaporation are based on salinity units of g salt kg MLW^{-1} (*see below*). Conductivity is converted to *TDS* and then salinity (g kg^{-1}) during the simulation with the above equations.

A MLW latent heat of evaporation of 2.45x10^{6} J kg^{-1} was estimated from linear interpolation between values of seawater and the Dead Sea (Steinhorn 1991). A kinematic viscosity of 1.27x10^{-6} m^2 s^{-1} and specific heat of 3865 J kg^{-1} °C^{-1} were obtained from Mason (1967).

The January 15, 1989, temperature profile and a isohaline profile served as the initial profile for simulations with daily meteorology and the January 18, 1992, CTD profile was the initial profile for the 6-hour simulations. The total salt content in the lake when converted with the TDS relationship is equivalent to 285 x 10^{6} tons of salt (SE = 3 x 10^{6}, n=64). The initial conductivity profile was determined from the total salt content on January 15,1989, for an initial elevation of 1943.25 m. The daily meteorological input simulation was run for 2177 days until December 31, 1994. The six hour meteorological input simulation was run for 1079 days until December 31, 1994. All other temperature and conductivity profiles are used for model validation only.

Hydrology Inputs and Methods

Daily total discharge of the five major streams was measured at gauges approximately 5 km upstream from the lake (Fig. 5). Temperatures of Convict Creek (not shown), at the Sierra Nevada Aquatic Research Laboratory located 45 km from Mono Lake at an elevation of 2160 m, served as stream temperature inputs.

Hour totals of precipitation were measured at Simis Ranch from 1988 to 1994 and at Cain Ranch prior to October, 1991. Vorster (1985) estimated annual precipitation to be 0.20 m yr^{-1} based on isohyetal maps of the Mono Basin, approximately 73% of the Cain Ranch annual average precipitation. Simis Ranch monthly precipitation was 65% of Cain Ranch values from October to March during 1988 to 1991 (r^2=86.9, n=21). The 1989 to 1994 Mono Lake daily precipitation totals were derived from Simis Ranch values by multiplying by 1.14 (73%/64%) (Fig. 5). Lake surface elevations were recorded weekly to monthly from staff gauges recorded to the nearest 0.03 m.

The evaporation rate can be estimated as $Z_E = E / \rho$, where E (kg freshwater m^{-2}) is calculated from equation 7 with χ equal to zero and ρ is the lake surface water density. However, in saline water bodies both the loss of volume due to evaporation and contraction of the water body from salinity increases must be computed. The lake level decrease from evaporation with constant temperature throughout the evaporation process, Z_E, was calculated as:

$$Z_E = \frac{(1+\beta S')E}{\rho'} \qquad (11)$$

where β is the linear expansion coefficient of salt (g $kg^{-1})^{-1}$, S' is the new salinity (g kg^{-1}), and ρ' is the new density (Steinhorn 1991). Equation (10) accounts for losses of volume from evaporation (E/ρ') and volume shrinkage from increased salinity ($\beta S'E/\rho'$). Similarly, the lake level increase from precipitation on the lake surface, Z_P was computed with (10) except E was replaced with the mass of precipitation, P_M (kg m^{-2}), where P_M/ρ' is the lake surface increase from precipitation and $\beta S'P_M/\rho'$ is the volume expansion from decreased salinity. The lake level increase from stream inputs, Z_S, was computed as Z_P, after dividing the volumetric input by the surface area.

The water balance of a terminal saline lake can be expressed as:

$$\Delta Z = Z_S + Z_G + Z_P - Z_E + \Delta Z_\rho \tag{12}$$

where ΔZ is the change in lake level (m d^{-1}), ΔZ_ρ is the lake level fluctuation from density changes throughout the water column (m d^{-1}), Z_P is the precipitation onto the lake surface (m d^{-1}), Z_S is stream discharge into the lake (m d^{-1}), Z_G is the ungauged surface runoff and groundwater inputs (m d^{-1}), and Z_E is the lake level decrease from evaporation with constant temperature (m d^{-1}). Lake level fluctuations caused by temperature changes in the surface layer, shortwave heating below the surface layer, and density changes from vertical mixing were computed for each sub-daily time step. The sum of lake level fluctuations from density changes is the term ΔZ_ρ in (12).

Vertical Mixing Model

The DYnamic REservoir Simulation Model, DYRESM, a 1D vertical mixing model, was used to simulate the six year period from 1989-1994. The surface fluxes of the model have been described. Descriptions of the mixed-layer parameterizations are given elsewhere (Imberger and Patterson 1981, 1990) and are briefly summarized here. Mixed-layer dynamics are based on an integral turbulent kinetic energy budget with four mechanisms: wind stirring, convective overturn, shear production, and Kelvin-Helmholtz billowing. The efficiency of the four mixing mechanisms are constants derived from theory, laboratory experiments, and field measurements (Sherman *et al.* 1978, Imberger and Patterson 1981) and are not calibrated.

The 1D assumption presumes that water column variations within the vertical are much greater than in the horizontal, a condition that is satisfied in small to moderate water bodies (*ca.* < 50 km^2). However, in larger lakes and oceans, (*ca.* > 10,000 km^2) significant persistent variations in the horizontal results in poor characterization of the entire water column with only one lakewide average vertical profile. In such cases the application of a 1D model is of limited use. In moderately-sized Mono Lake (~150 km^2), the seasonal dynamics have been characterized with lakewide averaged vertical profiles during monomixis (Chapter 1) and meromixis (Jellison and Melack 1993). However, modification of the vertical diffusivity parameterization was necessary and is discussed next.

Internal waves can cause mixing in the interior of the hypolimnion by breaking which is estimated in DYRESM as:

$$K_z = \alpha \frac{\varepsilon}{(N(z)^2 + 0.6 w_0^2 k_0^2)} \qquad \text{(Weinstock 1981)} \qquad (13)$$

where K_z is the diffusivity (m^2 s^{-1}), α is the efficiency (0.2-0.8), ε is dissipation (W kg^{-1}), w_0 is the wave speed (m s^{-1}), k_0 is the wavelength (m^{-1}), and $N(z)$ is the buoyancy frequency (s^{-1}) at depth z defined as,

$$N^2 = -\frac{g \partial \rho}{\rho \partial z} \qquad (14)$$

where ρ is the water density, z is depth (positive downward), and g is gravitational acceleration. If the simulated stratification is strong at depth z (i.e. $N^2 >> w_0^2 k_0^2$) then $K_Z = \alpha\varepsilon / N(z)^2$. For the case of weak stratification at depth z (i.e. $N^2 << w_0^2 k_0^2$) then $K_Z = \alpha\varepsilon/(0.6 w_0^2 k_0^2)$ where w_0 is assumed to equal u_*. The wave number, k_0, is given by,

$$k_0 = \left(\frac{12.4 A_S}{V_B h_0}\right)^{0.5} \tag{15}$$

where A_S is the surface area, V_B is the upper lake volume which contains 85% of the total buoyancy frequency distribution, and h_0 is the depth of the mixed layer.

The internal dissipation, ε, is modeled after Imberger (1982) as

$$\varepsilon = \frac{C_D^{1.5} \rho_A^{1.5}}{\rho_W^{0.5}} \frac{A_S}{V_B \rho_0} \alpha_W u_*^3 \tag{16}$$

where α_W is the efficiency (=0.24), u_* is surface water friction velocity ($=U_{10}\rho_A/\rho_W$), and ρ_0 is a reference density. If one assumes that the introduced energy can only be distributed throughout the lake by internal wave propagation, little energy will be dissipated in the hypolimnion so V_B is used instead of the total volume. Further, the parameterization in DYRESM assumes that local dissipation will become weaker away from the region of severe stratification below $z = H - h_1$. The dissipation is distributed vertically through the water column as,

$$\varepsilon = \varepsilon \qquad z > H - h_l \tag{17}$$

$$\varepsilon = \varepsilon \exp\{-(\frac{H - h_1 - z}{\sigma})\} \qquad z < H - h_l \tag{18}$$

where H is the total depth, h_l is the depth relative to the bottom of the center of area of the N^2 distribution, and σ is the variance of the first moment of the N^2

distribution (Imberger 1982). Hence, for a two layer stratification (i.e. a thin pycnocline), σ is small and the dissipation decreases rapidly with depth. Alternatively, if a thick metalimnion is simulated, σ is large and dissipation decreases moderately with depth.

Recent research indicates that the main source of turbulent kinetic energy in small to medium-sized lakes may be caused by shear at the interface of the well-mixed benthic boundary layer (Imboden and Wüest 1995). A simple parameterization for the diffusivity of the bottom boundary layer is given by Wüest *et al.* (1994) as:

$$K_Z = \frac{\gamma}{N^2}\left(\frac{\partial A}{\partial V}\frac{u_{*B}{}^3}{k}\left(1+\ln\left(\frac{\delta_B}{\delta_M}\right)\right)\right) \tag{19}$$

where K_z is the vertical diffusivity (m^2 s^{-1}), γ is the mixing efficiency (=0.2), A is the sediment area, V is the volume, u_{*B} is the friction velocity of the sediment-boundary layer, δ_B is the thickness of the Prandtl layer, δ_M is the thickness of the well-mixed benthic boundary layer, and k is the von Karman constant. Though δ_B, δ_M, and u_{*B} depend on internal wave dynamics and lake bottom characteristics such as bottom roughness and slope, estimates of these parameters were used to evaluate the potential importance of this mechanism. In particular, δ_B equal to 10 m, δ_M equal to 1 m, and $u_{*B} = C_{1m}{}^{0.5}\, U_{1m}$ $= (1.5\times10^{-3})^{0.5}$ 0.1 m s^{-1} = 4×10^{-3} m s^{-1} were set as constants, then equation 19 simplifies to:

$$K_Z = \frac{\gamma}{N^2}\left(5\times10^{-7}\frac{\partial A}{\partial V}\right). \tag{20}$$

A current velocity of 0.1 m s^{-1} 1 m above the sediment-water interface is considered an upper limit in lakes (Wüest and Imboden 1995).

The lake number, L_N, is an indicator of mixing below the base of the mixed layer and is defined as:

$$L_N = \frac{gS_t(1 - {z_t}/{H})}{\rho_0 u_*^{2} A_0^{1.5}(1 - {z_g}/{H})} \tag{21}$$

where g is the gravitational acceleration, S_t is the lake stability, z_t the height to the center of the metalimnion, z_g is height to the center of volume of the lake, u_* is the shear velocity, and A_0 is the lake surface area (Imberger and Robertson 1991, Imberger and Patterson 1990). For large L_N (>>1), the bottom of pycnocline remains horizontal. For small L_N (<1), the entire pycnocline tilts with the generation of currents below the pycnocline which results in increased hypolimnetic mixing.

Greater metalimnetic and hypolimnetic mixing during low L_N periods was simulated by increasing the dissipation as:

$$\varepsilon_{LN} = \frac{a}{L_N^{\,b}}\varepsilon \qquad \text{where } \varepsilon_{LN} = a\varepsilon \text{ for } L_N < 1 \tag{22}$$

where a and b are constants. If the L_N is small (i.e. tilting of the pycnocline with generation of internal waves and currents), an increase in mixing below the pycnocline is simulated.

Simulation Results

Water and Heat Balance

The annual surface energy balance indicates that the meteorological approximations from 1989-1991 were similar to the 1992-1994 period (Table 2). Simulated lake surface temperatures compared well with observed data during the stratified period except minimum lake surface temperatures during

December-February were cooler (Fig. 6). Daily evaporation rates ranged from nearly 0 to 12 mm d^{-1} (Fig. 6). Monthly evaporation totals were greatest in July or August (0.13-0.16 m $month^{-1}$) and lowest in January or February (0.02 m $month^{-1}$). The average annual evaporation rate over the six years was 0.93 m yr^{-1} (SE = 0.05 m yr^{-1}). An annual evaporation of 0.95 m yr^{-1} from 1992 to 1994 was simulated when all measurements were made on Paoha Island. Differences in annual evaporation rates (Table 3) reflected interannual differences in wind speed and vapor pressure. Other water balance components are given in Table 3.

The simulated lake level matched observations from 1989-1992 reasonably well except small winter lake level rises (e.g. 0.02-0.07 m) were not predicted (Fig. 6). Ungauged runoff and groundwater are probably significant to the water balance of the lake during this period. During 1993 the predicted lake level was 0.12 m below observations. The 1994 precipitation total is misleading. If November-December, 1994 is excluded, the precipitation total is 0.14 m, a similar precipitation total to the other years. In 1993, a relatively wet year, we hypothesize that significant snow accumulation around the perimeter of the lake and subsequent spring melt caused the additional lake level increase. Less snow on the basin floor in the other years resulted in less ungauged runoff.

An evaporation coefficient of -3.3 instead of -3.5 resulted in an accurate simulation of seasonal peak lake levels, but minimum seasonal lake levels were greater than observed. Surface temperatures were nearly equivalent for both simulations, and the annual evaporation for the lower evaporation coefficient was 0.90 m yr^{-1} over the 6-year period (SE = 0.05 m yr^{-1}). The simulated stratification dynamics are presented for the lower evaporation rate which simulated the observed lake level fluctuations with greater accuracy.

Field Observations

During the six year period mixed-layer temperatures were lowest in February (2-3 °C) and highest in July or August (> 20 °C) (Fig. 7A). Hypolimnetic temperatures were lowest in February (2-3 °C) and increased 1-4 °C by September of each year. The largest seasonal hypolimnetic temperature increase (4°C, May 4-September 12), earliest turnover date (late October/early November), and lowest thermocline temperature gradients during the six years characterized the 1989 thermal dynamics. The 1990 and 1991 thermal dynamics were characterized by a 2-3°C hypolimnetic temperature rise from early May to mid-October. The 1992 temperature dynamics were similar to 1990 and 1991 except the seasonal thermocline established at a lower depth in the spring with less thermocline deepening afterwards. Vertical temperature profiles in 1993 and 1994 were similar from May to October prior to turnover characterized by low rates of hypolimnetic heating (1-2°C).

Years 1989 and 1993 represent the two extremes of hydrological effects on salinity stratification dynamics during monomixis in Mono Lake (Fig. 7B). Stable salinity stratification throughout 1993 resulted from a positive water balance where freshwater inputs exceeded evaporation (Table 3). Stable salinity stratification resulted in strong stability throughout stratification until turnover in late November to early December. During drought conditions in 1989, a decrease in lake level resulted from low freshwater inputs. During thermal stratification, evaporative concentration of the mixed-layer resulted in unstable salinity stratification, weak density stratification, and a large downward heat flux. The other four years were intermediate cases between these two extremes. Stable salinity stratification in the spring persisted for a longer duration in 1990 and 1994 than 1991 and 1992 from greater precipitation and stream discharge inputs. However, all these years had unstable salinity profiles by mid-summer.

Published Version Simulation

The simulation with the published version of DYRESM (Imberger and Patterson 1981) predicted the mixed-layer thermal dynamics adequately for 1990-1992 and 1994 (Fig. 7C). In 1989 turnover was simulated several months early and in 1993 the mixed-layer depth was underestimated. The simulated salinity dynamics (Fig. 7D) from 1991-1992 match reasonably well with field profiles, but the 1993 dynamics incorrectly predicted the onset of meromixis.

If the 5 and 25 m water properties are used as indices of mixed-layer and hypolimnetic dynamics, comparisons between simulation and field profiles elucidate several problems with the simulation. The mixed-layer temperature was predicted accurately for all six years (Fig. 8A). Even the August to October 1989 mixed-layer temperatures were predicted accurately, though turnover was simulated several months early and the mixed-layer depths were greater than field profiles. After the onset of thermal stratification, modeled hypolimnetic temperatures remained constant except in 1989. The 5 m conductivity dynamics from 1991 to 1992 were predicted adequately (Fig. 8B). Mixed-layer dilution during rising lake level from January to March, 1993 was predicted accurately, however, the simulation predicted too much dilution after April. Hypolimnetic conductivity dynamics after the onset of thermal stratification from 1990 to 1992, and salinity stratification in January, 1993, remained constant whereas field profiles varied as a function of mixed-layer concentrations (Fig. 8C). Mixed-layer density dynamics were predicted accurately for 1991-1992, but excessive stream discharge dilution resulted in the prediction of a 2-4 kg m^{-3} less dense mixed-layer than field profiles from May, 1993 to September, 1994 (Fig. 8D). The predicted onset of meromixis in 1993 and 1994 resulted in a 1-3 kg m^{-3} denser hypolimnion (Fig. 8E) which further increased the density difference across the pycnocline relative to field profiles.

The model results indicate that the mixed-layer parameterizations are valid. However, the simulation results (i.e. constant hypolimnetic water properties) suggests problems with the eddy diffusivity formulation. A reasonable match between the 1990 to 1992 depth of the maximum temperature gradient for field profiles and simulated depths of the center of the daily buoyancy frequency distribution were modeled (Fig. 9A). Further, buoyancy frequency estimates were simulated reasonably well during 1991 and 1992 (Fig. 9B). Simulated dissipation rates ranged from $3x10^{-8}$ to $<1 \times 10^{-10}$ W kg^{-1} (Fig. 9C). Lakewide average dissipation estimates on a daily time scale are not available to compare with simulation values. Dissipation rates derived from microstructure measurements are within the range reported for the interior of Lake Alpanach (surface area=5 km^2, maximum depth=34 m, maximum N^2 $=2.5x10^{-3}$ s^{-2}) over a period of nine days by Wüest *et al.* (1994). Since dissipation and N^2 are the primary inputs for diffusivity calculations during the thermally stratified period ($N^2 >> w_0^2\ k_0^2$ in eq. 12) some insight can be inferred by comparing the field and model eddy diffusivities. The modeled vertical diffusion coefficient was underestimated by at least a factor of 10 throughout most of the thermally stratified period (Fig. 9D).

Simulation with Increased Dissipation

A simulation with the dissipation increased by a factor of 15 throughout the simulation did not effect mixed-layer dynamics significantly (Fig. 10), yet improved the simulation of hypolimnetic temperature, conductivity, and density dynamics (Fig. 11). The modeled buoyancy frequency and eddy diffusion coefficients matched field estimates well (Fig. 12).

The simulation suggests model dissipation estimates are too low. However, if the dissipation is increased by a factor of 15 during the 1983 to 1988 meromictic period, meromixis is predicted for only a 3 year period (1983 to 1985) (not shown). Hence, mixing mechanisms which occurred during monomixis but not meromixis must account for the discrepancy. Mixing mechanisms associated with internal waves are hypothesized to account for differences in the magnitude of metalimnetic and hypolimnetic vertical mixing between the two periods. Stability during meromixis was much stronger and likely suppressed internal wave amplitudes in the thermocline from wind forcing relative to monomictic years.

The comparison between the model results and field data suggest the most significant mixing mechanism(s) below the mixed-layer are not parameterized in the model. Alternatively, calculation of interior dissipation rates from daily average wind speeds may underestimate values, and sub-daily inputs (wind speeds in particular) are required. Both approaches are discussed next.

Benthic Boundary Layer Simulations

Benthic boundary layer mixing has previously been hypothesized to be an important mixing mechanism in Mono Lake (Chapters 1, 2, and 3). Maximum current speeds 1 m above the sediments in lakes are *ca.* 0.1 m s^{-1} (Wüest and Imboden 1995). Dissipation rates for a range of current speeds based on equation 20 and the Mono Lake bathymetry are illustrated in Figure 13. Dissipation estimates increase with depth below the surface since $\partial A/\partial V$ increases in equations 19 and 20 (i.e. there is a greater sediment area to volume ratio with increased depth so benthic boundary layer turbulence affects a greater volume with depth). Dissipation rates for the 0.1 m s^{-1} current speed at 1 m above the sediments sustained over the entire simulation still resulted in meromixis in 1993 (Fig. 14B). Hence, shear-induced mixing along the well-mixed benthic boundary layer is likely not the single primary mechanism of metalimnetic transport.

Published Version Simulation with Six Hour Inputs

A simulation with six hour meteorological inputs was performed to evaluate whether higher wind speeds resulted in an improved simulation of hypolimnetic dynamics. Excessive mixed-layer deepening during the setup of spring stratification was modeled (Fig. 14C and 14D). Mixed-layer parameterizations in DYRESM assume that a fixed proportion of the wind energy is used for mixed-layer deepening. A closure hypothesis in the diurnal version of DYRESM retains the average mixed-layer turbulent kinetic energy as an explicit variable (Spigel *et al.* 1986) and is likely required with six hour inputs in Mono Lake. More importantly, simulated dissipation rates below the mixed-layer were not significantly increased with the six hour wind speeds as isotherms and isopleths of conductivity remained horizontal during the stratified period in 1993 and 1994.

Simulations with Dependence on L_N

Simulations of lake stability with the published model version and a factor of 15 increase in dissipation matched field estimates in 1991 and 1992, but overestimated stability in 1993 (Fig. 15A). Stability was overestimated in 1993 from strong stable salinity stratification (> 1 mS cm^{-1}) whereas weak salinity stratification (0.5 mS cm^{-1}) was measured. The simulation with increased dissipation nearly resulted in holomixis by January, 1994, so that stability nearly matched field estimates through the remainder of the year.

L_N estimates from 1991 to 1994 (Fig. 15B) were much lower than the published version simulation in 1993 and 1994 (Fig. 15C) from overestimates in lake stability (Fig. 15A). The simulation with increased dissipation (Fig. 15D) agreed well with L_N estimates except from December 1993 to February 1994, when lakewide stability was again overestimated. The onset of inverse chemical stratification in early 1989 lead to weak stability (Fig. 15A) and low L_N (Fig. 15 C and D) during both simulations. The 1D assumption is not valid in 1989 (i.e. $L_N < 3$ during the entire year) and one can expect significant horizontal variations throughout the year from moderate to high wind forcing. Only during the summer of 1993 was the L_N greater than 10 for a significant period.

In Chapter 3, vertical diffusivities were approximately proportional to the L_N^{-1}. We assume that the maximum deflection of the metalimnion from 1990 to 1994 was just below the lake surface with no upwelling (i.e. no intersection of thermocline isotherms with the lake's surface for L_N less than

1). Utilization of equation 22 with *b* equal to -1 assumes that increased mixing during pycnocline tilting is caused by shear in the interior and boundary mixing along the margins proportional to L_N^{-1}.

Simulations with the *a* constant equal to 20 (Fig. 16A and 16B) and 30 (Fig. 16C and 16D) in equation 22 compare well with field profiles (Fig. 7A and 7B). Holomixis from 1990 to 1992 and 1994 is predicted several weeks to a month early. Inverse salinity stratification across the pycnocline from September to October likely causes double diffusive salt fingering (Chapter 1). The enhanced downward double diffusive salt flux may increase the simulated total stability long enough to prolong stratification.

Simulated hypolimnetic water properties with *a* equal to 20 tracked field measurements reasonably well (Fig. 17). The largest inconsistency between the field and model profiles is the amount of dilution of the mixed-layer in 1993. In particular, vertical mixing during the high spring wind forcing period (Fig. 2) appears to be reasonably well simulated, but discharge from summer snowmelt caused too much mixed-layer dilution. Mixed-layer depths were underestimated in 1993 (Fig. 18A) so that excessive dilution was caused by underestimates in mixed-layer volumes.

Buoyancy frequency was simulated reasonably well except during the summer of 1993 (Fig. 18B). Eddy diffusivities matched well with field estimates except in the summer of 1993 and to a lesser degree the summer of 1994 which were underestimated (Fig. 18D).

Discussion

Previous applications of DYRESM to Mono Lake utilized the lake elevation as the primary hydrological input. The amount of freshwater added was equivalent to the volume needed to raise the lake surface to the daily input elevation (Chapter 1). Groundwater and ungauged runoff were estimated as the difference between the daily volume needed to simulate the measured lake surface level and the volume of freshwater inputs (Chapter 2). The simulations here indicate that unmeasured freshwater inputs are a minor component of the water balance for years with below average hydrological inputs (1989-1992, 1994). The annual evaporation rate of 0.93-0.95 m yr^{-1} was less than values derived from water balance models of Mono Lake (1.06 m - Vorster (1985); 1.02 m - Los Angeles Department of Water and Power, *unpub.*).

In lakes of sufficient depth to undergo seasonal thermal stratification, it has been presumed that accurate simulations of temperature dynamics are needed to adequately estimate surface temperatures and evaporation rates (Morton 1983, Hostetler and Bartlein 1990). However, simulations presented here poorly reproduced the vertical temperature distribution in 1989, yet lake surface temperatures matched field measurements. Comparisons of modeled surface temperatures and evaporation rates of 1989 were nearly equivalent even though thermal dynamics varied significantly. Similarly, the mixed-layer was shallower relative to field profiles in 1993, yet lake surface temperatures were modeled accurately. The heat budget on a daily time scale is self-regulating. If the simulated mixed-layer depth is too shallow, more heating during the day results in greater heat loss during the night. Alternatively, when mixed-layer depth is too deep, less heat is lost during the night. Sensitivity of modeled evaporation rates and surface temperatures to the mass transfer coefficient was greater than the vertical temperature distribution.

Most lacustrine 1D vertical mixing model applications have been made in freshwater lakes (Patterson *et al.* 1984). Model validation generally consists of comparisons between measured and modeled temperature profiles to assess the quality of the simulation. Salinity dynamics in freshwater lakes generally are strongly influenced by inflow dynamics (Patterson *et al.* 1984). Application of DYRESM to an Australian reservoir with saline riverine inputs during the wet season adequately predicted salinity stratification at the bottom of the reservoir (Imberger 1982). However, the Australian reservoir case was not a test of vertical transport across the pycnocline from mechanisms other than inflow and outflow dynamics. Salinity stratification was caused by gravitational differences between the lake water and inflowing streams.

Application of DYRESM to hypersaline Mono Lake indicates the mixing parameterizations adequately modeled mixed-layer dynamics during stratification. However, the simulation with the published version of DYRESM underestimated vertical transport by a factor of 10 to 100 with an eddy diffusivity formulation which accounted only for mixing within the interior of the lake through internal wave breaking. The effect of methane bubble plumes in the lake with a ebullition rate of *ca.* 1.0 $m^3 s^{-1}$ was simulated and made a negligible contribution to hypolimnetic heating (Chapter 1).

Saline lakes are ideal systems to evaluate the validity of mixing parameterizations below the base of the mixed-layer since freshwater inputs occur at the surface and do not influence the hypolimnion directly. Temperature and salinity changes below the base of the mixed-layer can only occur from turbulent mixing processes within and below the pycnocline. Internal waves are initiated by wind forcing which causes deflections in the pycnocline and the generation of internal waves. Two types of boundary mixing can occur, internal wave breaking on the shallow sloping sides of the lake (Imberger and Ivey 1993) and shear-induced mixing along the interface of the benthic boundary layer (Gloor *et al.* 1994). Internal waves also cause horizontal velocity fluctuations at the base of the pycnocline which could lead to enhanced shear mixing within the interior of the lake (Münnich *et al.* 1992).

Boundary mixing from internal wave breaking along the margins of Mono Lake may be important along the southern portion of the lake in the region of relatively steep slopes (K. Flynn and S. MacIntyre *pers. comm.*). The northern and eastern sectors of the lake are characterized by shallow bottom slopes where internal waves likely cause metalimnetic isotherms to travel long distances along the sediment interface. For example, suppose the metalimnion is centered at 10 m below the surface, an internal wave with a 2 m amplitude could result in a *ca.* 1 km distance traversed along the bottom. Hence, the development of a well-mixed benthic boundary layer and resultant shear mixing along the margins are expected. In similarly-sized Lake Kinnert (A=168 km^2, z_{avg}=24 m), the development of a well-mixed benthic boundary layer has been documented which indicates cross-isopycnal mixing from internal seiche activity (Ostrovsky *et al.* 1996) in a region with similar slopes as the eastern and northern sectors of Mono Lake.

An increase in the vertical diffusivity within the interior of Mono Lake may result from the generation of currents and shear along the interface of the hypolimnion and metalimnion. The gradient Richardson number is defined as $Ri=N^2(\partial u/\partial z)^{-2}$ where $\partial u/\partial z$ is the horizontal velocity gradient. For Ri between 2 and 3, Peters *et al.* (1988) found diapycnal diffusivity to be approximately 1×10^{-6} m^2 s^{-1} in the Pacific equatorial undercurrent, the characteristic Mono Lake value. Typical maximum N^2 varied from 0.001 to 0.01 s^{-2} from 1991-1994 and would require 'sustained' horizontal velocity gradients of 0.01 s^{-1} for weak stratification to 0.1 s^{-1} for strong stratification to yield the characteristic

Mono Lake diffusivity. One must conclude that internal diffusivity from seiche induced horizontal velocity fluctuations may be important during weak stratification in the spring ($N^2 \sim 0.001\ s^{-2}$) but is not likely during strong stratification in the summer and fall ($N^2 \sim 0.01\ s^{-1}$).

When the L_N is used as an indicator of the occurrence of these metalimnetic and hypolimnetic mixing mechanisms improved simulations resulted (also *see* Chapter 2). Though the L_N may predict when these mechanisms are significant, differences in density structure and wind forcing on a sub-daily time scale are likely important parameters that determine the subtleties in the magnitude of mixing. Imberger and Robertson (1991) successfully applied the L_N as an indicator of deep turbulent mixing in a small (3 km^2), shallow (z_{avg}=5.6 m, z_{max}=20 m) Australian reservoir and reproduced changes in deep dissolved oxygen and other redox related parameters. As boundary mixing along the margins and internal shear within the interior are dependent upon lake bathymetry, the shortcoming to the the L_N as an indicator of deep mixing concerns calibration for different lake morphologies. Development of the L_N as an index of deep mixing in lakes is recommended since two- and three-dimensional circulation models are substantially more difficult to validate and require significantly more computational effort.

Accurate vertical mixing across the pycnocline must be validated for a stratification model prior to realistic seasonal ecological modeling in lacustrine settings. The published version of DYRESM would have underestimated the upward flux of the limiting algal growth nutrient (i.e. ammonia) in Mono Lake over the monomictic period. The L_N parameterization for mixing below the base of the mixed-layer can be used to model the upward flux of ammonia during years with a small to moderate negative water balance such as 1990-

1992 and 1994. Drought years with large water balance deficits such as 1989 do not conform to the 1D assumption during the thermally stratified period. Incorporation of double diffusive salt fingering parameterizations (Kunze 1987) may improve simulations of drought years with an increase in the downward salt flux.

References

Amorocho, J. and J.J. Devries. 1980. A new evaluation of the wind stress coefficient over water surfaces. J. Geophys. Res. 85:433-442.

Anati, D.A. and M. Stiller. 1991. The post-1979 thermohaline structure of the Dead Sea and the role of double-diffusive mixing. Limnol. Oceanogr. 36:342-354.

Benoit, G. and H.F. Hemond. 1996. Vertical eddy diffusion calculated by the flux gradient method: significance of sediment-water heat exchange. Limnol. Oceanogr. 4:157-168.

Gloor, M., A. Wüest, and M. Münnich. 1994. Benthic boundary mixing and resuspension induced by internal seiches. Hydrobiologia 284:59-68.

Hostetler, S.W. and P.J. Bartlein. 1990. Simulation of lake evaporation with application to modeling lake level variations of Harney-Malheur Lake, Oregon. Wat. Resour. Res. 26:2603-2612.

Imberger, J. 1982. Reservoir dynamics modelling. In: "Prediction in Water Quality", E.M. O'Loughlin and P. Cullen (ed.), pp. 223-248. Australian Academy of Science, Canberra.

Imberger, J. and G.N. Ivey. 1993. Boundary mixing in stratified reservoirs. J. Fluid Mech. 248:477-491.

Imberger, J. and J.C. Patterson. 1990. Physical limnology. Adv. Appl. Mech. 27:303-475.

Imberger J. and J.C. Patterson. 1981. A dynamic reservoir simulation model - DYRESM. In: "Transport Models for Inland and Coastal Waters", H.B. Fisher (ed.) pp. 310-361.

Imberger, J. and D.M. Robertson. 1991. Estimating changes in water quality using Lake Number, a new quantitative indicator of mixing. International Hydrology & Water Resources Symposium. Perth. 8 pp.

Imboden, D.M. and A. Wüest. 1995. Mixing mechanisms in lakes, p. 83-135. *In.* A. Lerman, D.M. Imboden, and J.R. Gat [ed.], Physics and Chemistry of Lakes. Springer-Verlag.

Jassby, A. and T. Powell. 1975. Vertical patterns of eddy diffusion during stratification in Castle Lake, California. Limnol. Oceanogr. 20:530-543.

Jellison, R. and J.M. Melack. 1993. Meromixis in hypersaline Mono Lake, California. 1. Stratification and vertical mixing during the onset, persistence, and breakdown of meromixis. Limnol. Oceanogr. 38:1008-1019.

Jewell, P.W. 1995. A simple surface water biogeochemical model. 2. Simulation of selected lacustrine and marine settings. Wat. Resour. Res. 31:2059-2070.

Kunze, E. 1987. Limits on growing, finite length salt fingers: a Richardson number constraint. J. Mar. Res. 45:533-556.

Likens, G.E. and N.M. Johnson. 1969. Measurement and analysis of the annual heat budget for the sediments in two Wisconsin Lakes. Limnol. Oceanogr. 14:115-135.

Lowe, P.R. 1977. An approximating polynomial for the computation of saturation vapor pressure. J. Appl. Meteorol. 16:100-103.

Mason, D.T. 1967. Limnology of Mono Lake, California. Univ. Calif. Publ. Zool. 83:1-110.

Morton, F.I. 1983. Operational estimates of lake evaporation. J. Hydrol. 66:77-100.

Münnich, M., A. Wüest, and D.M. Imboden. 1992. Observations of the second vertical mode of the internal seiche in an alpine lake. Limnol. Oceanogr. 37:1705-1719.

Ostrovsky, I., Y.Z. Yacobi, P. Walline, and I. Kalikhman. 1996. Seiche induced mixing: Its impact on lake productivity. Limnol. Oceanogr. 41:323-332.

Patterson, J.C., P.F. Hamblin, and J. Imberger. 1984. Classification and dynamic simulation of the vertical density structure of lakes. Limnol. Oceanogr. 29:845-861.

Peters, W.H., M.C. Gregg, and J.M. Toole. 1988. On the parameterization of equatorial turbulence. J. Geophys. Res. 93:1199-1218.

Price, J.F., R.A. Weller, and R. Pinkel. 1986. Diurnal cycling: observations and models of the upper ocean response to diurnal heating, cooling, and wind mixing. J. Geophys. Res. 91:8411-8427.

Salhotra, A.M., E.E. Adams, and D.F. Harleman. 1985. Effect of salinity and ionic composition on evaporation: analysis of Dead Sea evaporation pans. Wat. Resour. Res. 21:1336-1344.

Sherman F.S., J. Imberger, and G.M. Corcos. 1978. Turbulence and mixing in stably stratified waters. Ann. Rev. Fluid Mech. 10:267-288.

Spigel, R.H., J. Imberger, and K.N. Rayner. 1986. Modeling the diurnal mixed layer. Limnol. Oceanogr. 31:533-556.

Steinhorn, I. 1991. On the concept of evaporation from fresh and saline water bodies. Wat. Resour. Res. 27:645-648.

Tennessee Valley Authority. 1972. Heat and mass transfer between a water surface and the atmosphere. Lab Rept. No. 14, Norris, Tennessee.

Turner, J.S. 1985. Multicomponent convection. Ann. Rev. Fluid Mech. 17:11-44.

Vorster, P. 1985. A water balance forecast model for Mono Lake. Calif. Water. Resour. Monogr. 10. US Dep. Agric. Forest Serv. Region 5.

Weinstock, J. 1981. Vertical turbulence diffusivity for weak or strong stable stratification. J. Geophys. Res. 86:9925-9928.

Wüest, A., D.C. van Senden, J. Imberger, G. Pieplke, and M. Gloor. Diapycnal diffusivity measured by microstructure and tracer techniques: a comparison. Symp. on Turbulent flow, Grenoble. 8 pp.

Table 1. Relations used to fill gaps in the meteorology. PI = Paoha Island, CR = Cain Ranch, SR = Simis Ranch, LV = Lee Vining.

Wind Speed	PI = 1.08 SR	r^2=0.77, n = 1415
	PI = 1.06 LV	r^2=0.65, n = 1513
Air Temperature	PI = 0.93 SR + 0.72	r^2=0.99, n = 1605
	PI = 0.91 LV + 1.10	r^2=0.98, n = 1571
Relative Humidity	RH = -1.51 AirT + 67.6	r^2=0.61, n = 1200
PAR	PI = 0.95 CR	r^2=0.93, n = 1104
SW	SW = 0.455 PAR	r^2=0.99, n = 1095

Shortwave Attenuation Coefficients

Wavelength (nm)	Attenuation Coefficient (m^{-1})	% of Shortwave	
280-400	1.5	4	(Jellison and Melack 1993)
400-700	*see* Figure 3	45	
700-800	1.1	13	(Jassby and Powell 1975)
800-900	3.4	9	(Jassby and Powell 1975)
> 900	26.0	29	(Jassby and Powell 1975)

Table 2. Annual surface heat balance (MJ m^{-2} yr^{-1}) during the six year simulation.

Year	SW	LW	Black Body	Sensible	Latent	Inflow
1989	68.41	97.63	-131.93	-5.25	-26.52	0.15
1990	68.60	100.71	-136.38	-7.14	-27.68	0.31
1991	69.29	95.45	-134.87	-5.44	-24.49	0.26
1992	69.71	96.34	-135.90	-5.08	-25.95	0.30
1993	74.12	94.43	-135.27	-6.59	-28.37	0.61
1994	72.19	94.57	-134.78	-5.06	-27.31	0.27
Average	70.39	96.52	-134.86	-5.76	-26.72	0.32
SE	2.28	2.37	1.56	0.88	1.39	0.15

Table 3. Annual depth water balance (m yr^{-1}) during the six year simulation.

Year	Stream	Rain	Evap	Density	Annual
1989	0.293	0.070	-0.923	0.013	-0.546
1990	0.614	0.129	-0.963	0.003	-0.217
1991	0.484	0.175	-0.852	0.005	-0.189
1992	0.575	0.163	-0.903	0.001	-0.164
1993	1.051	0.233	-0.987	-0.002	0.294
1994	0.591	0.238	-0.950	0.002	-0.118
Average	0.601	0.168	-0.930	0.004	-0.157
SE	0.250	0.064	0.048	0.005	0.269

Figure 1. Mono Lake bathymetry with locations of sampling stations (●), meteorology stations (+), Lee Vining Creek confluence (■), and Rush Creek confluence (◆).

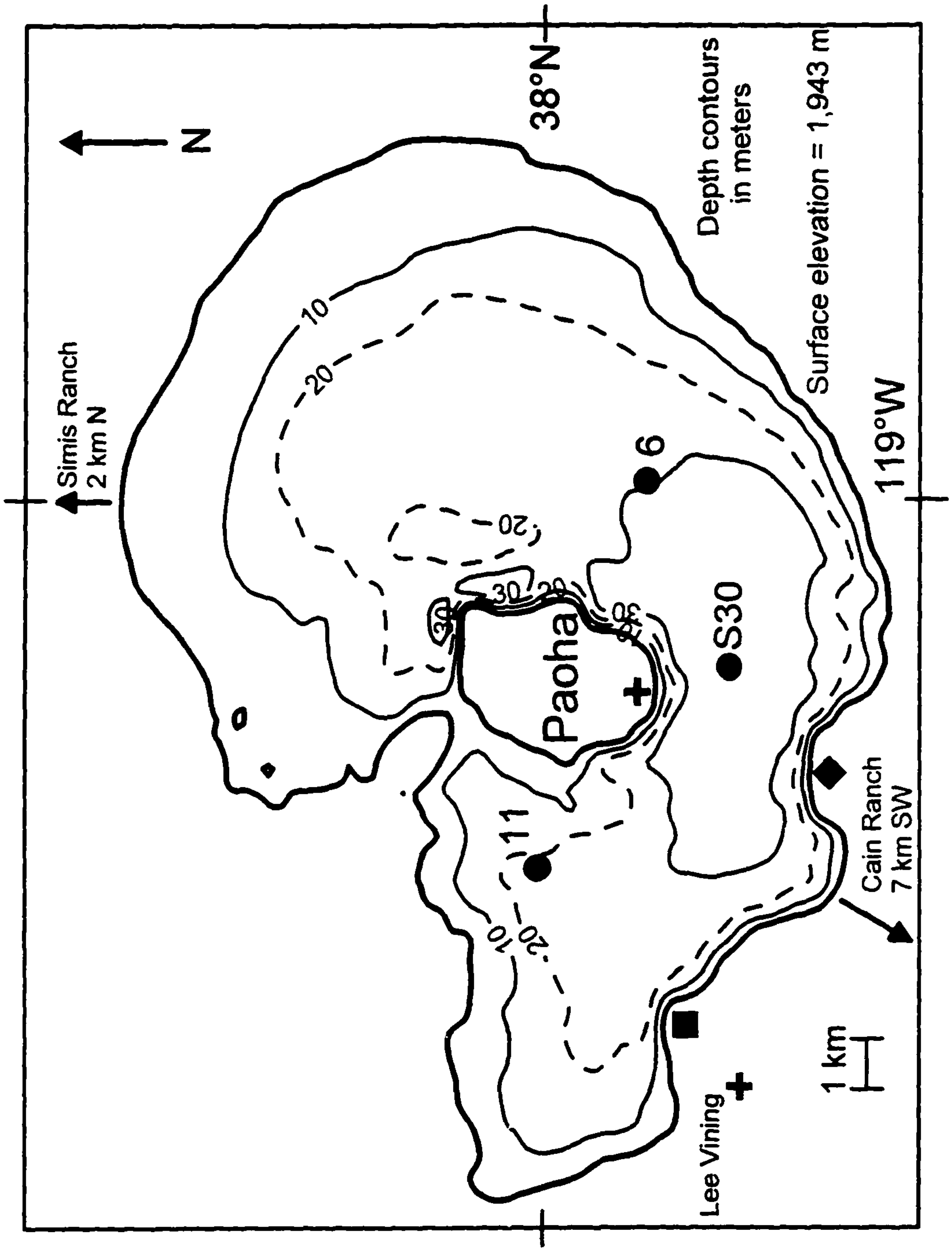
N
Simis Ranch
2 km N
38°N
Depth contours
in meters
Surface elevation = 1,943 m
119°W
10
20
30
Paoha
6
S30
11
Cain Ranch
7 km SW
Lee Vining
1 km

Figure 2. Daily averages of wind speed, air temperature, and vapor pressure for the period 1989-1994.

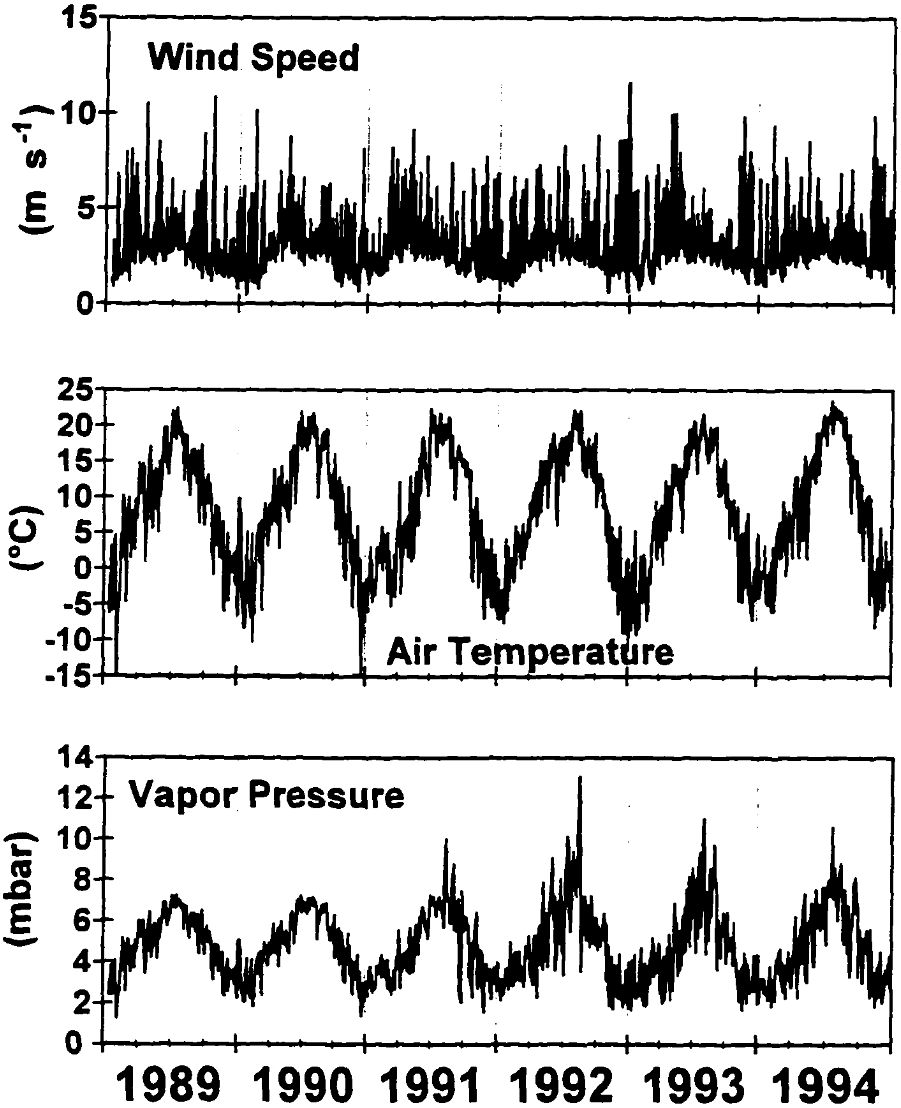
Wind Speed
(m s-1)
15
10
5
0
Air Temperature
(°C)
25
20
15
10
5
0
-5
-10
-15
Vapor Pressure
(mbar)
14
12
10
8
6
4
2
0
1989 1990 1991 1992 1993 1994

Figure 3. Six hour averages of wind speed, air temperature, and vapor pressure for the period 1992-1994.

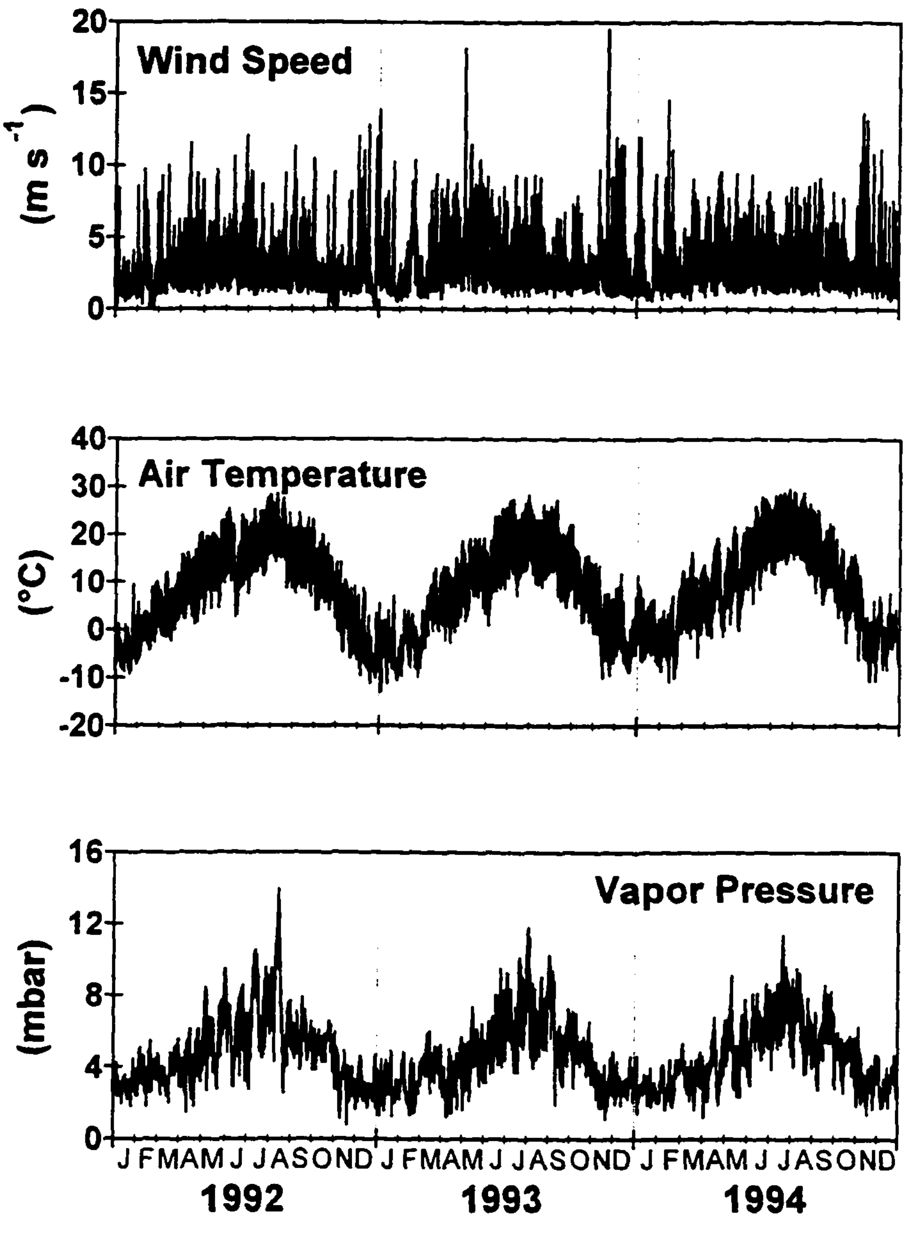
Wind Speed
(m s -1)
20
15
10
5
0
Air Temperature
(°C)
40
30
20
10
0
-10
-20
Vapor Pressure
(mbar)
16
12
8
4
0
J F M A M J J A S O N D J F M A M J J A S O N D J F M A M J J A S O N D
1992
1993
1994

Figure 4. Longwave and shortwave radiation daily totals and underwater PAR attenuation for the period 1989-1994.

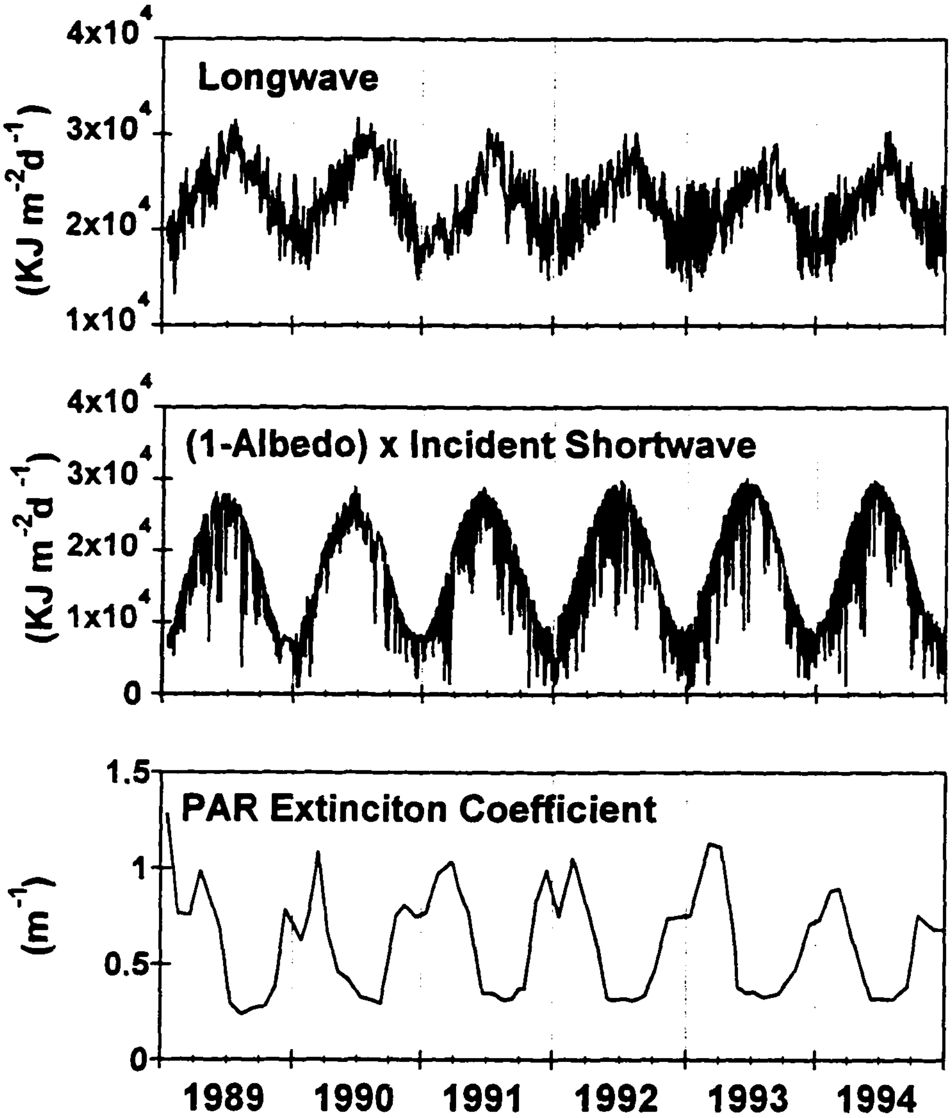
Longwave
(1-Albedo) x Incident Shortwave
PAR Extinciton Coefficient
(KJ m-2d-1)
(KJ m-2d-1)
(m-1)
4x10^4
3x10^4
2x10^4
1x10^4
0
1.5
1
0.5
1989
1990
1991
1992
1993
1994

Figure 5. Daily totals of stream discharge and precipitation for the period 1989-1994.

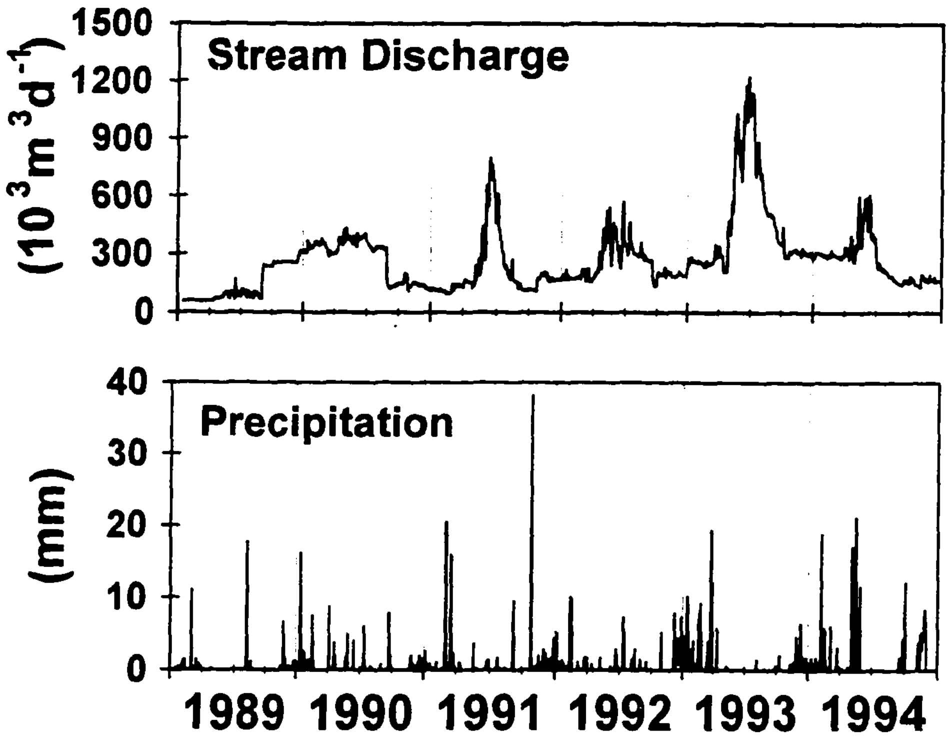

Stream Discharge
(10^{3}m^{3}d^{-1})
1500
1200
900
600
300
0
Precipitation
(mm)
40
30
20
10
0
1989 1990 1991 1992 1993 1994

Figure 6. Measured (•) and simulated surface temperature, simulated daily evaporation, and measured (•) and simulated lake levels. Evaporation mass transfer coefficients equal to 3.5 (thick line) and 3.3 (thin line) are shown in lake level panel.

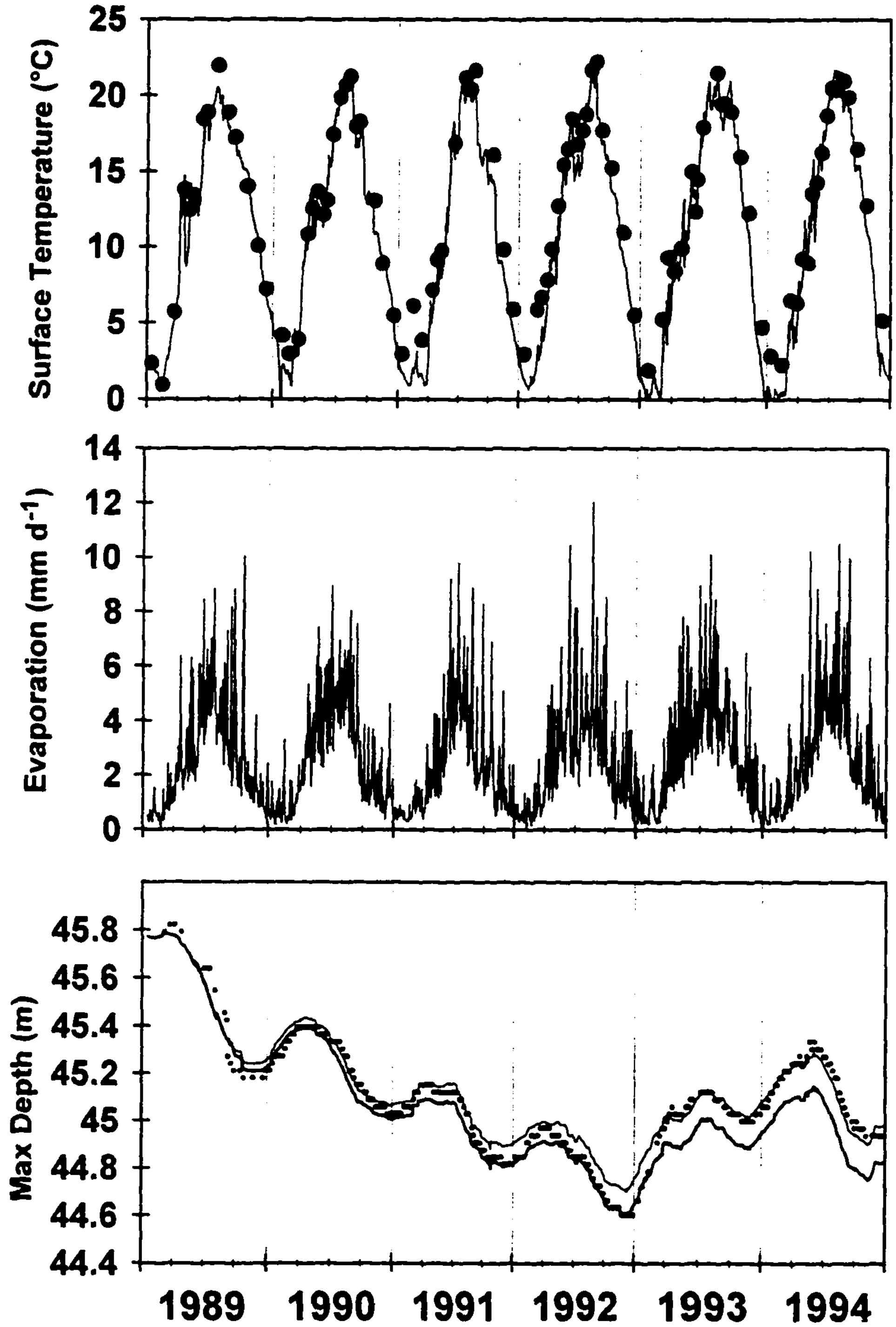
Surface Temperature (°C)
25
20
15
10
5
0
Evaporation (mm d-1)
14
12
10
8
6
4
2
0
Max Depth (m)
45.8
45.6
45.4
45.2
45
44.8
44.6
44.4
1989
1990
1991
1992
1993
1994

Figure 7. Field (A) temperature (°C) and (B) conductivity at 25 °C (mS cm^{-1}) profiles and simulation (C) temperature (°C) and (D) conductivity at 25 °C (mS cm^{-1}) profiles with isotherm intervals of 3°C and intervals of conductivity isopleths of 0.5 mS cm^{-1}.

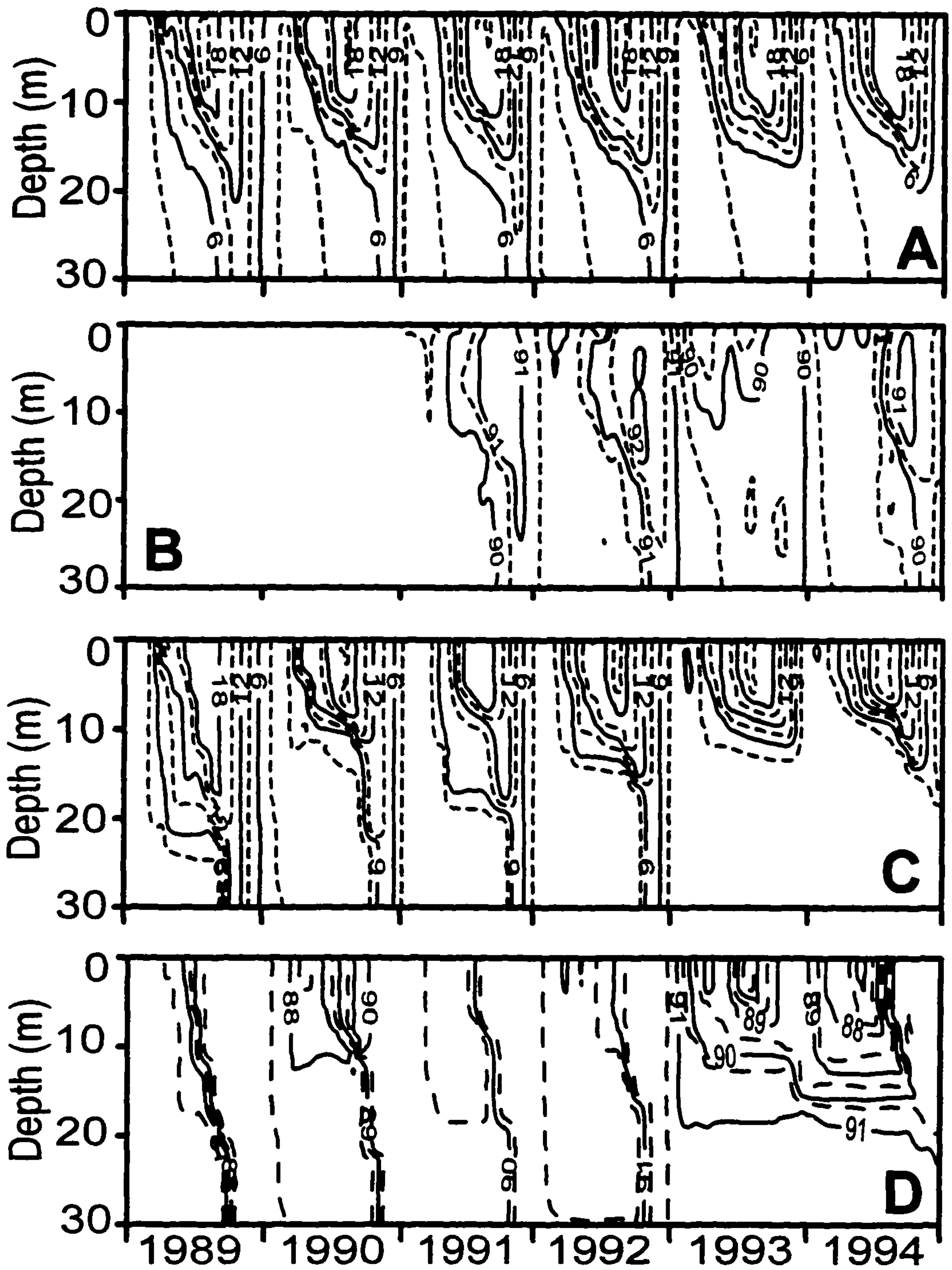
Depth (m)
0
10
20
30
A
B
C
D
1989
1990
1991
1992
1993
1994

Figure 8. Comparison between field measurements at 5 m (■) and 25 m (●) with simulated (A) 5 m (thin) and 25 m (thick) temperatures, (B) 5 m conductivity, (C) 25 m conductivity, (D) 5 m density, and (E) 25 m density.

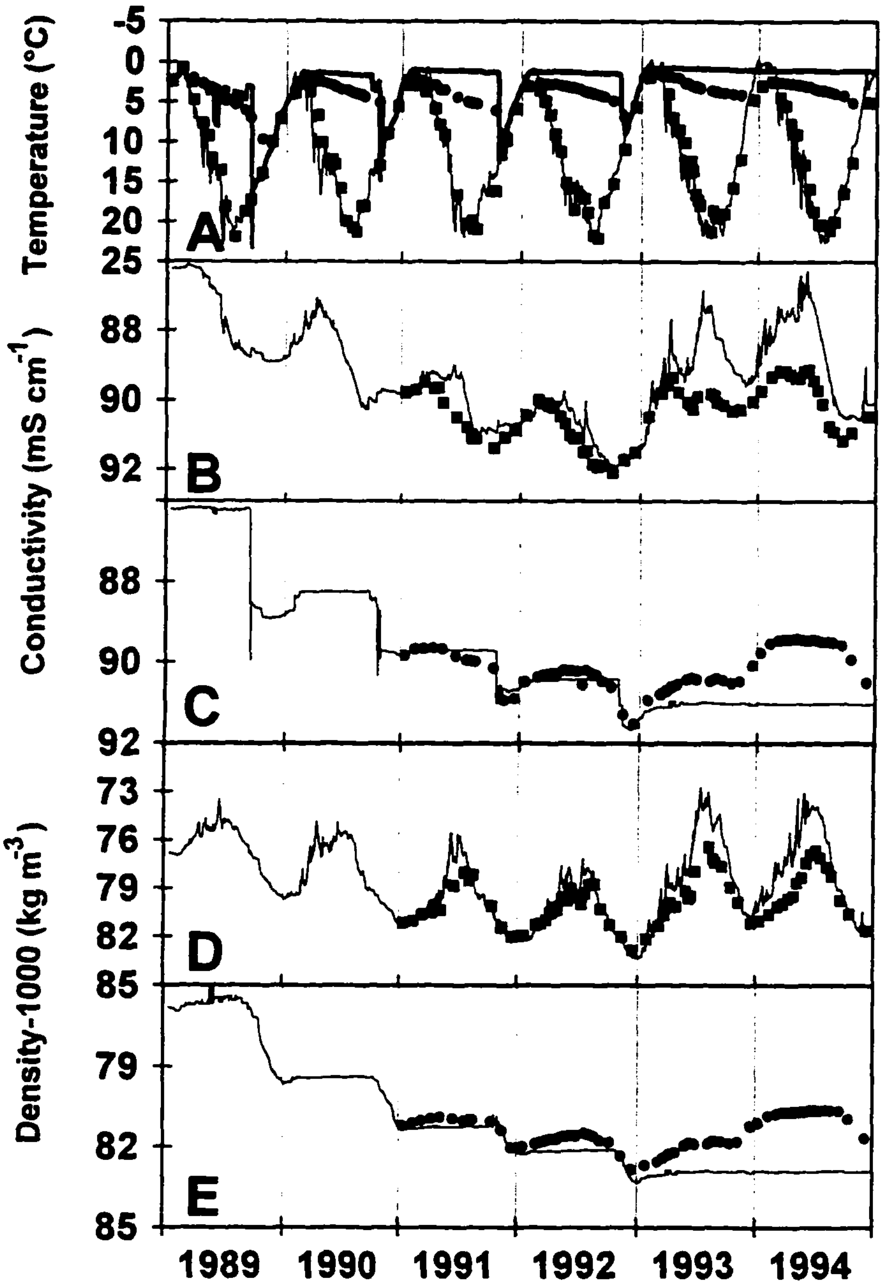
Temperature (°C)
Conductivity (mS cm-1)
Density-1000 (kg m-3)
-5
0
5
10
15
20
25
88
90
92
73
76
79
82
85
A
B
C
D
E
1989
1990
1991
1992
1993
1994

Figure 9. (A) Depth of field profile maximum temperature gradient (●) and simulated depth of the center of the vertical N^2 distribution (solid line). (B) Comparison of field (●) and simulated (solid line) N^2 at depths shown in panel (A). (C) Dissipation estimates from simulation at depths shown in panel (A). (D) Comparison of field (●) and simulated (solid line) vertical diffusivities, K_z, at depths shown in panel (A). Field K_z estimates calculated from field temperature profiles with the heat flux gradient method corrected for solar heating (Jassby and Powell 1974, *see* Chapter 3).

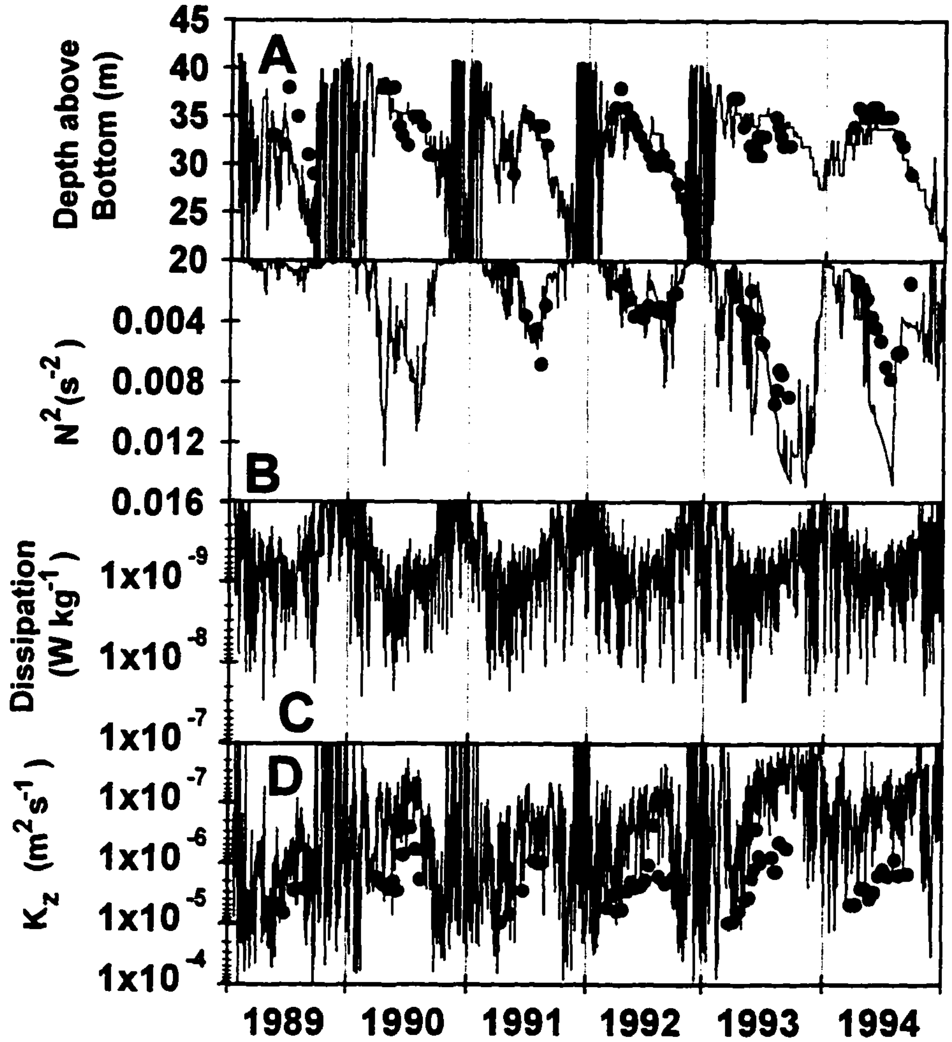
A
B
C
D
Depth above Bottom (m)
45
40
35
30
25
20
$N^2(s^{-2})$
0.004
0.008
0.012
0.016
Dissipation (W kg^{-1})
$1x10^{-9}$
$1x10^{-8}$
$1x10^{-7}$
K_z (m^2s^{-1})
$1x10^{-7}$
$1x10^{-6}$
$1x10^{-5}$
$1x10^{-4}$
1989
1990
1991
1992
1993
1994

Figure 10. As fig. 7 for simulation with dissipation increased by a factor of 15 throughout the simulation.

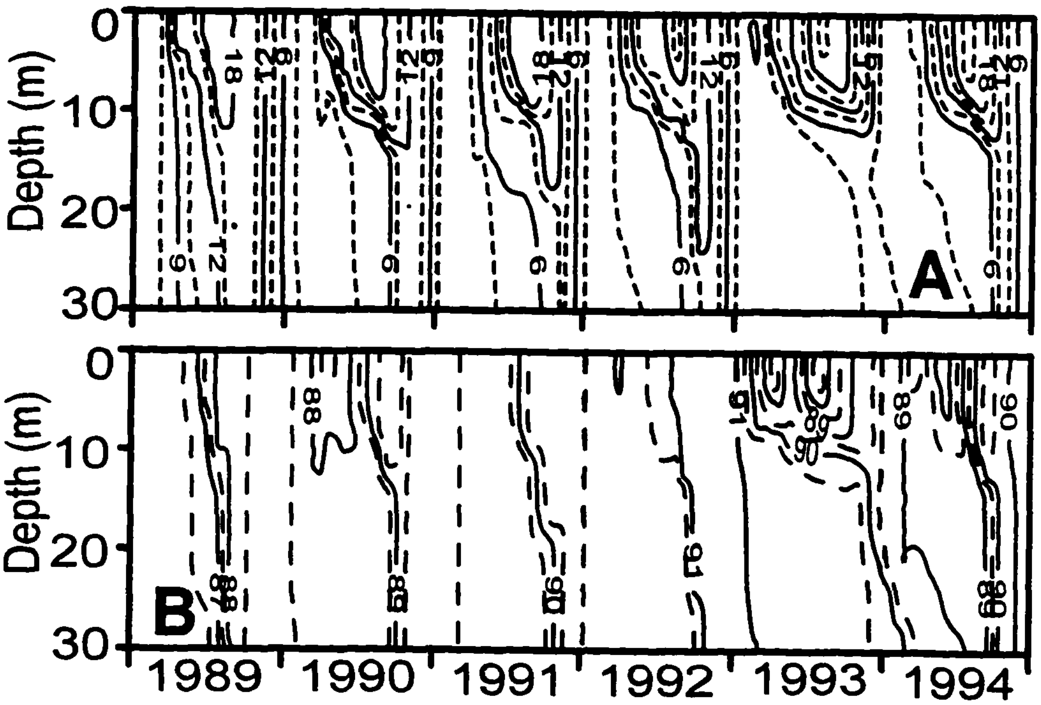

Depth (m)
0
10
20
30
A
B
1989
1990
1991
1992
1993
1994

Figure 11. As fig. 8 for simulation with dissipation increased by a factor of 15 throughout the simulation.

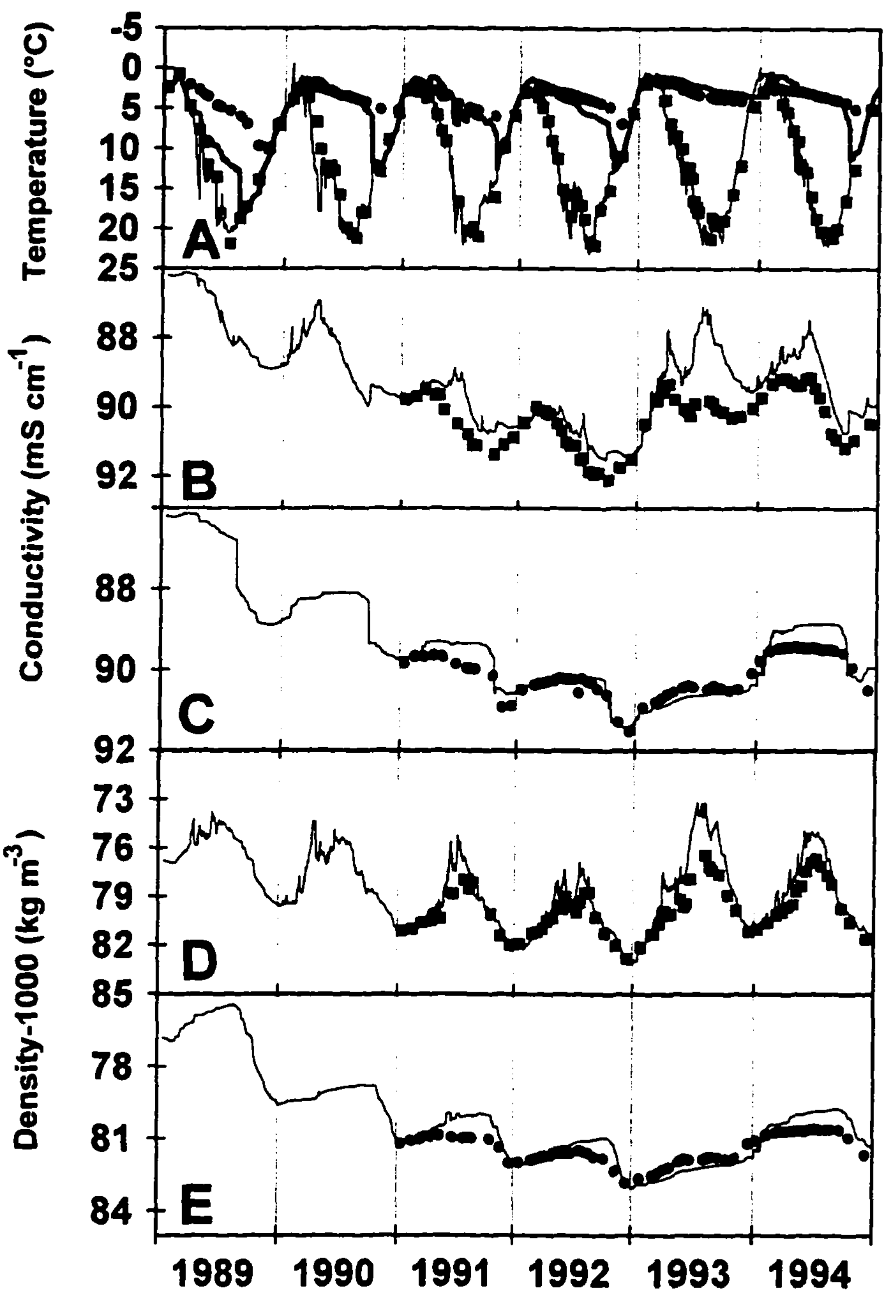
Temperature (°C)
-5
0
5
10
15
20
25
A
Conductivity (mS cm^{-1})
88
90
92
B
88
90
92
C
Density-1000 (kg m^{-3})
73
76
79
82
85
D
78
81
84
E
1989
1990
1991
1992
1993
1994

Figure 12. As fig. 9 for simulation with dissipation increased by a factor of 15 throughout the simulation.

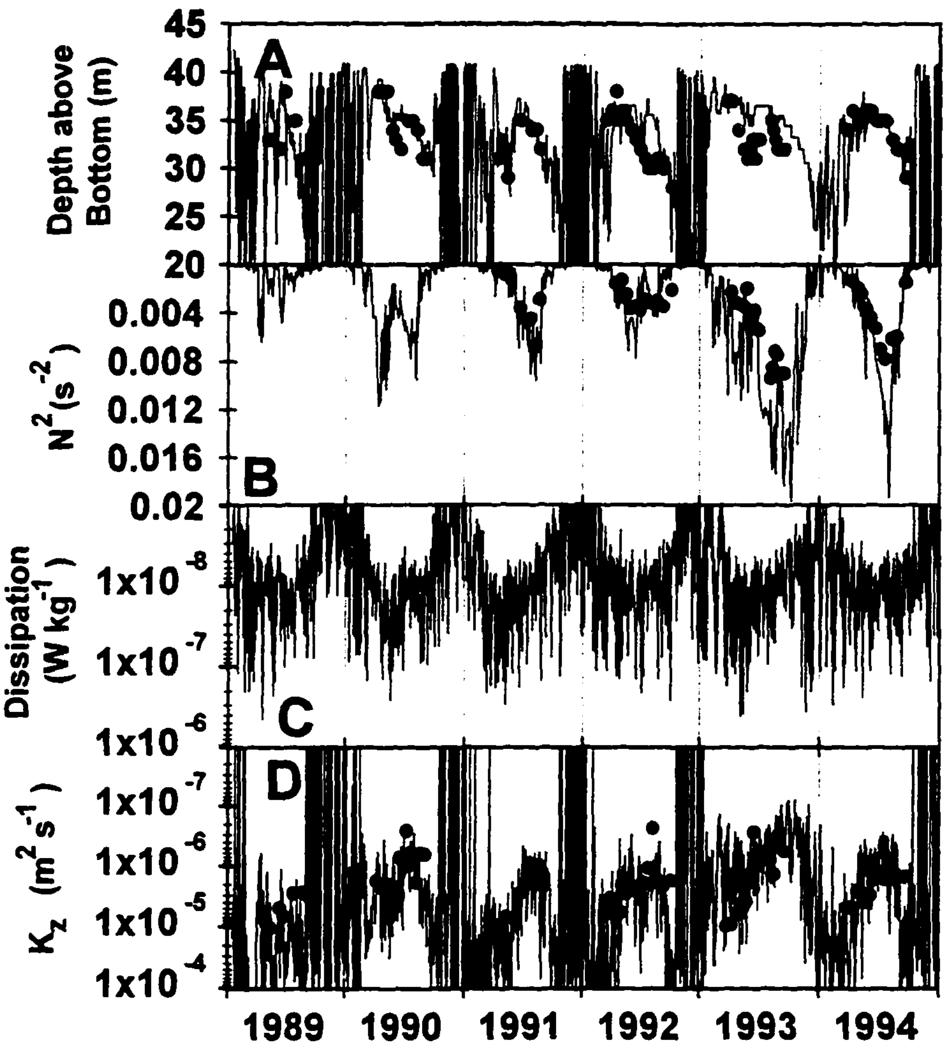
Depth above Bottom (m)
45
40
35
30
25
20
A
N^2(s^{-2})
0.004
0.008
0.012
0.016
0.02
B
Dissipation (W kg^{-1})
1x10^{-8}
1x10^{-7}
1x10^{-6}
C
K$_z$ (m^{2}s^{-1})
1x10^{-7}
1x10^{-6}
1x10^{-5}
1x10^{-4}
D
1989
1990
1991
1992
1993
1994

Figure 13. Dissipation estimates from benthic boundary layer turbulence (equation 18) for 0.1 (solid line), 0.05 (dash line), 0.01 (dash-dot line), and 0.05 (dash-dot-dot line) m s^{-1} current velocities 1 m above the sediments.

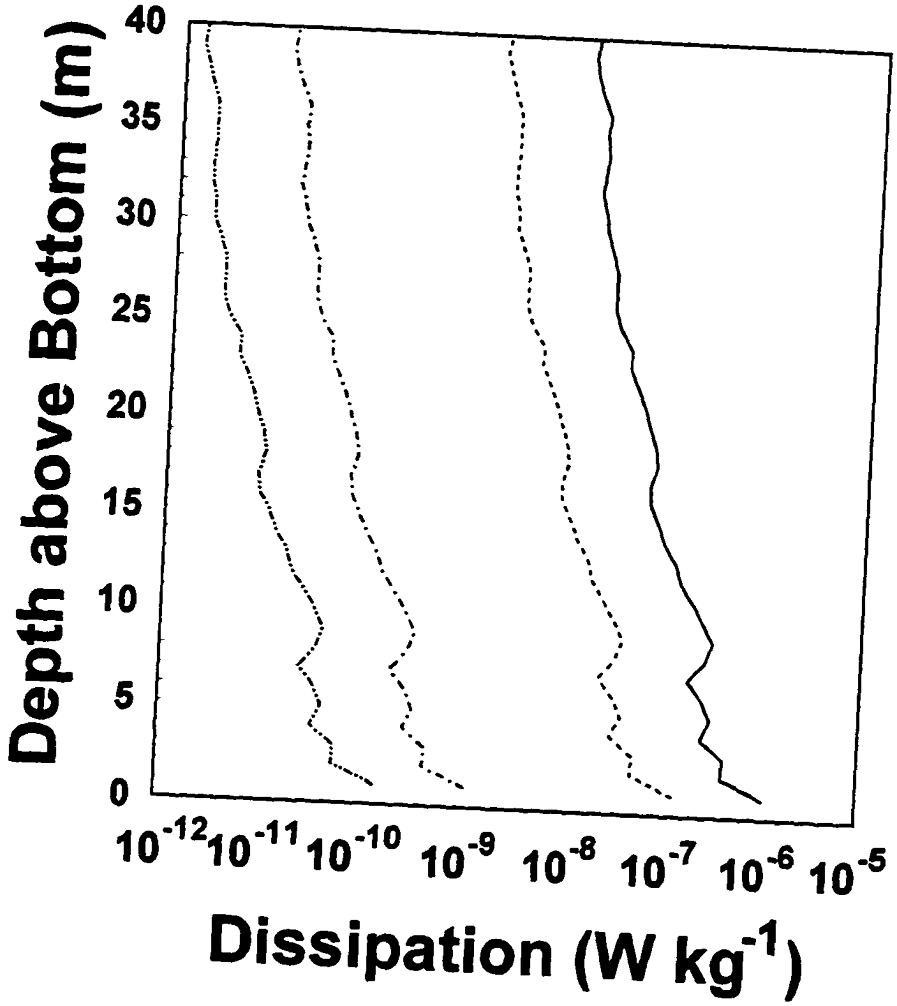
Depth above Bottom (m)
40
35
30
25
20
15
10
5
0
10^-12 10^-11 10^-10 10^-9 10^-8 10^-7 10^-6 10^-5
Dissipation (W kg^-1)

Figure 14. As fig. 7 for benthic boundary mixing simulation with 0.1 m s^{-1} over the entire duration of the simulation (Panels A and B). Simulation with six hour meteorological inputs (Panels C and D).

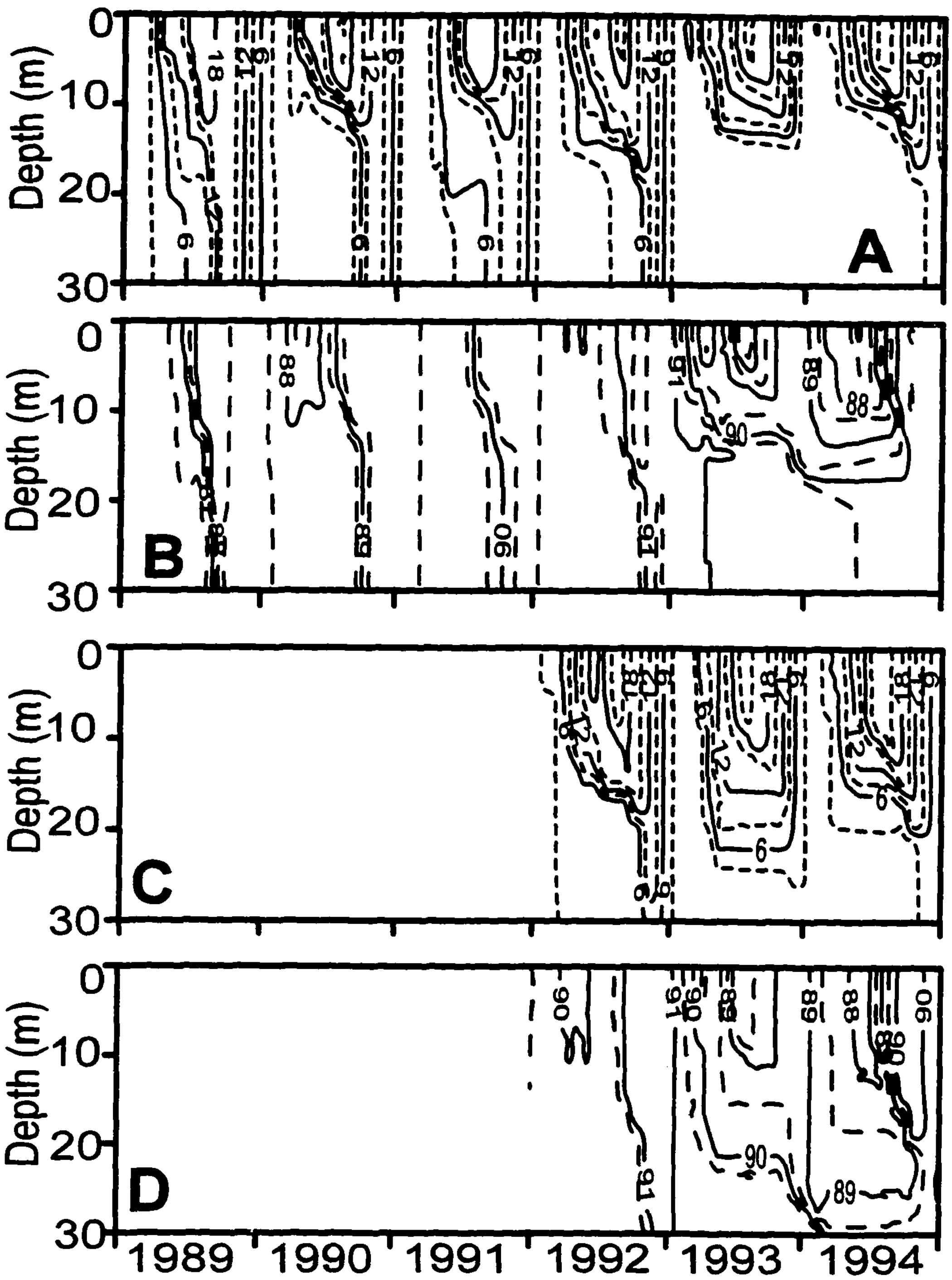
A
B
C
D
Depth (m)
0
10
20
30
1989
1990
1991
1992
1993
1994

Figure 15. (A) Stability, S_t, defined as the energy required to mix the entire water column against the potential energy of its stratification and calculated as,

$$S_t = \int_0^{H} (z - z_g) A(z) \rho(z) dz$$

where z is the vertical coordinate from the bottom of the lake, $A(z)$ is the area of the lake at height z, $\rho(z)$ is the water density at z, H is the water depth, and z_g is height to the center of volume of the lake defined as,

$$z_g = \frac{\int_0^{H} z A(z) dz}{\int_z^{H} A(z) dz}$$

for field profiles (●), published version simulation (thick line), and simulation with a factor of 15 increase in dissipation (thin line). L_N calculations from (B) field profiles, (C) simulation with published version, and (D) simulation with L_N dependence.

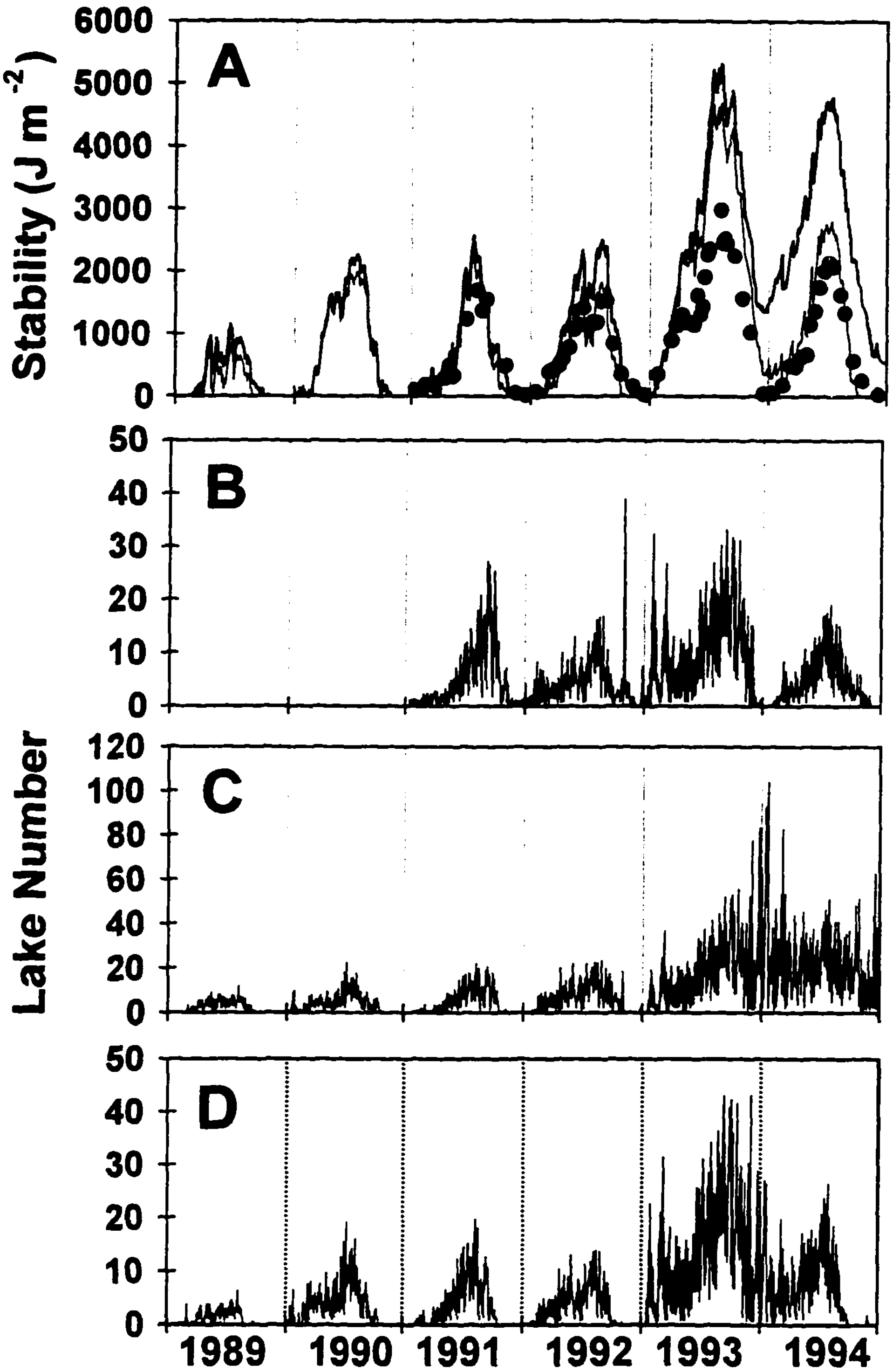
6000
5000
4000
3000
2000
1000
0
A
Stability (J m $^{-2}$)
50
40
30
20
10
0
B
120
100
80
60
40
20
0
C
Lake Number
50
40
30
20
10
0
D
1989
1990
1991
1992
1993
1994

Figure 16. As fig. 7 of the simulations with the diffusivity as a function of L_N with the constant a equal to 20 (Panels A and B) and 30 (Panels C and D) and constant b equal to -1.

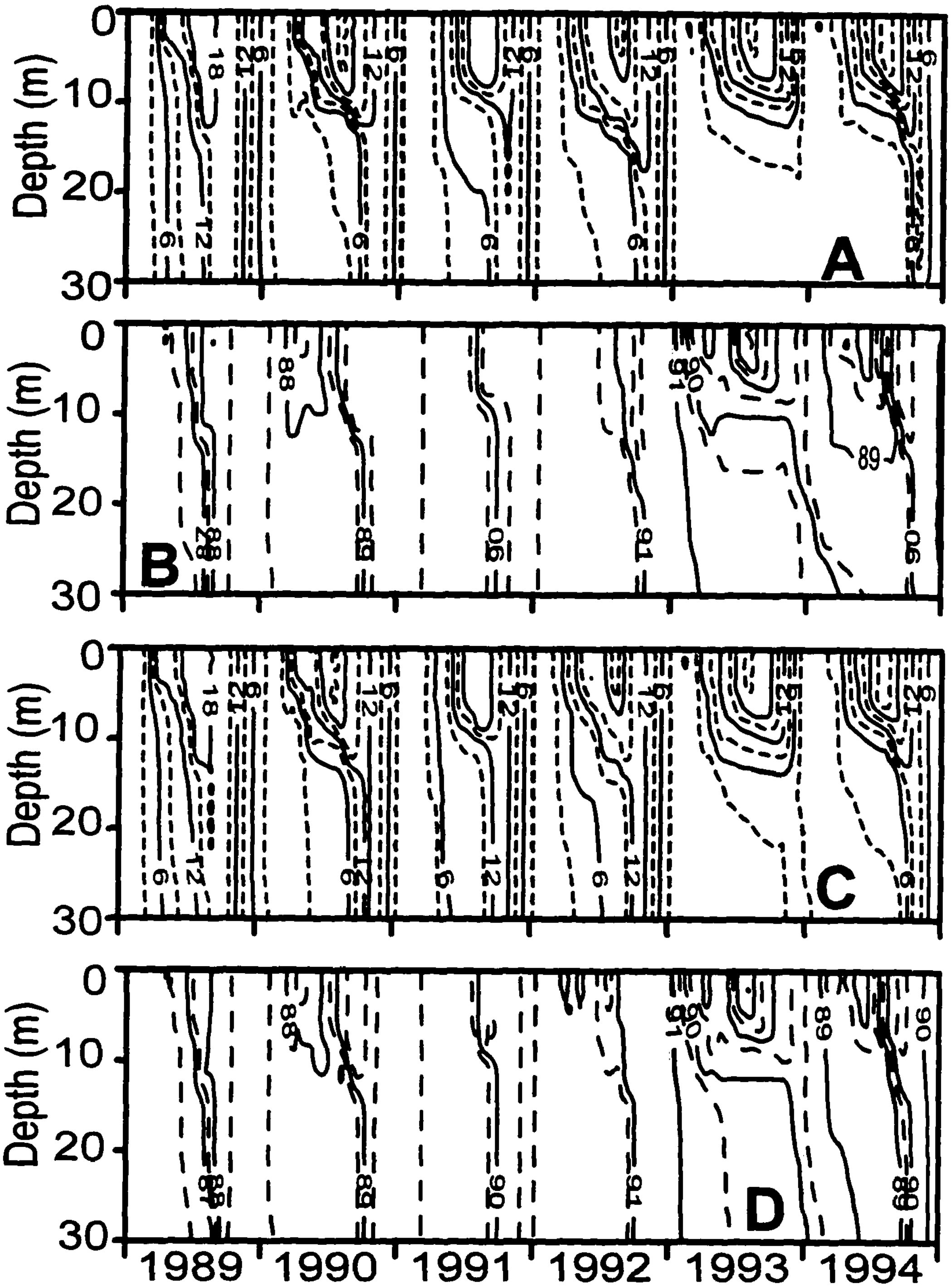
Depth (m)
0
10
20
30
A
B
C
D
1989
1990
1991
1992
1993
1994

Figure 17. As fig. 8 of the simulation with the diffusivity as a function of L_N and constants a equal to 20 and b equal to -1.

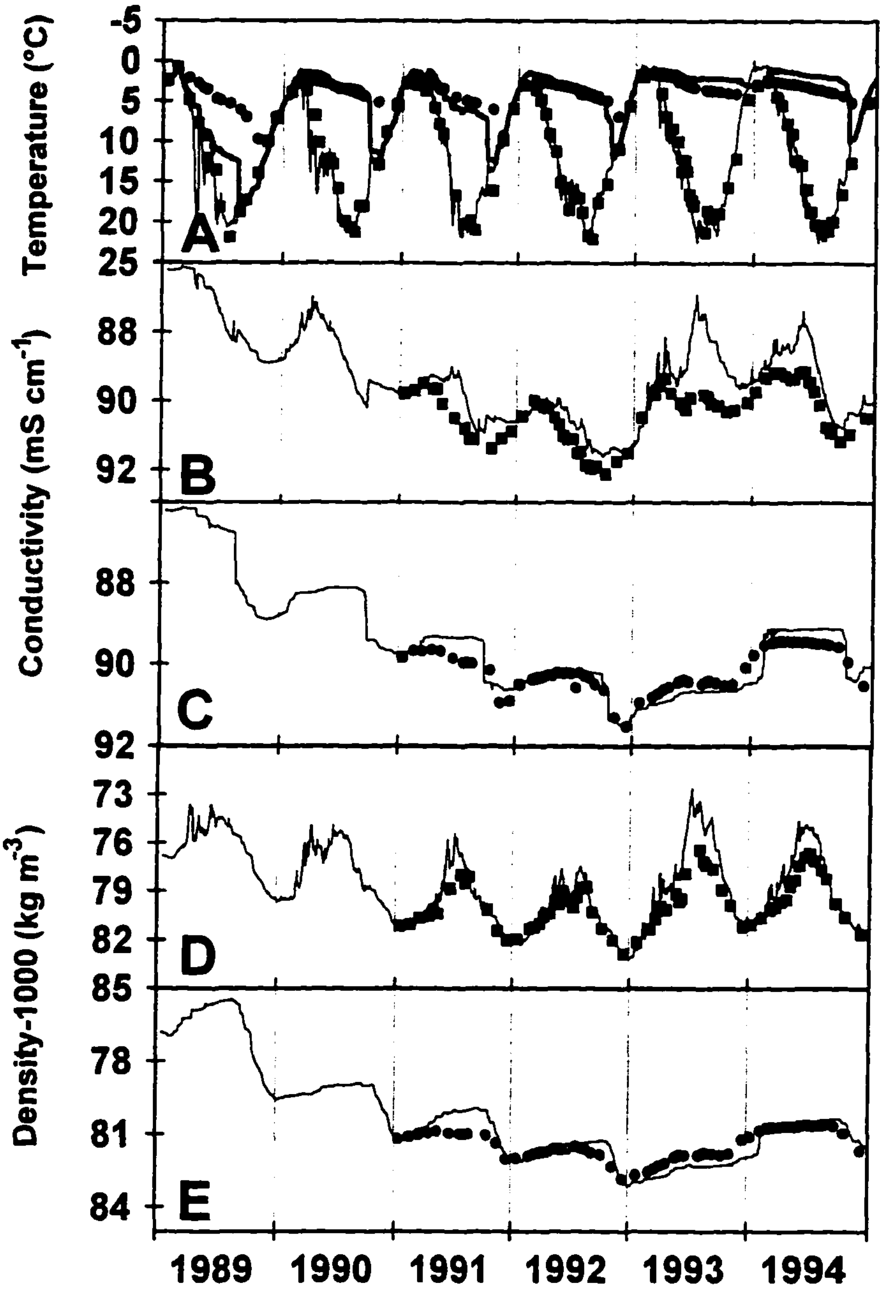
Temperature (°C)
-5
0
5
10
15
20
25
A
Conductivity (mS cm^{-1})
88
90
92
B
88
90
92
C
Density-1000 (kg m^{-3})
73
76
79
82
85
D
78
81
84
E
1989
1990
1991
1992
1993
1994

Figure 18. As fig. 9 of the simulation with the diffusivity as a function of L_N and constants a equal to 20 and b equal to -1.

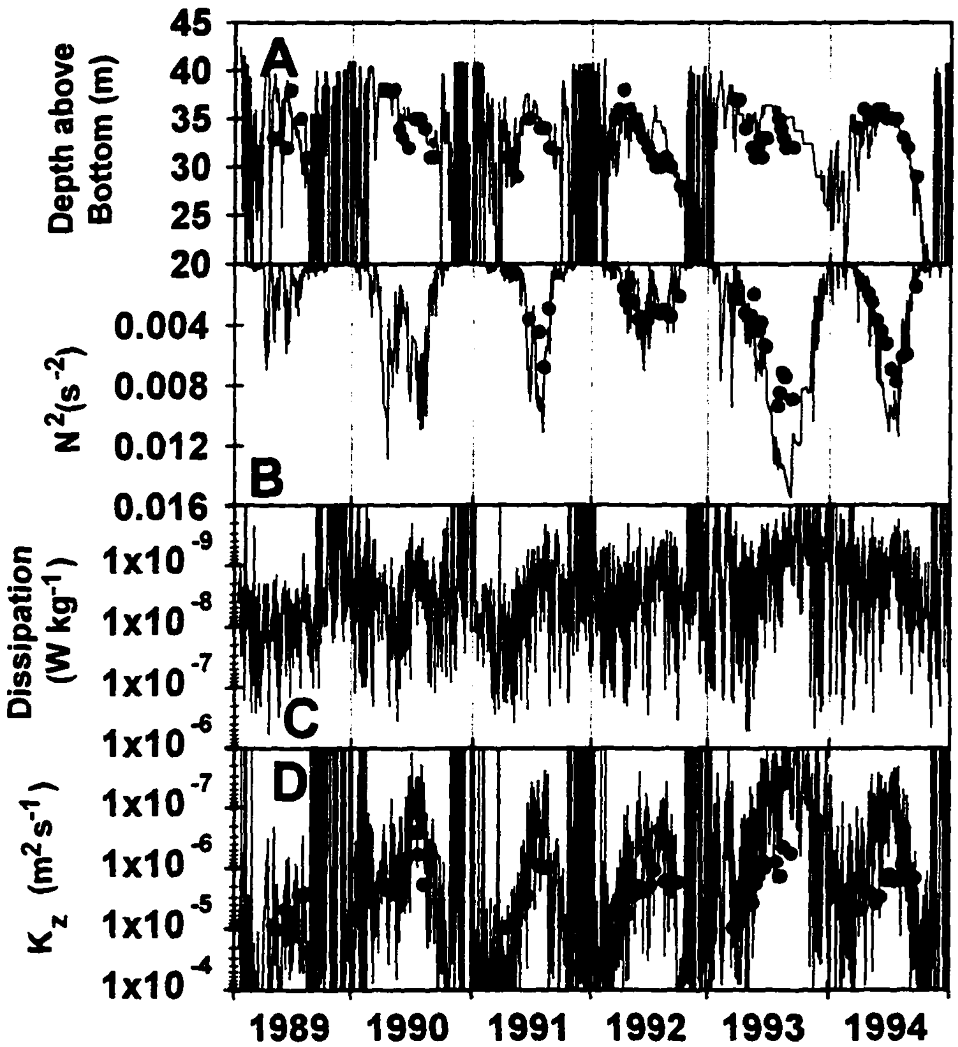

Depth above Bottom (m)
45
40
35
30
25
20
A
N2(s-2)
0.004
0.008
0.012
0.016
B
Dissipation (W kg-1)
1x10-9
1x10-8
1x10-7
1x10-6
C
Kz (m2s-1)
1x10-7
1x10-6
1x10-5
1x10-4
D
1989
1990
1991
1992
1993
1994